University of Liege

Modeling of aerodynamic forces in flapping flight with the Unsteady Vortex Lattice Method

---

Author:
Thomas Lambert

Supervisor:
G. Dimitriadis

*A thesis submitted in fulfillment of the requirements
for the degree of Master in Aerospace Engineering*

Academic Year 2014-2015

President of the Jury:	J-P. Ponthot
Members of the Jury:	T. Andrianne, O. Brüls,
	G. Dimitriadis, T. Gillet
	V. Terrapon

UNIVERSITY OF LIEGE
Faculty of Applied Sciences
Master in Aerospace Engineering

**Modeling of aerodynamic forces in flapping flight with the Unsteady
Vortex Lattice Method**

by Thomas LAMBERT

Abstract

This thesis concerns the extensive study and comparison of two approaches commonly used to compute the aerodynamic forces with the unsteady vortex lattice method. The first approach was introduced by Katz and Plotkin and is based on Bernoulli's equations, the second approach was based Joukowski's equations for the computation of forces.

This report is divided in two main sections: the study of one wing undergoing simple movements (steady, pure harmonic pitching and pure harmonic plunging) and the study of two separate wings undergoing a combination of flapping and pitching such as seen in avian flight.

For the simple test cases, the results obtained with both methods of computation were first compared to an analytical solution for a (quasi) 2D case. Then the comparison of both methods was made for finite wings. For the 3D problem a convergence study was done with respect to the chordwise discretisation of the airfoils. This section showed that for all the cases, the two methods give almost the same answer and therefore they could be considered as equivalent. The convergence study realised for finite wings showed however that Joukowski's method converges quicker than Katz's for symmetric airfoils, but it is the other way around when it comes to cambered airfoils.

The study of the flapping and pitching motion is based on the work of N. Abdul Razak in [2]. The influence of pitch leading was extensively studied as this phenomenon presents a flow attached at all time, so these kinematics are well suited for the vortex lattice method. Both pure flapping and pitch lagging were also discussed but more briefly.
For pitch leading, the study showed that in general both methods give the same results for the drag and the lift. Moreover, the UVLM solutions were very close to the experimental ones, especially for the drag. The convergence showed a small advantage for the Katz method for the coarser meshes, but in the end both methods appear to reach convergence for the same discretisation.

Acknowledgements

I would like to express my deepest appreciation to all the people that helped me during the realisation of this project.

In particular, I would like to thank my supervisor, Greg Dimitriadis for giving me the opportunity to work on this thesis. I am forever grateful for his guidance, his wise advice and for being available to answer my numerous questions, even during his vacations. It goes without saying that without him I would not have been able to carry out this project.

I would also like to thank my family and friends and especially Maud Bocar for her support and encouragements during this last year.

Contents

List of Figures

List of Tables

Nomenclature

a	nondimensional distance between airfoil midchord and center of rotation	-
b	semichord	m
C_D	wing drag coefficient	-
C_d	sectional drag coefficient	-
C_L	wing lift coefficient	-
C_l	sectional lift coefficient	-
C_s	sectional leading-edge suction coefficient	-
c	airfoil chord	m
h	plunge displacement	m
k	reduced frequency	-
M	number of chordwise panels	
N	number of spanwise panels	
$\mathbf{n}$	panel normal vector	
P	orthogonal projection operator	
$\mathbf{U}$	velocity vector	$\text{m} \cdot \text{s}^{-1}$
U_∞	freestream velocity	$\text{m} \cdot \text{s}^{-1}$
Δt	time step	s
α	angle of attack	rad
α_{eff}	effective angle of attack	rad
α_p	pitching angle	rad
γ	flapping angle	rad
Γ	circulation	$\text{m}^2 \cdot \text{s}^{-1}$
Φ	Velocity potential	-
ρ_∞	freestream density	$\text{kg} \cdot \text{m}^{-3}$
$\boldsymbol{\tau}$	panel tangential vector	
ω	angular frequency	$\text{rad} \cdot \text{s}^{-1}$

Chapter 1

Introduction

Since the beginning of time, man has been fascinated by the way birds fly. Using the technological improvements of the past two centuries, this dream finally came true in December 1903 thanks to the Wright brothers.
During the following years, people tried to develop similar planes, all based on fixed wings systems, taking advantage of their simplicity. Eventually, Leonardo Da Vinci's dream of mimicking bird flight was abandoned during the first war as all the efforts were focused on fixed wing configurations.

Lately, due to many technological advancements such as micro-chips, composite materials, piezoelectric actuators,... the development of small Unmanned Aerial Vehicles (UAV) became more and more affordable and generalized. Thanks to these new kind of aircrafts, interest in flapping flight has been revived.

Recent progresses in biological engineering were able to describe more accurately the flight of birds and insects. This initiated the rise of new types of Micro Aerial Vehicles: ornithopters and entomopters, that are based respectively on imitating birds and insects flights – where the main difference lies in the flapping frequency. In these peculiar type of flights, the lift and thrust are generated using only the motion of the wing (usually flapping and pitching), without any engine. The flapping aircrafts present the advantages of high maneuverability, the possibility to hover in space and the high efficiency in low Reynolds flows. At low frequency, the flapping motion of the wings should also produce less noise than a rotary motion. Moreover, technological breakthroughs can now allow exceptionally small flappers [3], making them extremely useful for defense, intelligence gathering, surveillance, but also civilian purposes (toys, camera recording).

In order to study the flapping flight, specific methods need to be used. This work will review a very common tool employed for the modeling of such flights: the Unsteady Vortex Lattice Method (UVLM). In particular, emphasis will be made on the way the aerodynamic forces are computed within this method. A full study of two different computation processes for the aerodynamic loads will be conducted; first for simple cases (steady , pure harmonic pitching, pure harmonic plunging), then for a more complex motion combining flapping and pitching of two separate wings. The flapping and pitching case will be entirely based on the

experiments conducted by N. Abdul Razak at the University of Liege during his PhD Thesis [2]. These results will be used as reference to compare the validity of both aerodynamic computation methods with the UVLM in flapping flight.

Aerodynamic loads

The main purpose of this thesis is to compare two different methods used to compute the aerodynamic loads. Both methods are well known and commonly applied to solve problems with vortex ring elements. However the literature suffers from a lack of discussions and comparisons between them, especially regarding the induced drag computation.
The first method discussed in this thesis is based on Bernoulli's equations and was proposed by Katz and Plotkin in [1]. This method will be referred in this work as the *Katz* method.
The second one is based on Joukowski's equations for the computation of forces and will be referred as the *Joukowski* method.

A small technical note written in 2013 by Simpson *et al.* [4] discusses precisely these methods. However, it focuses only on flat plates in pure harmonic pitching or pure harmonic plunging. In this technical note, the results for the drag coefficient obtained with the UVLM are compared with the results given by a closed-form solution introduced by Garrick [5]. This paper will be used as a start for the study of the simple cases in this thesis, bit the study will also be extended in order to analyse the effect of the airfoil's camber.

In the end, the ambition of this thesis is to determine if one method is better than the other from a qualitative point of view but also from a convergence aspect, in the case of more general kinematics and for different types of airfoil.

Chapter 2

Unsteady Vortex Lattice Method

The unsteady vortex-lattice method is an approach commonly used to study the aerodynamic loads in unsteady, subsonic flows. It is perfectly suited for the analysis of flapping flight as it can provide time accurately simulations and can account the changing of circulation distribution on the wing, the time-dependent velocity potential and the movement of the circulatory wake [6], as long as the flow remains attached to the wing.

This method is based on the resolution of potential flows which is very convenient because of its simplicity of implementation and the low computational cost in regard to CFD tools. However, it is obviously less precise than a full CFD analysis of the flow, and therefore it is mostly used during the initial phase of a project.
A complete description of this method is given by Katz and Plotkin in [1]. Other recommended lectures on this topic include also Anderson [7] and Murua *et al.* [8].

2.1 Concept of potential flow methods

As said earlier, the UVLM is based on the potential theory and on the resolution of Laplace's equation using potential flows. In order to use this equation, different strong hypothesis must be made.
The flow must remain at all time:

- sub-sonic,
- non-viscous,
- incompressible,
- irrotational.

Moreover, in order to match the irrotationality condition, the flow has to remain attached everywhere and the rotational areas must be negligible (locked in the

boundary layer or in the wake). This attached flow hypothesis is of crucial importance in the vortex lattice method and will be discussed in detail in Chapter 4. Under these hypothesis, the velocity potential Φ can be defined as

$$\mathbf{U} = \nabla\Phi \tag{2.1}$$

leading to the definition of Laplace's equation from the continuity:

$$\nabla \cdot \mathbf{U} = 0$$
$$\Leftrightarrow \quad \Delta\Phi = 0 \tag{2.2}$$

The resolution of Laplace's equation (Eq. (2.2)) is based on finding elementary solutions, also called singularities. These elementary solutions have the form of algebraic functions of unknown strength that satisfy Laplace's equation. Using the superposition principle, the singularities are then combined to form the flow field. Thus, the problem becomes a limit values problem expressed as a set of algebraic equations for the unknown distribution of singularities over the surface, which is easier and faster to solve.

Laplace's equation requires a pair of boundary conditions in order to describe totally the problem. The first one is usually an impermeability condition across the surface (mathematically expressed by canceling the component of velocity normal to the surface). The second condition, relates the loss of influence of the flow in the far-field and therefore imposes that the disturbances vanish at infinity. Obviously, the combination of singularities must also follow these two conditions in order to represent the flow around the object.
Moreover, in the case of lifting bodies, the flow must detach smoothly at the trailing edge to form a thin wake. This requirement is referred as the Kutta condition (or Kutta-Joukowski condition) and must also be fulfilled by the combination of singularities.

Concretely, for general geometries, the singularities are disposed on the surface of the body. Hence, the differential equation is replaced by a system of algebraic equations. The far-field boundary condition is automatically satisfied for the singularities since their influence decays with the distance. The strength of the singularities is then determined by applying the impermeability at different control points over the surface.
Finally the Kutta condition is imposed to remove the indetermination about the circulation around the body, leading to a unique solution.

2.2 Classification of potential flow methods

There is plenty of methods that can solve the potential flow equations like it was explained in the previous section. These methods can be differentiated accordingly to various criteria.

The first distinction is evidently related to the steadiness or unsteadiness of the flow (introduced through the boundary conditions).
A second classification can be made upon the discretisation of the domain and therefore the types of singularity used: sources, doublets, vortices or even computer generated high-order elements.
A third differentiation is based on the wake model employed. It is known that the wake can have a crucial effect on the aerodynamic properties of the wing in unsteady flow. In fact, the wake induces aerodynamic lags, which are delays in the development of the aerodynamic forces over the wing. In real cases, the wake is force-free and moves with respect to the local flow velocity. This particular type of wake is called a *free wake*. Nevertheless, capturing this behavior is computationally expensive. A more common and cheaper approach is to use a *flat wake*. In this scenario, the wake is simply convected by the free stream and is not deformed afterwards.
An other classification relies on the thickness of the body. For a thin body, computational resources can be spared by modeling the airfoil using only its camberline. In that case, the singularities are placed along this camberline with respect to the thin airfoil theory. The singularities used are vortices to generate circulation (and therefore loads) and doublet (to represent thickness). However, for relatively thin airfoils, the thickness does not impact significantly the aerodynamic forces. As long as the thickness does not exceed 30% of the chord, its influence is minimal in non-stationary flow, and it can be neglected [8].

This thesis will focus on pitching, plunging and flapping wings, with a maximum camber equal to 6% of the chord. Therefore the unsteady vortex lattice method applied to thin airfoils is one of the best ways to solve the potential flow equation.

2.3 Discrete-time state-space UVLM

The unsteady vortex lattice method is a very useful tool to solve 3D potential flow problems and to represent lifting surfaces. These surfaces, along with the wake are modeled with vortex rings elements. One vortex ring is a quadrangle consisting in a closed loop of four vortex segments, each of constant and equal intensity.
The unsteady vortex lattice method is solved by the means of a time-marching algorithm: at the beginning of the resolution, the vortex rings of the wake are shed freely at the trailing edge of the wing and then they deform with respect to the local flow (free wake model) or they are simply convected by the free stream (flat wake model).

Specifically, the lifting surfaces are discretised in quadrilateral panels along the camberline of the airfoil. A vortex ring is then associated to each panel, as it is shown in Fig. 2.1, and the impermeability condition is imposed at the collocation point. Usually, the vortex rings attached to a lifting panel are called *bound vortices*. The vortex ring's leading segment must be placed on the the

panel's quarter chord line in order to satisfy (implicitly) the Kutta condition. Note that the Kutta condition can also be enforced explicitly [9], but it is not usually employed because it requires more computations. The collocation points are placed at the center of the three-quarter chord line of the corresponding panel. For each vortex ring, a normal vector $\mathbf{n}$ is defined at the collocation point. Finally, the vorticity $\mathbf{\Gamma}$ is defined on each segment with respect to the right-hand rule, as shown in Fig. 2.1.
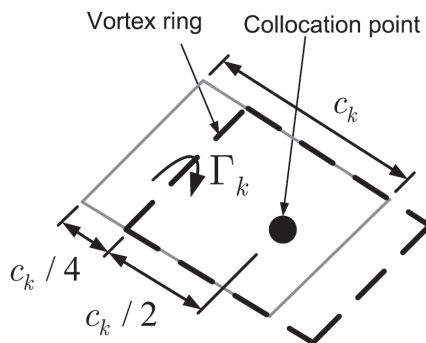
FIGURE 2.1: Surface panels, vortex rings and collocation points. Illustration from [8].

The wake is made of a vortex sheet produced at the trailing edge of the wing and shed freely as explained previously, these vortices are usually called *wake vortices*. The vortex ring model for the two first time steps is presented in Fig.2.2.

At the discrete time step $n+1$, the impermeability condition is imposed at each collocation point, which leads to the determination of the vorticity for each ring. This condition is traduced mathematically by canceling the normal component of the local velocity at the collocation point of each panel:

$$A_{cb}\mathbf{\Gamma}_b^{n+1} + A_{cw}\mathbf{\Gamma}_w^{n+1} + \mathbf{w}^{n+1} = 0 \qquad (2.3)$$

where A_{cb} and A_{cw} are the wing-wing and wing-wake aerodynamic influences matrices computed at the collocation points, $\mathbf{\Gamma}_b$ and $\mathbf{\Gamma}_w$ are the circulation strengths respectively in the bound and wake panels, and $\mathbf{w}$ is the vector of the components normal to the panel of all velocities other than the ones induced by the vorticity (free stream, wing motion, gusts,etc.).
This relation means that the sum of each contribution to the normal speed at the collocation point is zero.

The velocity induced by the vortex rings is computed for each panel thanks to the Biot-Savart law. The influence of panel l of unit vortex strength $\mathbf{\Gamma}_l$ on the collocation point k is given by:

$$\mathbf{q}_{kl} = \oint_{\mathcal{C}_l} \frac{\mathrm{d}\mathbf{s}_j \times \mathbf{r}_{kl}}{4\pi r_{kl}^3} \qquad (2.4)$$
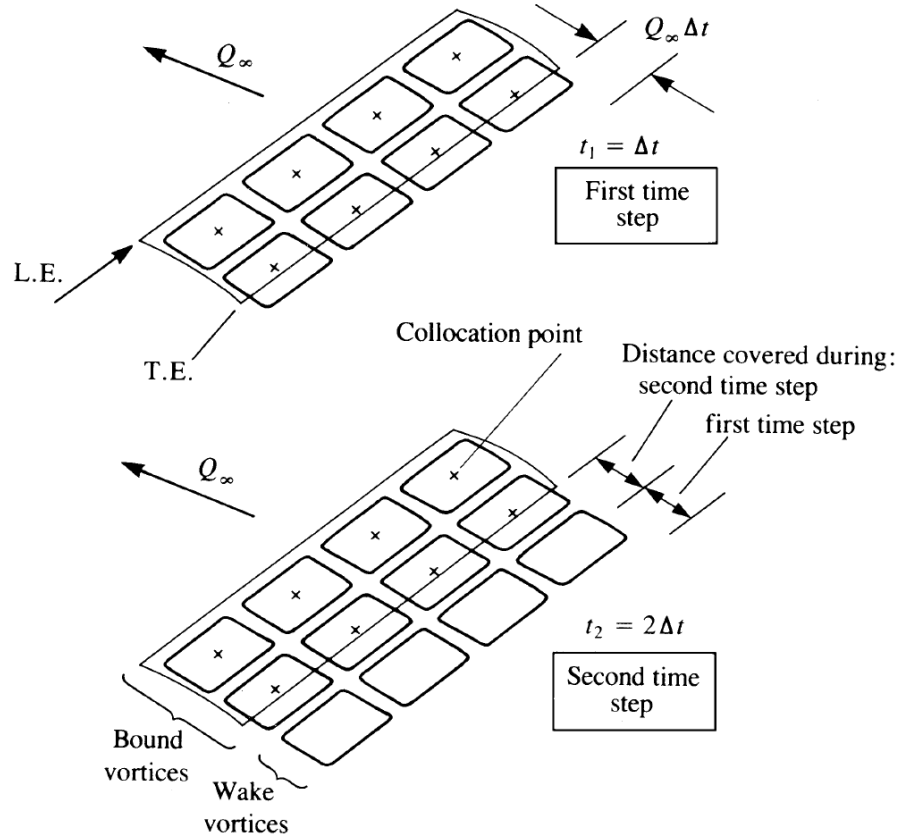
FIGURE 2.2: Vortex ring model for the unsteady lifting surface during the first time step (upper figure) and during the second time step (lower figure). Illustration from [1].

where $\mathbf{ds}_j$ are the vortex elements that made the ring $\mathcal{C}_l$ and $\mathbf{r}_{kl}$ the vector from the collocation point k to the right vortex segment in the ring. The matrices of influences A_{cb} and A_{cw} are computed using the projection of each $\mathbf{q}_{kl}$ onto the normal $\mathbf{n}_k$ associated with the collocation point

$$\begin{cases} (A_{cb})_{kl} & = \mathbf{q}_{kl} \cdot \mathbf{n}_k & k, l = 1...N_b \\ (A_{cw})_{kv} & = \mathbf{q}_{kv} \cdot \mathbf{n}_k & k = 1...N_b; \ v = 1...N_w \end{cases} \tag{2.5}$$

In order to reduce the computation time, only the influence of the wake panels close to the wing can be taken into account. This approximation is justified as the wake panels have less influence when they are far away from the body. In the codes developed for this thesis, only the portion of the wake smaller than five time the chord was taken into account for the computation of the wake influences matrix.

Finally, the non-circulatory velocity is given by:

$$(\mathbf{w})_k = (\mathbf{U}_\infty + \mathbf{U}_{\text{wing}}) \cdot \mathbf{n}_k \tag{2.6}$$

where $\mathbf{U}_\infty$ is the velocity of the free stream and $\mathbf{U}_{\text{wing}}$ is the velocity due to the rigid body motion of the the wing. Additional contributions can be added in order

to extend the model: gusts, deformation of the wing,etc. but these are not studied in the problems of pitching, plunging and flapping wings presented in this thesis.

The shedding of the wake should now be addressed. As the wake is not linked directly to a surface, only rings of vorticity have to be generated. These rings are defined using four corner points. In order to account for the movement of the wing, the trailing segment (= the first wake segment) should be placed in the interval covered by the trailing edge during the latest time step: $\mathbf{U}_\infty(t)\Delta t$. Nonetheless, this approach would lead to an underestimation of the induced velocity when compared with the continuous wake vortex sheet result. ("This is mainly due to the small distance (zero distance) of the continuous wake from the trailing edge during the time interval, compared to the relatively larger distance of an equivalent discrete vortex with similar vorticity placed amid the interval of the latest time step" [1]). As a result, the usual numerical approach is to place the first wake vortex closer to the trailing edge, typically at $0.2 - 0.3\,\mathbf{U}_\infty(t)\Delta t$.

At each time step, the whole procedure is repeated: two new points are created at a distance of $0.2 - 0.3\,\mathbf{U}_\infty(t)\Delta t$ for each panel and a new vortex cell is created, as shown in Fig. 2.3.

The strength of the newly shed wake vortex is set equal to the one of the bound vortex situated at the trailing edge in the previous time step:

$$\Gamma_w^{n+1} = \Gamma_{\text{T.E.}}^n \tag{2.7}$$

Note that, because the dissipation of vorticity is zero (due to Kelvin's theorem), the vortex ring's strength remains unchanged.
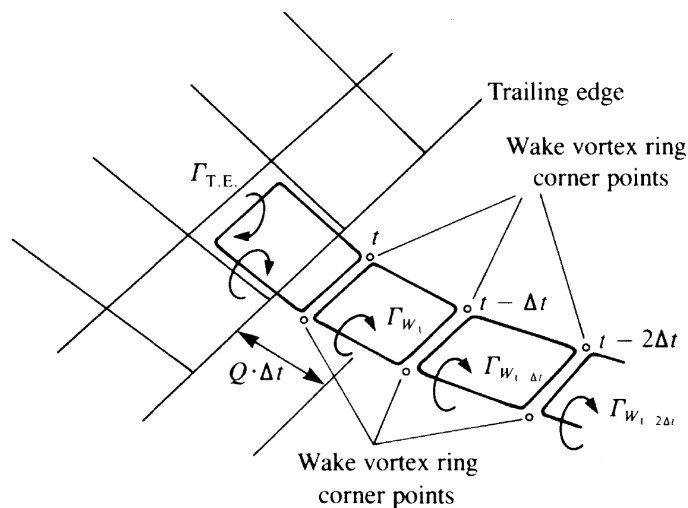
FIGURE 2.3: Nomenclature for the wake shedding procedure at a typical trailing-edge panel. Illustration from [1].

In the case of a flat wake, all the wake rings are simply transported with the flow in straight line and therefore no further computations are required.

If a free wake model is chosen, the newly shed rings are liberated at each time step as already explained but the previously shed rings are deformed with respect to the local flow (wake roll-up). This procedure leads to a wake shape closer to

the reality but is extremely time consuming, as more and more rings have to be deformed when the wake grows.

The position of the four corner of each ring is given by

$$x_v^{n+1} = x_v^n + \int_{t_n}^{t_{n+1}} \mathbf{u}(t) \, \mathrm{d}t \tag{2.8}$$

with $\mathbf{u}(t)$ the velocity of the fluid at the corner. This velocity is computed just like the one at the collocation points:

$$\mathbf{u}(t) = A_{cb}\mathbf{\Gamma}_b + A_{cw}\mathbf{\Gamma}_w + \mathbf{U}_\infty \tag{2.9}$$

Finally, using the impermeability condition and the equations for the wake, all elements of the problem are known except for the strength of the bound vortices. Starting from a differential problem, the system is now made of simple algebraic equations where the only unknown is $\mathbf{\Gamma}_b$. This system can be solved really quickly and efficiently using numerical tools.

2.4 Aerodynamic loads

Once the velocity and the vorticity fields have been determined, the aerodynamic loads must be calculated. This thesis will focus on two different methods to compute them: the *Katz* method based on Bernoulli's equations and the *Joukowski* method based on the theory of circulatory forces.

2.4.1 Joukowski method

In order to capture efficiently the effects of leading-edge suction, the contribution of all bound vortices must be included. The total force can be divided in two parts: (quasi)steady and unsteady.

The steady contribution of one vortex segment is calculated simply with the Joukowski theorem as

$$\delta\mathbf{F}^{\mathrm{st}} = \rho\Gamma_{\delta l}(\mathbf{U} \times \delta\mathbf{l}) \tag{2.10}$$

with $\delta\mathbf{l}$ the vortex segment, $\mathbf{U}$ the local flow velocity taken at the middle of the segment $\delta\mathbf{l}$ and $\Gamma_{\delta l}$ the circulation of that segment.

In order to lower the number of computation, some twisting was done to this formula. In most of the cases each segment is counted twice: one time for each ring it delimits. For example, the leading segment of the panel (i, j) is also the trailing segment of panel $(i - 1, j)$. Due to the right-hand rule used for the definition of the vortex segments, it is counted in opposite direction if it is the leading edge of panel (i, j) or the trailing edge of panel $(i - 1, j)$. But while the circulation of the segment is different for both panel (respectively $\Gamma_{i,j}$ or $\Gamma_{i-1,j}$), the local velocity computed in the middle of the segment is the same for both panels. So, in order to compute the velocity only once, this segment will only be counted as the leading

edge of panel (i, j), but with a net circulation $\Gamma_{i,j} - \Gamma_{i-1,j}$. And it will not be counted as the trailing segment for the panel $(i - 1, j)$. The same reasoning can be applied for the left and right segments instead of leading and trailing segments. In the end, only the leading and the left segments will be computed for each panels, but with their net circulation, respectively $\Gamma_{i,j} - \Gamma_{i-1,j}$ and $\Gamma_{i,j} - \Gamma_{i,j-1}$.

Obviously, a special treatment should be reserved for the borders of the wings. In the case of the leading segment of the leading edge panels, the net circulation is only $\Gamma_{i,j}$. The same goes for the left segment at the left wing tip. For the right wing tip panels, the circulation of the right segment must be taken into account (as it is not shared with any other ring). And finally, the trailing segment of the trailing edge panel is taken into account in the trailing bound vortex ring with a circulation strength equal to $\Gamma_{\delta l} = \Gamma_{ij} - \Gamma_{1,j}^{wake}$.

This procedure is equivalent to the one described rigorously in Eq. 2.10, however it allows to compute the velocity only at two points for each panel instead of four (except for the panels at the border of the wing).

Note that the impermeability condition is imposed at the collocation points only, so $\mathbf{U} \times \delta\mathbf{l}$ does not necessarily act along the normal of the panel.

The unsteady contribution rises from the unsteady part of Bernoulli's equation and acts along the normal of each vortex ring panel. Therefore it can be expressed simply as

$$\mathbf{F}_{ij}^{\text{unst}} = \rho \frac{\partial \Gamma_{ij}}{\partial t} S_{ij} \mathbf{n}_{ij} \tag{2.11}$$

With Γ_{ij} the circulation strength of the panel. Finally the total force contribution from each panel is

$$\mathbf{F}_{ij}^{\text{tot}} = \sum_{\delta\mathbf{l}} \delta\mathbf{F}^{\text{st}} + \mathbf{F}_{ij}^{\text{unst}} \tag{2.12}$$

2.4.2   Katz method

This method was developed by Katz and Plotkin in [1]. Here, the unsteady Bernoulli's equations are applied in order to determine the pressure jump across each panel:

$$\Delta p_{ij} = \rho \left((\mathbf{U}_{ij}^m + \mathbf{U}_{ij}^w).\boldsymbol{\tau}_{ij}^c \frac{\Gamma_{ij} - \Gamma_{i-1,j}}{\Delta c_{ij}} + (\mathbf{U}_{ij}^m + \mathbf{U}_{ij}^w).\boldsymbol{\tau}_{ij}^s \frac{\Gamma_{ij} - \Gamma_{i,j-1}}{\Delta b_{ij}} + \frac{\partial \Gamma_{ij}}{\partial t} \right) \tag{2.13}$$

where $\mathbf{U}_{ij}^m$ is the velocity due to the surface motion (relative inertial velocity) and $\mathbf{U}_{ij}^w$ is the velocity due to the wake vorticity, all taken at the panel collocation point. The bound vorticity contribution is approximated by the gradient of circulation along the direction of the panel tangential vectors $\boldsymbol{\tau}_{ij}^c$ and $\boldsymbol{\tau}_{ij}^s$, respectively for chordwise (Δc_{ij}) and spanwise (Δb_{ij}) directions.

Using this pressure jump, the lift can be easily computed with:

$$\Delta L_{ij} = \Delta p_{ij} S_{ij} \cos(\alpha_{ij}) \tag{2.14}$$

with S_{ij} the surface of the panel and α_{ij} its angle of attack.

This procedure leads to some problems since it does not account leading-edge suction force. The lifting properties will be in general well predicted but the induced drag will be overestimated.

Thus, Katz and Plotkin introduce a correction for the induced drag using the component of downwash that acts along the local lift vector:

$$\Delta D_{ij} = \rho \left((\mathbf{U}_{ij}^{bc} + \mathbf{U}_{ij}^{w}).(P_{\widehat{\mathbf{U}}_{ij}^m}\mathbf{n}_{ij})(\Gamma_{ij} - \Gamma_{i-1,j})\Delta b_{ij} + \frac{\partial \Gamma_{ij}}{\partial t} S_{ij}\sin(\alpha_{ij}) \right) \quad (2.15)$$

with $\mathbf{U}_{ij}^{bc}$ the velocity calculated considering only the bound chordwise vortices and $\mathbf{U}_{ij}^{w}$ the velocity due to the wake vorticity. The second term simply accounts for the acceleration of the fluid. The term $(P_{\widehat{\mathbf{U}}_{ij}^m}\mathbf{n}_{ij})$ is an orthogonal projection of the normal to the panel in the plane of the flow and therefore it ensures that only the downwash component of the velocities is taken. The projection operator is defined as $P_{\widehat{\mathbf{U}}_{ij}^m} = I - \widehat{\mathbf{U}}_{ij}^m\widehat{\mathbf{U}}_{ij}^{m^T}$, where the unit vector $\widehat{\mathbf{U}}$ describes the direction of the local flow velocity.

Finally, the total aerodynamic load applied to each panel is

$$\mathbf{F}_{ij} = \Delta D_{ij}\widehat{\mathbf{U}}_{ij}^m + \Delta L_{ij}(P_{\widehat{\mathbf{U}}_{ij}^m}\mathbf{n}_{ij}) \quad (2.16)$$

2.4.3   Comments on the methods

It is obvious that the procedure used by Katz is more complex than the one used for Joukowski. Moreover, only the chordwise-oriented vorticity of the bound segment is taken into account in the drag computation. Also, the leading-edge suction and therefore the drag is computed using an approximation of velocities at the collocation points and not directly on the vortex segments.

All of these introduce approximations errors and therefore the result found may be not as good as the one obtained using Joukowski. Finally the Katz method is based on a small angle assumption for the angle of attack and may show some discrepancies in pure flapping and pitch lagging cases, or at least diverge from the experiment results sooner than the Joukowski's solution (where there is no assumption regarding the angle of attack).

One of the main drawback of the Joukowski solution is that the velocity has to be computed at four points for each ring instead of only one for Katz. It is possible to reduce the number of computation as some points are shared by different panels, but still the total number of points is higher than the number of collocation points. This will result in a larger computational time compared to the Katz method.

2.5   UVLM for systems of multiple bodies

The configuration studied in Chapter 4 consists of two separate wings, where each of these sheds a different wake. Therefore, for multiple bodies system, the computation process for the velocity and vorticity fields must be adapted.

Especially, in order to compute the vorticity at one point, the impact of all the wings and all the wakes should be taken into account.

For instance, in a single body system, the A_{cb} matrix accounts for the influences of the wing over itself. In a two wings system, the A_{cb} matrix is made of influences from wing 1 over itself, wing 1 over wing 2, wing 2 over wing 1 and wing 2 over itself. The same principle accounts for the wake influences.

Thus, for n different bodies, the total number of computation is increased by a factor n^2.

2.6 Matlab implementation

The code used for the resolution of all the geometries studied here is largely based on the one developed by G. Dimitriadis for the simulation of bird flapping [10].

This original code was designed to compute the loads applied during the motion of one symmetrical wing using the Katz method.

Therefore, it had to be adapted for this thesis in order to take into account systems of multiple wings and to compute the aerodynamic loads using the Joukowski method in parallel of the Katz. The computation of the loads with the two methods is done in the same code to take advantage of the fact that the firsts steps (definition of the wings, enforcement of boundary conditions, computation of velocities and vorticities, shedding of the wake,...) are shared by both methods. This will reduce consequently the total time needed to find the solution.

The first step of the calculation consists in determining the position of the wing for the current time step. As the wing is rigid, its position is entirely determined by the position of its four corner points. The wing is then divided into panels that match the imposed discretisation. In the case of a two wings system (as the one studied in Chapter 4), the second wing and its panels are simply construed by symmetry of the first one.

The next step consists in the definition of the vortex rings applied to each panel using the position of the panels' corner points. The mid position of each vortex segment is also calculated (as it is required for Joukowski method). For each vortex ring the collocation point is computed and the normal and tangential vectors are calculated along with the panel area.

The latest vortex ring is then shed in the wake. Note that in the case of a two wings system, all these steps need to be done for each wing.

Both influences matrices can now be computed and the external velocities **w** are calculated. As explained in the previous section, in case of a two wing system, the influences matrices need to account for the effect of each element on the others. Knowing the values of the wake vorticities for the previous time step, the velocities induced by the wake can be computed at the collocation points and also at the mid point of each vortex segment (for the Joukowski method). All these data allow the calculation of the bound vorticities by enforcing the impermeability condition at the collocation points (Eq. 2.3). Finally the velocities due to the wing vorticity are computed at each collocation point and at the mid point of each vortex segment.

At this point everything is known and the calculation of aerodynamic loads can be addressed.

For the Katz method, the length of the bound vortices (Δc_{ij} and Δb_{ij}) must be calculated for each panel along with the projection operator $P_{\widehat{\mathbf{U}}_{ij}^m}$. Finally, the rate of change of vortex strengths on the wing panels is computed as

$$\frac{\partial \Gamma_{ij}}{\partial t} = \frac{\Gamma_{ij}^t - \Gamma_{ij}^{t-\Delta t}}{\Delta t} \tag{2.17}$$

Once all these are known, the pressure drop can be found using Eq. (2.13) and the induced drag correction is found with Eq. (2.15). Finally the total lift and drag are found with the projections of Eq. (2.16) in the right directions.

For Joukowski method, the vortex filament vectors are determined using the corner points of the vortex ring. The two components of the total force are simply computed using Eqs. (2.10) and (2.11). Note that the local flow velocity $\mathbf{U}$ used in Eq. (2.10) is the flow velocity calculated at the mid point of the vortex segment and not at the collocation point.

Finally, the entire wake is propagated and the position of the wake corners are calculated with respect to the wake model used (flat or free wake).

All the previous steps are then repeated for each time step, until the limit number of periods is reached (or until the wake is long enough in the steady cases). Once the loads are known for each panel at each time step, the total forces acting on the whole wing can be calculated for each time step.

Chapter 3

Test cases

This section will focus on the study of simple test cases. The methodology presented by Simpson *et al.* [4] will be reproduced for flat plates but also extended to different cambered airfoils. Three different airfoils will be studied here: NACA 0012, NACA 2412 and NACA 6409. These are the airfoils analysed by Abdul Razak in [2], and therefore the ones that will be used in the analysis of flapping flight in Chapter 4.
Note that as the resolution of the UVLM will be made accordingly to the thin airfoil theory, the NACA 0012 can be assimilated to a flat plate in this chapter.

First, a study of the steady case will be done in 2D for all airfoils. This study will be followed by the solution over finite wings. After, both 2D and 3D cases will be investigated for pure harmonic pitching and plunging motions. And finally, this chapter will be concluded by a small study of the wake parameters.

3.1 Discretisation of the problem

3.1.1 Spatial discretisation

This section addresses the study of one wing at a time. For each case, the wing used is perfectly rectangular, with no dihedral, taper, sweep or twist. Moreover, all the wings have the same dimensions; they only differ from each other because of their camber.

The paneling of the wing is made so that the chordwise panels have all the same length. The number of chordwise panels will be denoted M.
For the spanwise discretisation of finite wings, the panels are smaller at wing tip than at the center of the wing in order to detect more effectively the effects of the tip vortices on the drag. The number of spanwise panels will be noted N.
The Fig. 3.1 represents a zoom on a typical finite wing discretisation with the vortex rings and the collocation points associated with each panels.

In order to compute 2D problems with the UVLM — which is a 3D method — the wing will be modeled with an extremely large aspect ratio; this will ensure
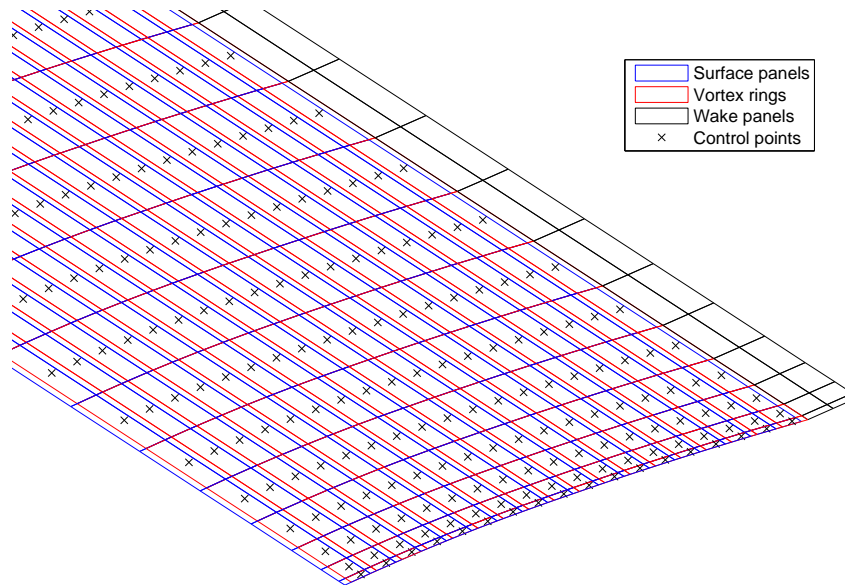
FIGURE 3.1: Surface and wake panels, vortex rings and collocation points.
3D wing - NACA 2412, $M = 18$, $N = 24$

that the wing tip effects remain negligible, and therefore the problem will be approximately 2D. Moreover, for a 2D model, there is no spanwise discretisation ($N = 1$).

For this specific chapter, the same dimensions and discretisation are used for all the wings, depending of the geometry of the problem (2D or 3D). These parameters are summed in Table 3.1.

	Chord [m]	**Span** [m]	**M** [-]	**N** [-]
2D	1	4000	18	1
3D	1	4	18	24

TABLE 3.1: Dimensions and discretisations of the wings for 2D and 3D geometries.

3.1.2 Time discretisation

In all the cases, the three same movements will be studied. In order to make valid comparisons nondimensional units must be used.
The nondimensional time is expressed as $s = U_\infty t / b$, and the reduced frequency is defined as $k = \omega b / U_\infty$.
For the UVLM it is practical to use also a nondimensional time step $\Delta t U_\infty / c$. With this definition and knowing that the chord is divided into M panels, the

time step can be set as

$$\frac{\Delta t U_\infty}{c} = \frac{1}{M} \tag{3.1}$$

Using this specific time step will ensure that the wake panels have the same area than the trailing edge panels from which they are shed. The drawback of this nondimensional time step is that the computational cost will increase dramatically with the number of chordwise panels, as not only the wing's discretisation will be finer, but also the wake's.

3.1.3 Wake modeling

In all the following simulations the flat wake model is used due to the rapidity of its computation. Furthermore, as stated in the previous chapter (Section 2.3), the first wake vortex segment will be placed at $0.25\,\mathbf{U}_\infty(t)\Delta t$ aft of the wing's trailing edge. The influence of these two parameters will be studied later in Section 3.6.

3.2 Kinematics

For the steady configuration, the airfoil will simply remain at a given angle of attack until the wake grows to 10 times the chord length (to ensure a perfectly steady flow on the airfoil during the last time steps). The aerodynamic loads will then be taken as the values of lift and drag at the last time step.

The plunging motion will be imposed in the form of an harmonic oscillation of amplitude $h = \overline{h}\cos(ks)$. The computation will be made over several periods, and only the results of the last one will be taken into account; once again this is done to ensure that the flow is fully stabilised during this last period.

The pitching motion will be imposed as an harmonic oscillation of the pitching angle $\alpha_p = \overline{\alpha}_p \sin(ks)$. Here again, the computations will be made over multiple periods and only the last one will be taken into account.

3.3 Steady solutions

This section addresses the analysis of the steady results obtained with the three different profiles for airfoils (2D) and finite wings (3D) cases. The computations have been made for various angles of attack ranging from -5 deg to +5 deg. These values for the angle of attack guarantee the validity of the UVLM results, as the flow is considered to remain attached at all time.

In order to simplify the comparisons, all the results of this thesis are represented in terms of sectional lift and drag coefficients. These coefficients are defined

as

$$C_d = \frac{\text{Drag}}{\frac{1}{2}\rho_\infty U_\infty^2 S} \tag{3.2}$$

$$C_l = \frac{\text{Lift}}{\frac{1}{2}\rho_\infty U_\infty^2 S} \tag{3.3}$$

where "Drag" and "Lift" are the total values of the drag and lift over the wing, ρ_∞ is the density of the freestream (considered equal to the density over the surface in incompressible flows), U_∞ is the airspeed and S is the total area of the wing.

3.3.1 Steady airfoils

Results

The results are presented in Fig. 3.2 for the sectional drag and lift coefficients of all the three airfoils.

The first thing to notice is that in all the cases, the differences between the two methods are negligible. This result was expected as the methods main difference lies in the computation of drag, yet in a 2D steady inviscid case the drag should be zero.

A more surprising result is that the drag is actually different from zero for all the airfoils. That is a clear violation of d'Alembert's paradox which states that the drag should be non-existent for steady incompressible and inviscid potential flows. However, the drag observed in Fig. 3.2 is very small. In fact, this effect comes from one of the limitations of the UVLM. As mentioned previously, the UVLM is a 3D method, and some hypothesis were made in order to model 2D flows. The vortex lattice method computes always a small downwash (about 0.2 m/s here). Due to the extreme value of the aspect ratio (4000 in these cases), the induced drag is very small $O(10^{-3})$ but still non zero. In conclusion, the 3D effects can be minimised using a very high aspect ratio but they will never be completely eradicated.

The lift coefficient is plotted in comparison with results given by `XFoil` for a steady inviscid flow. The results of the UVLM for the NACA 0012 and 2412 match quite well the ones given by `XFoil`, while there is a larger difference in the case of the NACA 6409. It is interesting to notice that the lift computed with the UVLM matches exactly the one given from `XFoil` for the angle of attack corresponding to the absence of drag.
This discrepancies between the results of vortex lattice and `Xfoil` come from the fact that some drag is modeled by the vortex lattice method and therefore the lift is slightly diminished. Moreover, as the drag modeled by the UVLM is higher for the NACA 6409 it as a larger influence on the lift, which explains the greater difference between the UVLM and `XFoil` for this specific airfoil.
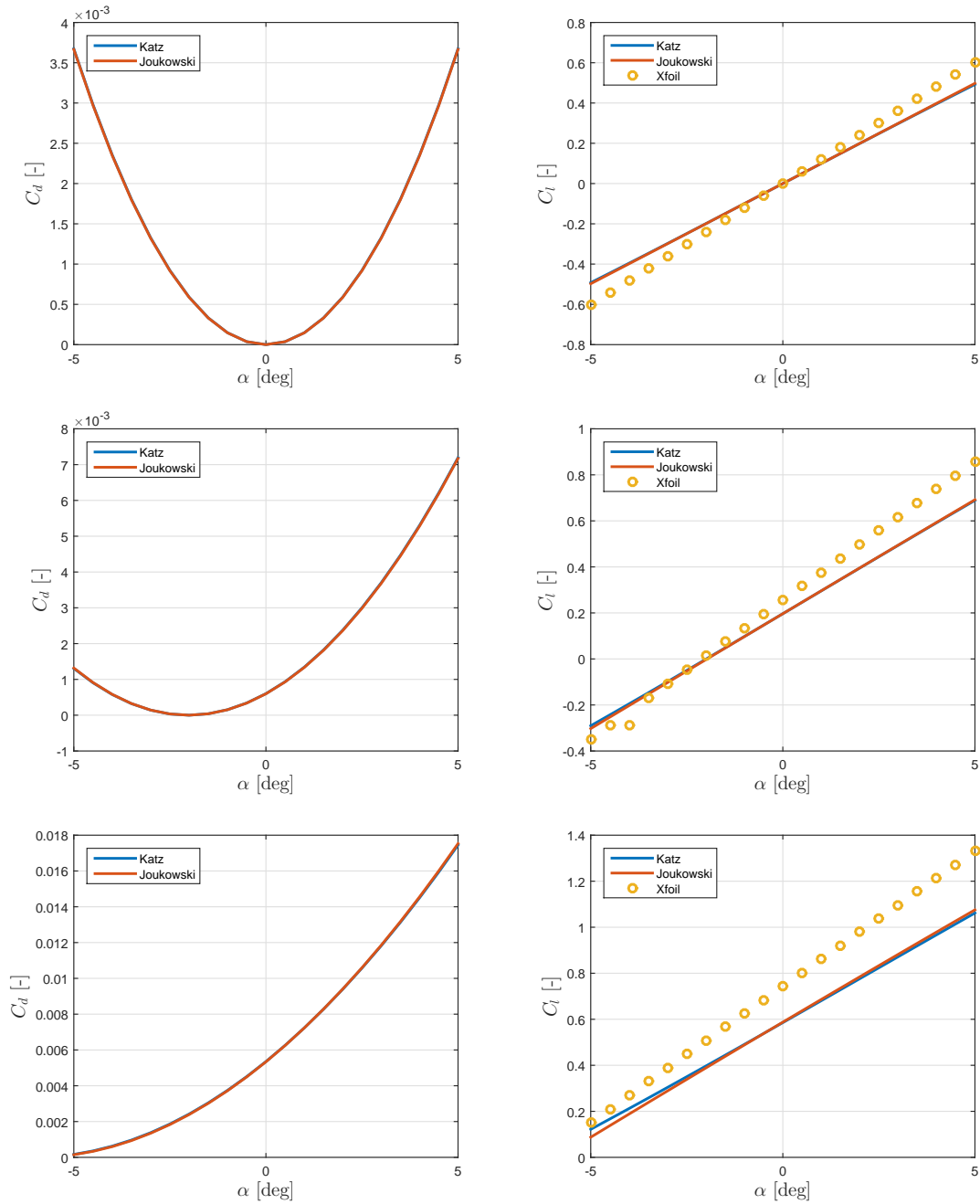
FIGURE 3.2: Drag and lift coefficients for steady NACA 0012 (top), 2412 (mid) and 6409 (bottom) airfoils – 2D.

Convergence

As the vortex lattice method fails to predict correctly the drag and also most of the lift, there is no point in studying the convergence for the steady 2D cases.

3.3.2   Steady finite wings

Results

The results for the sectional drag and lift coefficient of the three finite wings are presented in Fig. 3.3.
The aerodynamic coefficients have strictly the same shape that the ones of the 2D case, but this time the value of C_d is higher while the one of C_l is smaller. Unfortunately, `Xfoil` does not allow the modeling of finite wings, thus there is no available data for comparison.

However, it can be noticed that the drag modeled is slightly different from one method to another (especially for the most cambered airfoil), which was not the case for 2D airfoils. The differences between the two methods remain still negligible so that both methods can be considered equivalents for all types of steady wings (in 2D or 3D).

Convergence

A convergence study can be made for both methods. In this chapter, this exercise will be done with respect to the chordwise discretisation only. A more complete convergence study will be done later for the problem of two finite wings undergoing flapping and pitching motion.
The error made on any coefficient C_i is simply computed as

$$\text{error}_{C_i} = \left| \frac{C_i(M) - C_i(M-1)}{C_i(M)} \right| \times 100 \qquad [\%] \qquad (3.4)$$

with M the different chordwise discretisations tested.

The Fig. 3.4 shows the convergence study of Katz and Joukowski's methods in 3D for each NACA profile.
This convergence exercise is conducted on all the three profiles with an angle of attack fixed at $+4$ deg. The wings' geometry and discretisation (except for M obviously) used are still the same than in the previous exercise and are summed up in Table 3.1.

The first observation that can be done is that the lift convergence has almost the same shape for both methods with every profile. This is due to the fact that the lift computation is very similar from one method to another and they both give almost exactly the same results.
In all the cases the error on the lift coefficient is smaller than 1% with 18 chordwise panels or more. This means that, at least for the lift coefficient, the computation can be assumed converged with the discretisation used so far.
Note also that for the NACA 0012 airfoil, the error on the lift coefficient is always smaller than 1, which means that the lift could be considered as immediately converged in this case.
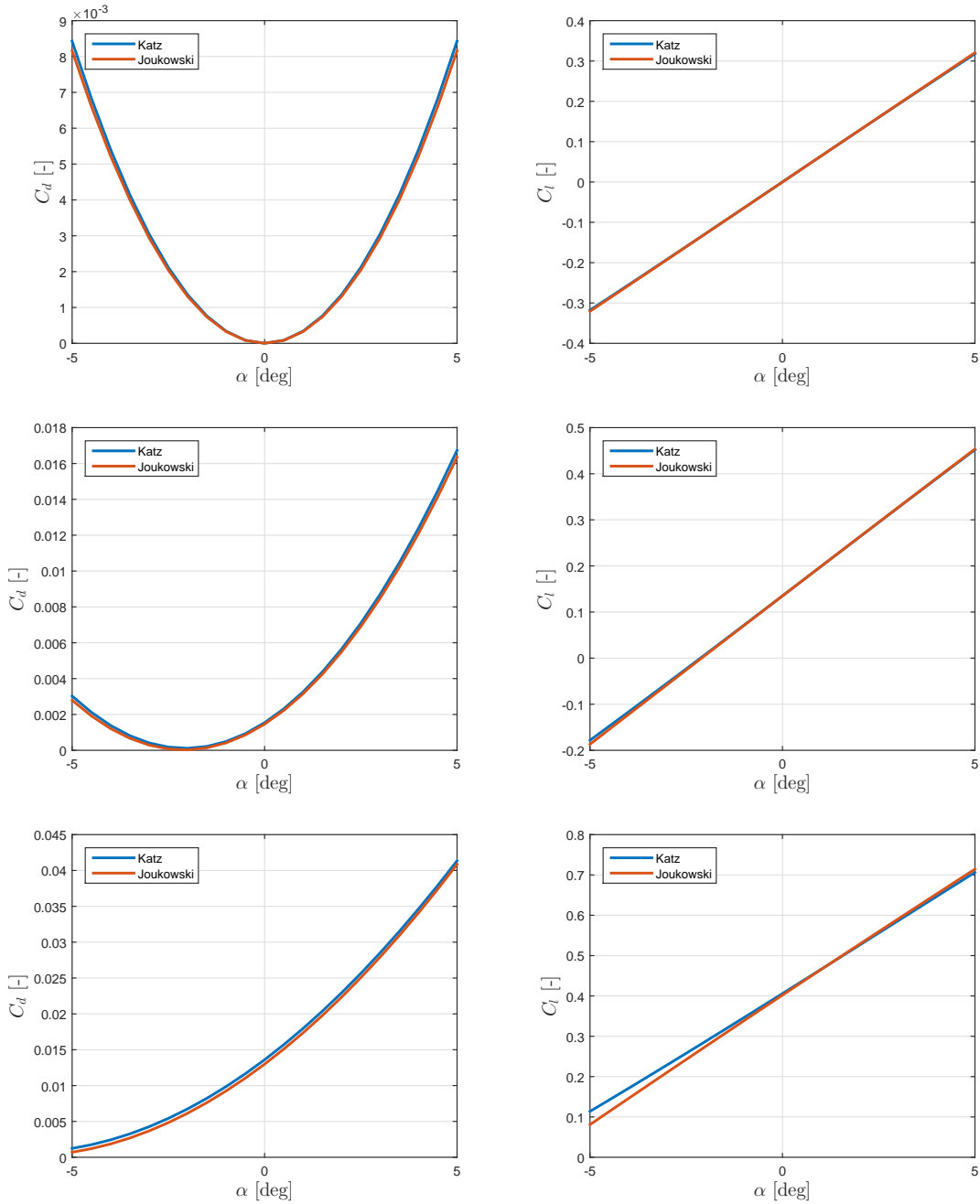
FIGURE 3.3: Drag and lift coefficient for steady NACA 0012 (top), 2412 (mid) and 6409 (bottom) finite wings – 3D.

For the drag coefficient, there is a very big difference in convergence between both methods. In particular for the flat plate (NACA 0012), it can be observed that the Joukowski method converges extremely quickly (instantly), while the Katz solution needs at least 14 chordwise panels to reach an error smaller than 2%. This is almost certainly due to the discretisation error incurred by calculating downwash at the collocation points [4].

For the cambered airfoils however, Katz method converges more rapidly than
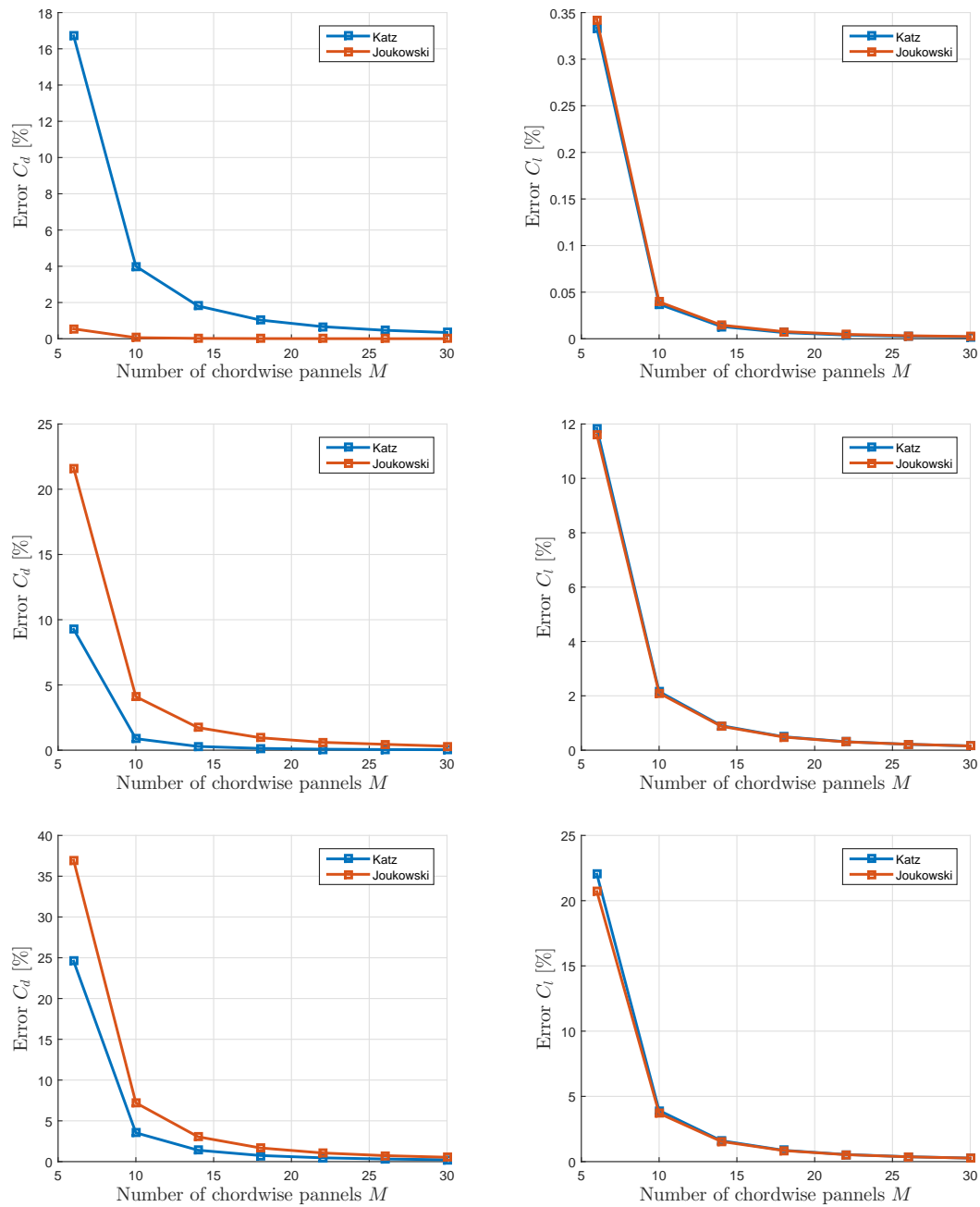
FIGURE 3.4: Convergence of sectional drag and lift coefficients for steady NACA
0012 (top), 2412 (mid) and 6409 (bottom) finite wings – 3D.

Joukowski's. Therefore a general conclusion for the convergence can not be deter-
mined with full certitude solely on the basis of these graphs.

3.4 Pitching and plunging airfoils

3.4.1 Symmetric airfoil: NACA 0012

As in the technical note of Simpson *et al.* [4], the solution obtained with both vortex lattice solutions will be compared to the one obtained using Garrick closed-form solution [5]. Note that the results given by these equations are only valid for flat plates and not for cambered airfoils.

Analytical solution

For the plunging motion described previously, Garrick's solution can be written in nondimensional form as [11]

$$C_d(s) = -2\pi k^2 \frac{\overline{h}^2}{b^2} \left[G(k)\cos(ks) + F(k)\sin(ks)\right]^2 \tag{3.5}$$

where C_d is the sectional drag as a function of the nondimensional time s.
$F(k)$ and $G(k)$ are the terms of the Theodorsen's function $C(k) = F(k) + iG(k)$.

For the pitching motion defined earlier, a center of rotation a must be defined. This parameter is nondimensionalised by the semichord and counted positive in the aft direction from the mid chord. The induced drag becomes then

$$C_d(s) = \alpha_p C_l(s) - C_s(s) \tag{3.6}$$

where the suction force coefficient $C_s(s)$ is

$$C_s(s) = \frac{\pi \overline{\alpha_p}^2}{2} \left[\Upsilon_1 \sin(ks) + \Upsilon_2 \cos(ks)\right]^2 \tag{3.7}$$

using

$$\begin{cases} \Upsilon_1 = 2\left[F(k) - kG(k)(\frac{1}{2} - a)\right] \\ \Upsilon_2 = 2\left[G(k) - kF(k)(\frac{1}{2} - a)\right] - k \end{cases} \tag{3.8}$$

and the lift coefficient in Eq.(3.6) is

$$\begin{aligned} C_l(s) = \pi\overline{\alpha_p}\Bigg[&k\cos(ks) + ak^2\sin(ks) \\ &+ 2F(k)\left(\sin(ks) + \left(\frac{1}{2} - a\right)k\cos(ks)\right) \\ &+ 2G(k)\left(\cos(ks) + \left(\frac{1}{2} - a\right)k\sin(ks)\right)\Bigg] \end{aligned} \tag{3.9}$$

The results computed using both Katz and Joukowski's methods are compared with the ones obtained with Eqs.(3.5) and (3.6) in Fig. 3.5 and 3.6. In these figures,

the aerodynamic coefficients are plotted against the kinematics for two reduced frequencies.

Note that in plunge, $\alpha_{\text{eff}} = \tan^{-1}\left[k(\overline{h}/b)\sin(ks)\right]$ with $(\overline{h}/b) = 0.1$. In pitch, $\overline{\alpha_p} = 4$ deg, and $a = -0.5$, which means that the pitching occurs around quarter chord.

Results

The results of plunging and pitching motion for the NACA 0012 airfoil can be found respectively in Fig. 3.5 and Fig. 3.6. Globally, there is a very good agreement between the UVLM and the linear theory.

(a) C_d at $k = 0.2$

(b) C_l at $k = 0.2$

(c) C_d at $k = 0.5$

(d) C_l at $k = 0.5$
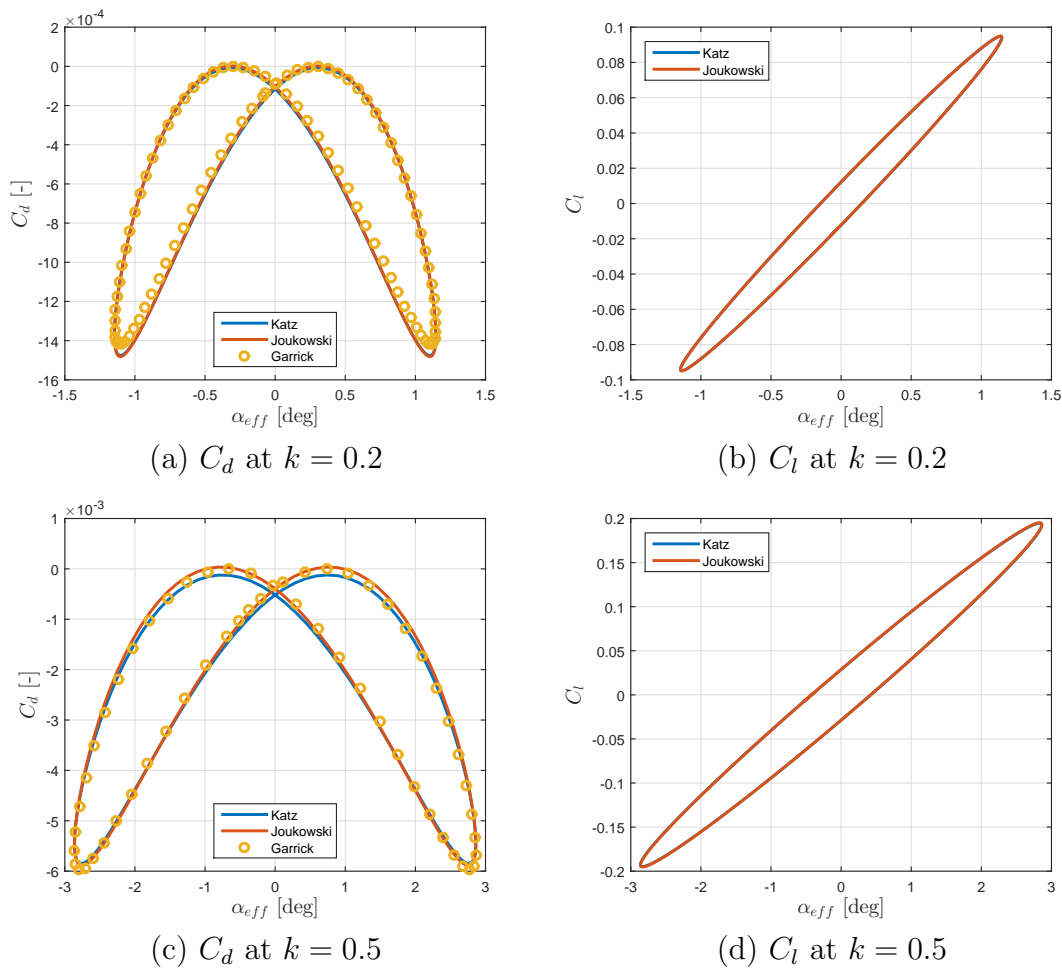
FIGURE 3.5: Drag and lift coefficients for a NACA 0012 airfoil in plunge – 2D.

The results concerning the pure harmonic plunging displacement in Fig. 3.5 show a good agreement between both vortex lattice results and the analytical solution, except for the case of plunging at $k = 0.5$ where there is a small difference at maximum drag. In this case, Joukowski's solution seems to be a little bit closer

to the analytical data.

The graphs representing the evolution of lift coefficient are exactly the same for both VLM solutions. This result was expected as the difference between these two methods lies mainly in the modeling of leading-edge suction effects and therefore the calculation of the drag. In this case, the drag is extremely small, but it is also almost exactly the same for the two different load computations. Therefore the lift appears to be exactly the same.

It is interesting to notice that, for the two reduced frequencies tested, the drag is always negative. This means that a net thrust is generated by the wing's motion at all time. Moreover, the mean lift is very close to 0, therefore this particular type of movement used along with flat plates is not suited for a real aircraft, as the lift will not be able to compensate the weight of the flapper.

In conclusion, for a flat plate in 2D undergoing harmonic plunge both methods give a similar solution. Furthermore, the solutions for the drag fit really well the analytical expectations.

The results obtained for the pure harmonic pitching are shown in Fig. 3.6. Once again, the two vortex lattice solutions are extremely close to each other,

(a) C_d at $k = 0.2$

(b) C_l at $k = 0.2$

(c) C_d at $k = 0.5$

(d) C_l at $k = 0.5$
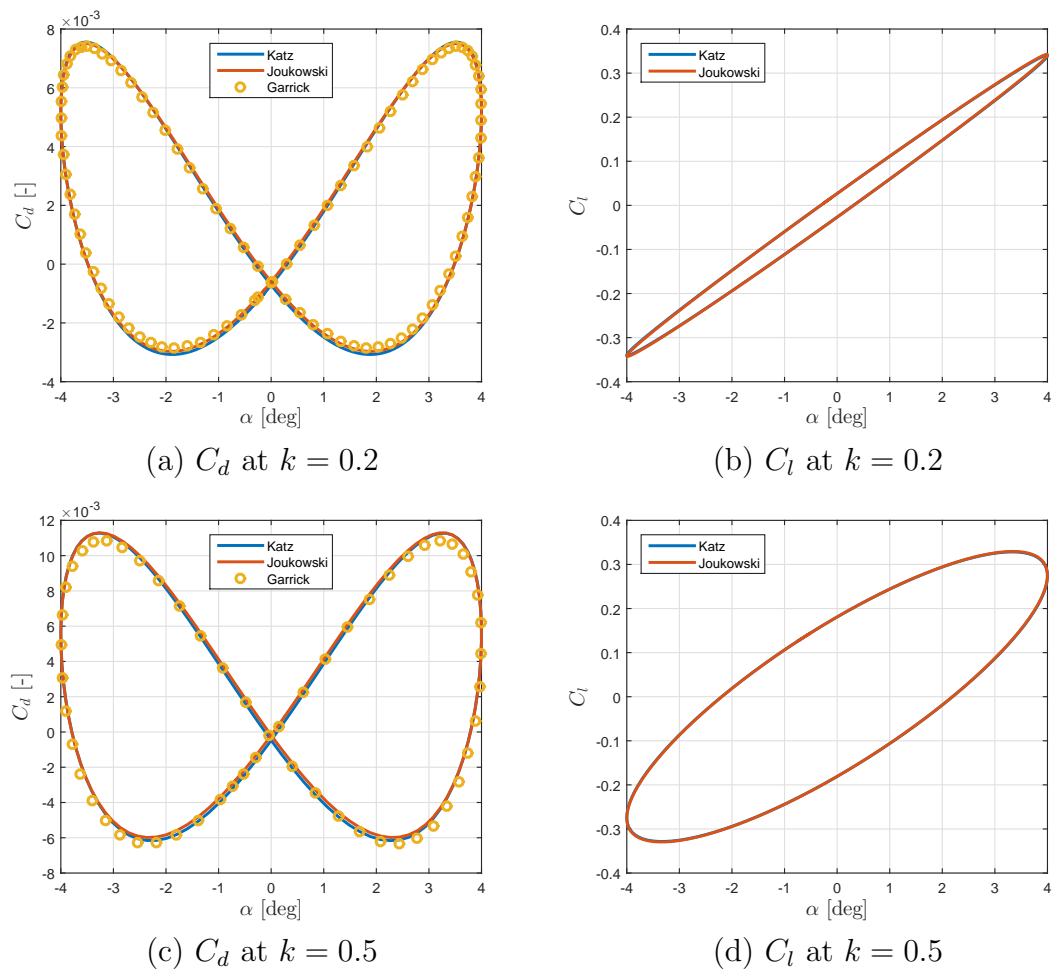
FIGURE 3.6: Drag and lift coefficients for of a NACA 0012 airfoil in pitch – 2D.

even closer than for the harmonic plunge.

The vortex lattice solutions match really well the analytical expectations for the drag. Just like for harmonic plunging, the lift coefficients given by both methods are exactly the same.

This time however, the wing produces some drag during the cycle. The net drag over the whole movement is positive, which means that this movement will not be able to propel any aircraft with a NACA 0012 wing by itself. In this case the net lift is also very close to 0.

Convergence

A convergence study can now be done for Katz and Joukowski methods. The convergence of each coefficient is computed using Eq. 3.4, except that the mean value of the coefficient over one period is taken into account instead of its value at the last time step. The results of the convergence analysis for the sectional drag and lift coefficients can be found in Fig. 3.7.

(a) Plunge, error$_{C_d}$

(b) Plunge, error$_{C_d}$

(c) Pitch, error$_{C_d}$

(d) Pitch, error$_{C_d}$
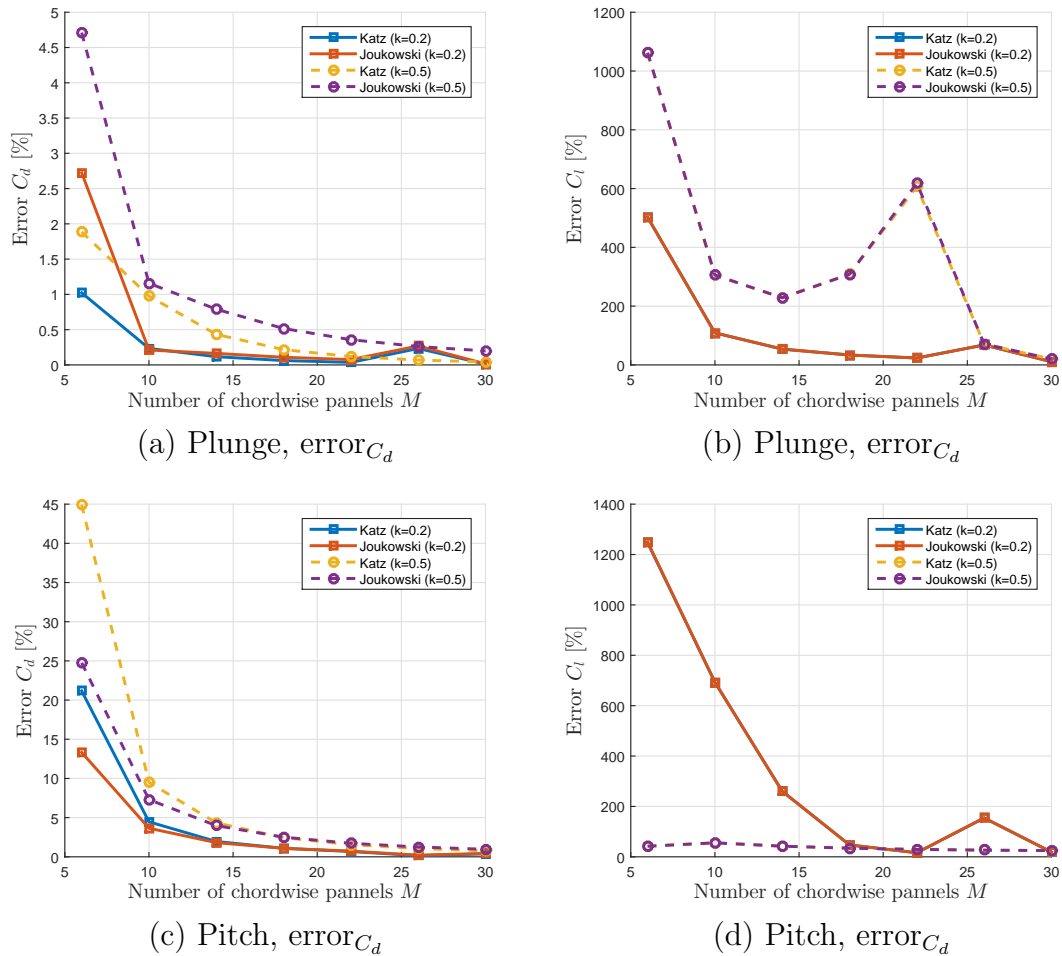
FIGURE 3.7: Convergence of drag and lift coefficients for of a NACA 0012 airfoil in plunge and in pitch – 2D.

The lift coefficient seems to follow an odd convergence scheme for both kinematics. This result is solely due to the very small value of the mean lift coefficient over one period, and the fact the the lift coefficient's sign changes from one discretisation to another. The Fig. 3.8 shows the actual value of the mean lift with respect to the chordwise discretisation. From the inspection of these graphs, it is clear that the results are well converged in reality (or almost converged for pitching with $k = 0.5$). Therefore, the odd aspect of the convergence graph is in fact solely due to analytical considerations.

Furthermore, the convergence of the lift is exactly the same for the two methods. This result was expected as the lift coefficients computed with each method have the exact same value.

(a) Plunge, C_l (b) Pitch, C_l
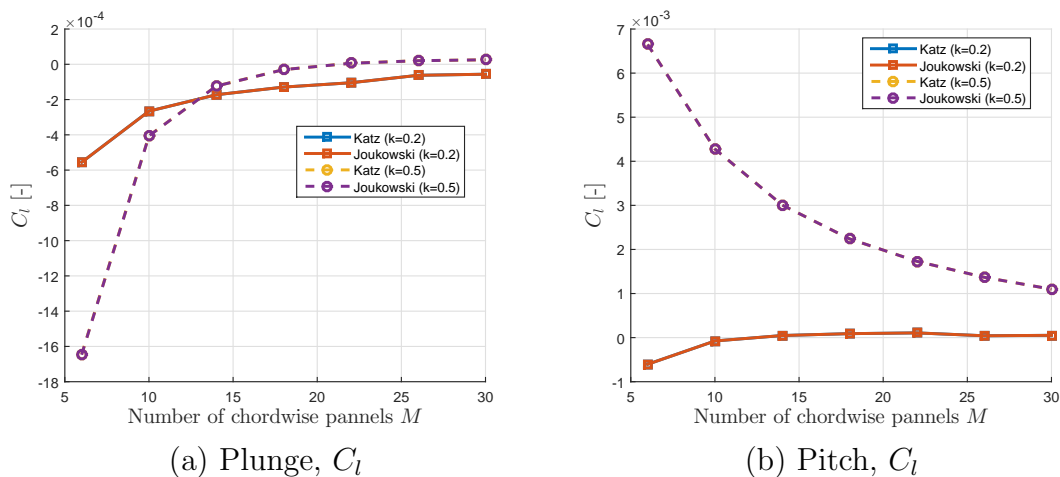
FIGURE 3.8: Evolution of mean lift coefficient with the chordwise discretisation for of a NACA 0012 airfoil in plunge and in pitch – 2D.

The drag coefficient shows a more classical convergence shape.

For the plunge, the Katz solution seems to converge faster than Joukowski's for both reduced frequencies. That result is in contradiction with the one presented in [4]. As a matter of fact, Simpson *et al.* computed the convergence of the drag in 2D using the result of Garrick's equations as the reference value for the drag:

$$\text{error} = \frac{\text{RMS}(C_{d_{\text{UVLM}}} - C_{d_{\text{Garrick}}})}{\max_t |C_{d_{\text{Garrick}}}|} \tag{3.10}$$

and as shown in Fig. 3.5, even if they are both really close to the analytical results, the Joukowski solution is a little bit more accurate. This leads to a smaller error with regard to the solution given by Garrick's equations.

Nonetheless, the error made on the drag coefficient in plunge is very small even for the coarsest discretisation. The value $M = 18$ used so far seems to be a good choice for the prediction of plunge.

For the drag computed for the pitching motion, the Joukowski method converges marginally faster than Katz. But for $M \geq 14$ the two methods are found to converge at the same rate. In the end, the error is smaller than 2% for $M = 18$,

which means that the value of M used so far is a good compromise between precision and computation time.

Note however that both method reach convergence (typically error $\leq 2\%$)for the same number of panels. So, none of them can be considered as better than the other in this case.

3.4.2 Cambered airfoil: NACA 6409

This section will focus on cambered airfoils in order to check if the previous conclusions are still valid for cases more complex than simple flat plates. This report will treat in detail the case of a NACA 6409 airfoil. The NACA 2412 was also studied but the results regarding this last airfoil are similar to the ones obtained for a NACA 6409, so only the convergence of the NACA 2412 coefficients will be discussed.

Results

As there is no empirical data available for cambered airfoils undergoing pure harmonic pitching and plunging motion, the validity of the model can not be concluded. Still, the results for the drag and lift coefficients are presented in Fig. 3.9 and 3.10 respectively for plunging and pitching at two different reduced frequencies; in order to see if there is any significant differences between the two models.

Once again, it is obvious that both methods give very similar results in all cases.
However, it is important to notice that the difference between the two methods is slightly larger than for a flat plate (especially for pitching at $k = 0.5$). This effect is due to the introduction of camber in the airfoil. The inspection of the results for a NACA 2412 (see Appendix A, Fig. A.1 and A.2) reveals that the difference between the methods increases with the camber of the airfoil. Moreover, this small difference tends to increase also with the reduced frequency.
Furthermore, the lift is no longer exactly the same for both methods, even though it remains really similar.

In plunge, this airfoil produces a net drag during the period when the reduced frequency $k = 0.2$. For higher reduced frequencies, the mean drag gets closer to 0. For both frequencies however, the mean lift is positive. This result is logical as the movement is of very small amplitude and quite low frequencies, so that the effective angle of attack α_{eff} remains small (and especially smaller to the zero-lift angle for a steady 6409 airfoil).

For the pitching motion, thrust is generated for a very small amount of time, and therefore a net drag is computed for the whole period. The thrust production seems however to be increased when the pitching frequency is increased. For too large values of k, the flow is expected to separate, leading to the generation of a

(a) C_d at $k = 0.2$ (b) C_l at $k = 0.2$

(c) C_d at $k = 0.5$ (d) C_l at $k = 0.5$
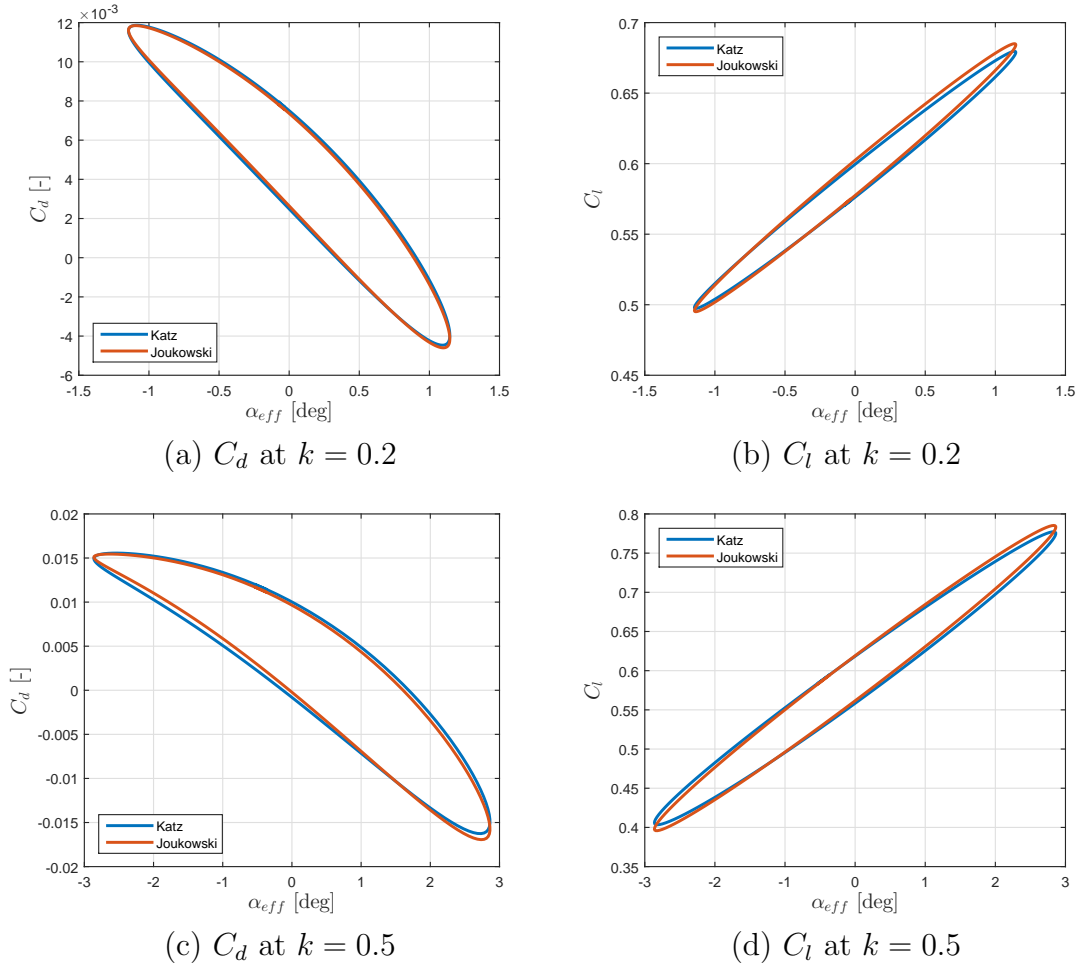
FIGURE 3.9: Drag and lift coefficients for a NACA 6409 airfoil in plunge – 2D.

significant amount of drag that could not be computed with the UVLM. Therefore it has no use to verify the behavior of the wing at $k \geq 0.5 - 0.6$ as the UVLM solutions will not reflect the reality.

Once again, the mean lift is always positive, which was expected as the pitching angle does not exceed -4 deg during its oscillations.

Convergence

Even though the validity of the methods can not be estimated due to the lack of experimental or analytical data for a comparison, a convergence study can be done on both methods. The results of the convergence of a NACA 6409 airfoil are shown in Fig. 3.11.

In all the graphs shown in Fig. 3.11 the convergence rates are very similar from one method to the other. For the lift coefficient, it is almost impossible to tell them apart.

However for the drag coefficient, Katz method shows a slightly better convergence

(a) C_d at $k = 0.2$ (b) C_l at $k = 0.2$

(c) C_d at $k = 0.5$ (d) C_l at $k = 0.5$
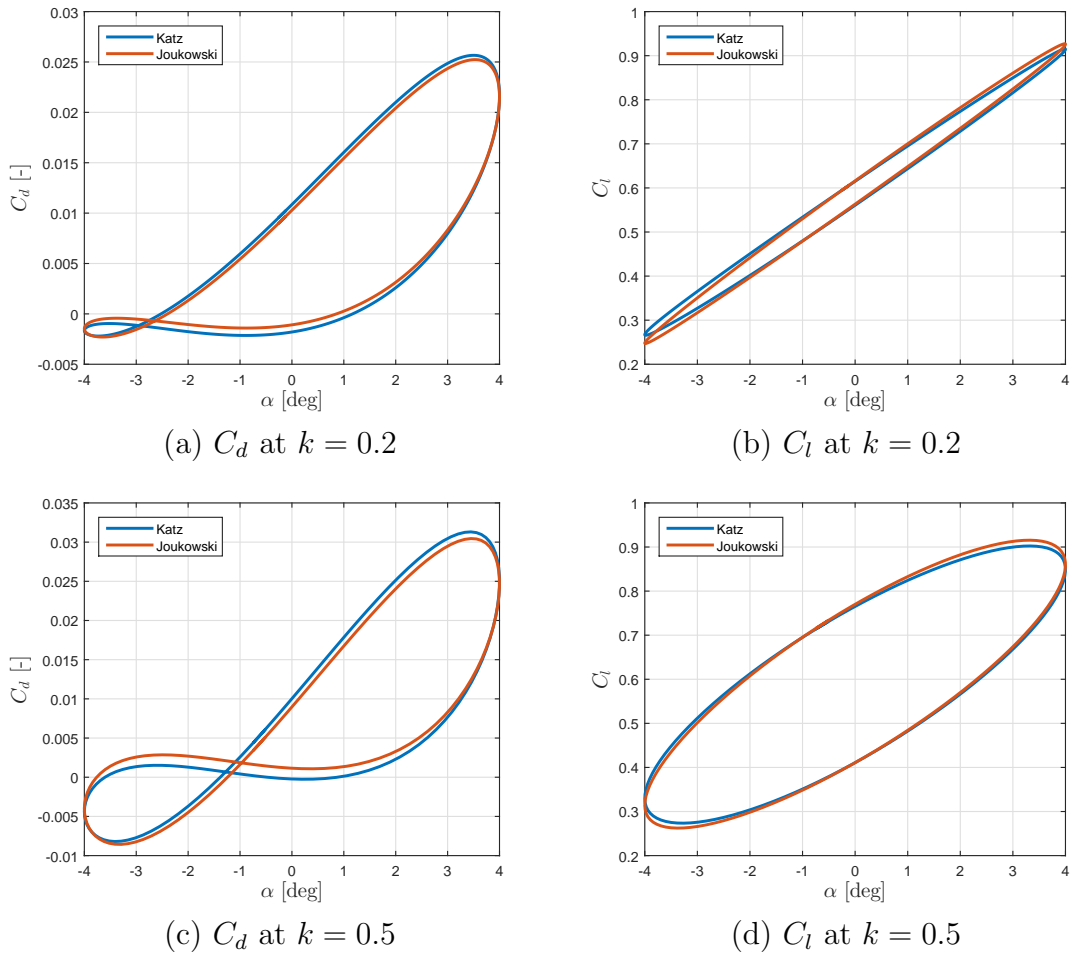
FIGURE 3.10: Drag and lift coefficients for a NACA 6409 airfoil in pitch – 2D.

than Joukowski's for the first discretisations. This is especially true in pitching for a large k, which was the case presenting the larger discrepancies between both results.

Note that for this airfoil, the lift convergence shows a much classical behavior than for the NACA 0012 because the mean lift computed for the NACA 6409 is always larger than 0 and is not close to it nor changes sign.

In all cases, $M = 18$ seems to be a good discretisation as the error on the coefficients is relatively small.
Note that even if Katz method converges a little bit faster than Joukowski for the first panels, they both reach an error smaller than 2% for the same discretisation, so in the end they need the same number of panel be considered as converged.

(a) Plunge, error$_{C_d}$

(b) Plunge, error$_{C_d}$

(c) Pitch, error$_{C_d}$

(d) Pitch, error$_{C_d}$
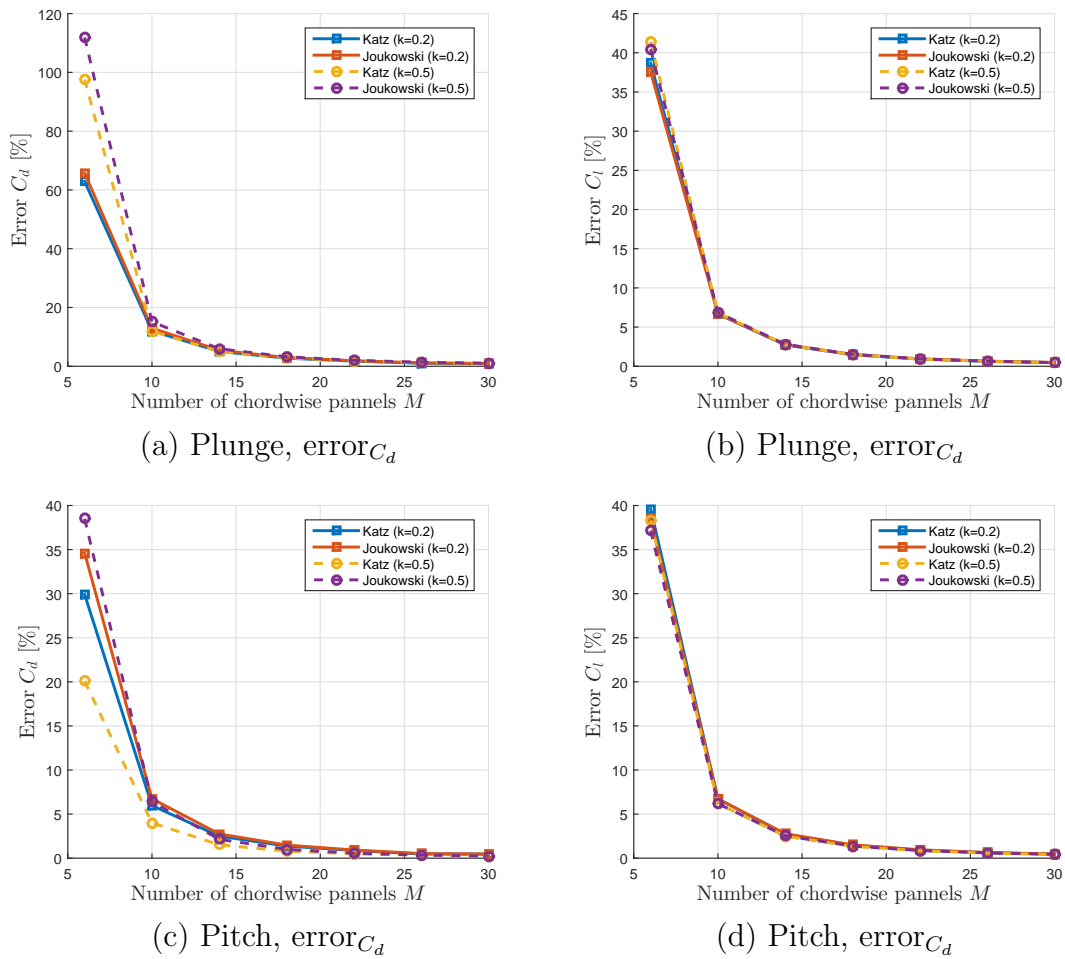
FIGURE 3.11: Convergence of drag and lift coefficients for of a NACA 6409 airfoil in plunge and in pitch – 2D.

3.4.3 Cambered airfoil: NACA 2412

Results

The results for this profile are redundant with the ones obtained for the NACA 6409. They will not be discussed in detail here. However, they can be found in Appendix A.

Convergence

Although the results for the NACA 2412 have not been discussed, the convergence can still be studied. The results are presented in Fig. 3.12.

For this airfoil, the convergence of the lift coefficient is once again exactly the same from one method to another, just like for the the airfoils. In this case also, the lift converges following a more regular pattern due to the fact that its mean

(a) Plunge, error$_{C_d}$

(b) Plunge, error$_{C_d}$

(c) Pitch, error$_{C_d}$

(d) Pitch, error$_{C_d}$
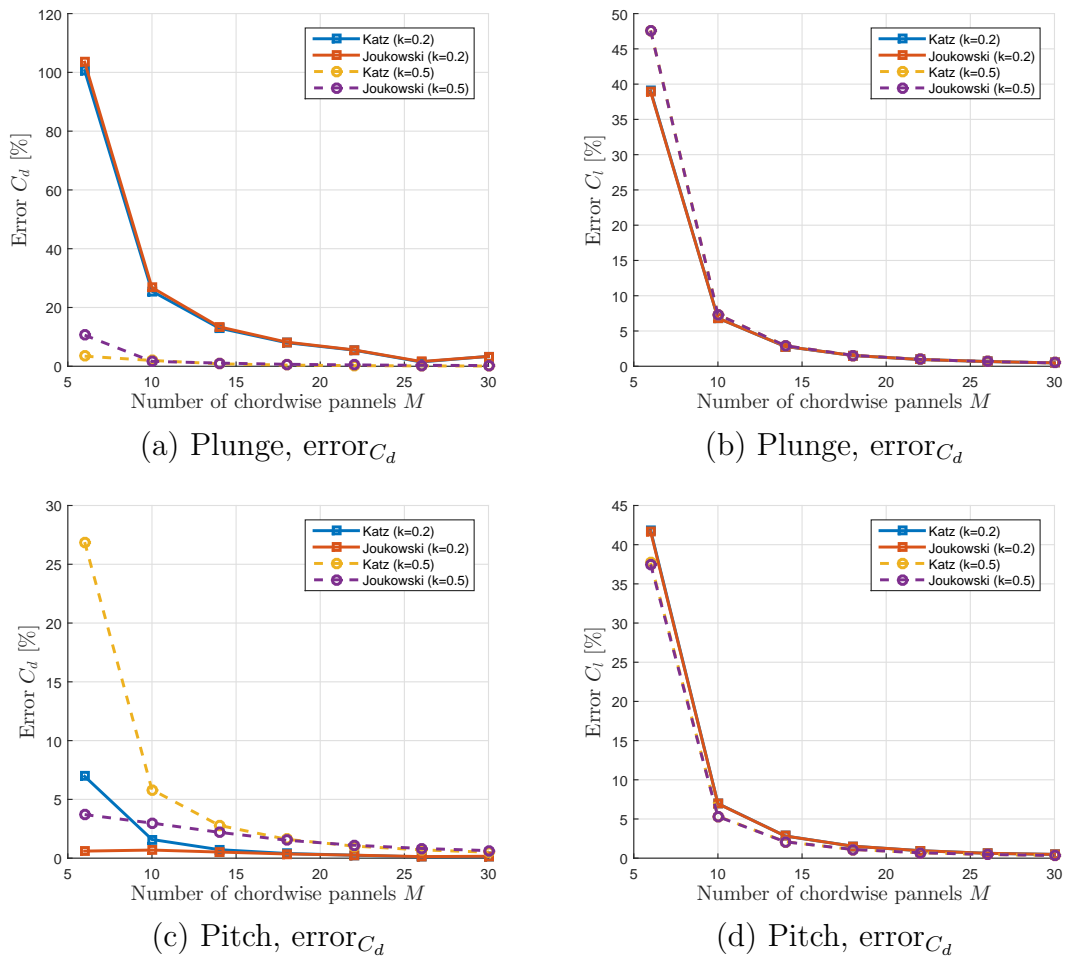
FIGURE 3.12: Convergence of drag and lift coefficients for of a NACA 2412 airfoil in plunge and in pitch – 2D.

value over one period is far enough from 0.

The drag convergence is here a little bit more similar to the results of the NACA 0012 than to the ones of the NACA 6409. Indeed, for the plunging motion, Katz method seems to converge a little bit faster than Joukowski. While for the pitching motion, the Joukowski method presents a small overhead.

Anyway, the choice of $M = 18$ for the chordwise discretisation seems to be a good choice, as usually the error made on the coefficients is smaller than 2% (except in plunge at $k = 0.2$).

Note that once again, both method reach convergence for the same discretisation.

3.5 Pitching and plunging of finite wings

3.5.1 Symmetric airfoil: NACA 0012

Results

The results produced for 3D cases are very close to the ones concerning the 2D cases, the only difference lies in the values taken by the coefficients, but the shape of their phase diagram remains the same. In order to lighten this report, only the convergence of the methods will be discussed for finite wings.

Convergence

The Fig. 3.13 shows the convergence of the drag and lift coefficient with respect to the chordwise paneling for a flat plate.

(a) Plunge, error$_{C_d}$

(b) Plunge, error$_{C_d}$

(c) Pitch, error$_{C_d}$

(d) Pitch, error$_{C_d}$
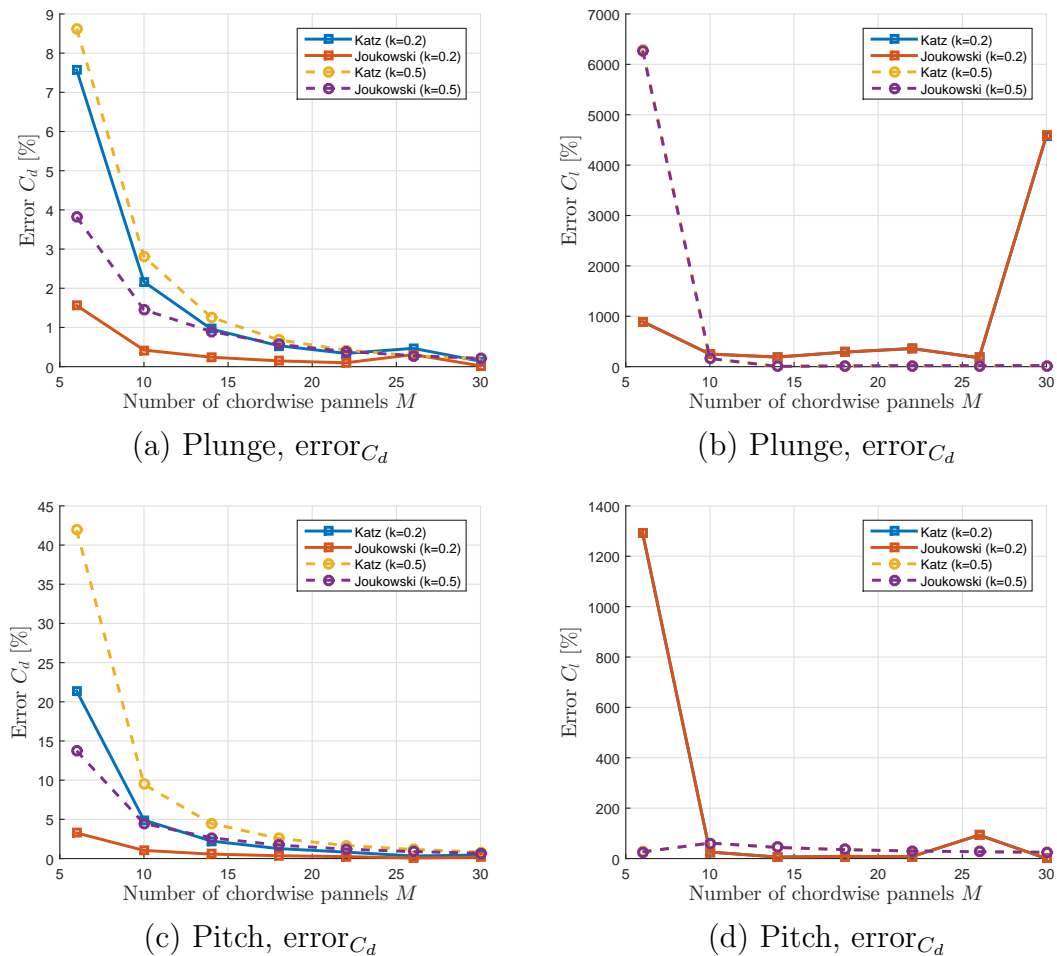
FIGURE 3.13: Convergence of drag and lift coefficients for of a NACA 0012 finite wing in plunge and in pitch – 3D.

The graphs obtained for the drag are quite different than the ones obtained for a 2D case (see Fig. 3.7). It clearly shows that the drag benefits from a really good convergence of the Joukowski method for both types of motion. This result is valid for all the reduced frequencies tested. Note that the same conclusion was already done for a steady NACA 0012 finite wing in Section 3.3.2.

As in the 2D case (see Fig. 3.7), the lift coefficient shows an odd convergence pattern. Once again, the values taken by the error are extremely high. This result is due to the fact that for 3D wings the mean lift is also very close to 0 and even changes sign with increasing M, which leads to the computation of excessive values. By observing the values of the mean lift coefficient with respect to the chordwise discretisation in Fig 3.14, one can see that the solution is in fact converged for $k = 0.2$ and the results observed in Fig. 3.13 are simply due to analytical properties (division by a number close to 0).

(a) Plunge, C_l (b) Pitch, C_l
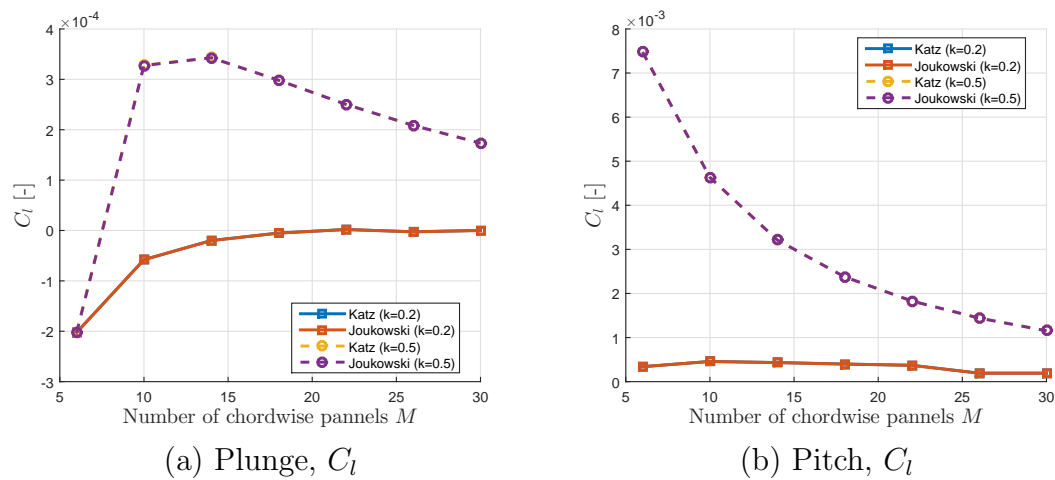
FIGURE 3.14: Evolution of mean lift coefficient with the chordwise discretisation for of a NACA 0012 finite wing in plunge and in pitch – 3D.

Note that the drag coefficient can be considered converged for $M \geq 18$ as the error in pitch and plunge are less than 2%.

3.5.2 Cambered airfoil: NACA 6409

Results

The results for a finite wing are once again very close to the ones observed for a 2D airfoil. Therefore, only the convergence will be studied for finite wings.

Convergence

The convergence of the aerodynamic coefficients with respect to the chordwise paneling is shown in Fig. 3.15 for the NACA 6409 finite wing.

(a) Plunge, error$_{C_d}$

(b) Plunge, error$_{C_d}$

(c) Pitch, error$_{C_d}$

(d) Pitch, error$_{C_d}$
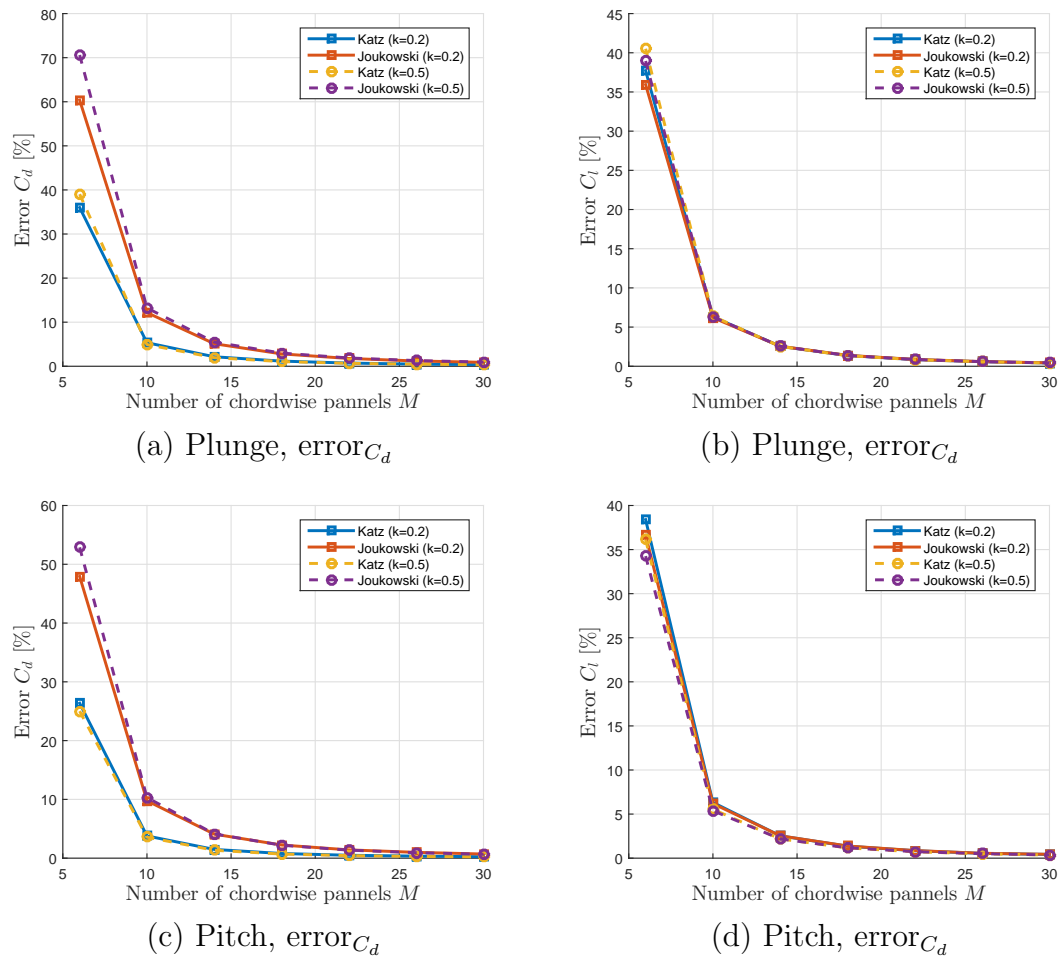
FIGURE 3.15: Convergence of drag and lift coefficients for of a NACA 6409 finite wing in plunge and in pitch – 3D.

First of all, in this case the lift converges following a more typical shape. It clearly shows that the convergence rate is the same for both method and is independent of the reduced frequency. This result traduces the fact that the lift coefficient is similar for both methods and evolves in the same way with the discretisation.

The drag convergence shows a very interesting behavior. First, for both kinematics, the Katz method converges faster than Joukowski's. Note that this behavior was already proven for the same wing in steady case (see Fig 3.4) but also for the 2D case (see Fig. 3.11),even though the difference was more marginal in 2D.
Also, it appears that the reduced frequency has very little influence on the convergence rate of each method.

Finally, convergence is said to be reach for $M \geq 18$ as the error is smaller than 2%.

3.5.3 Cambered airfoil: NACA 2412

Results

Once again, the results are very close to the ones obtained with the 2D airfoil. Therefore they are not discussed in this section.

Convergence

The Fig. 3.16 represents the convergence of drag and lift coefficients with respect to the chordwise discretisation of the NACA 2412 finite wing.

(a) Plunge, error$_{C_d}$ (b) Plunge, error$_{C_d}$

(c) Pitch, error$_{C_d}$ (d) Pitch, error$_{C_d}$
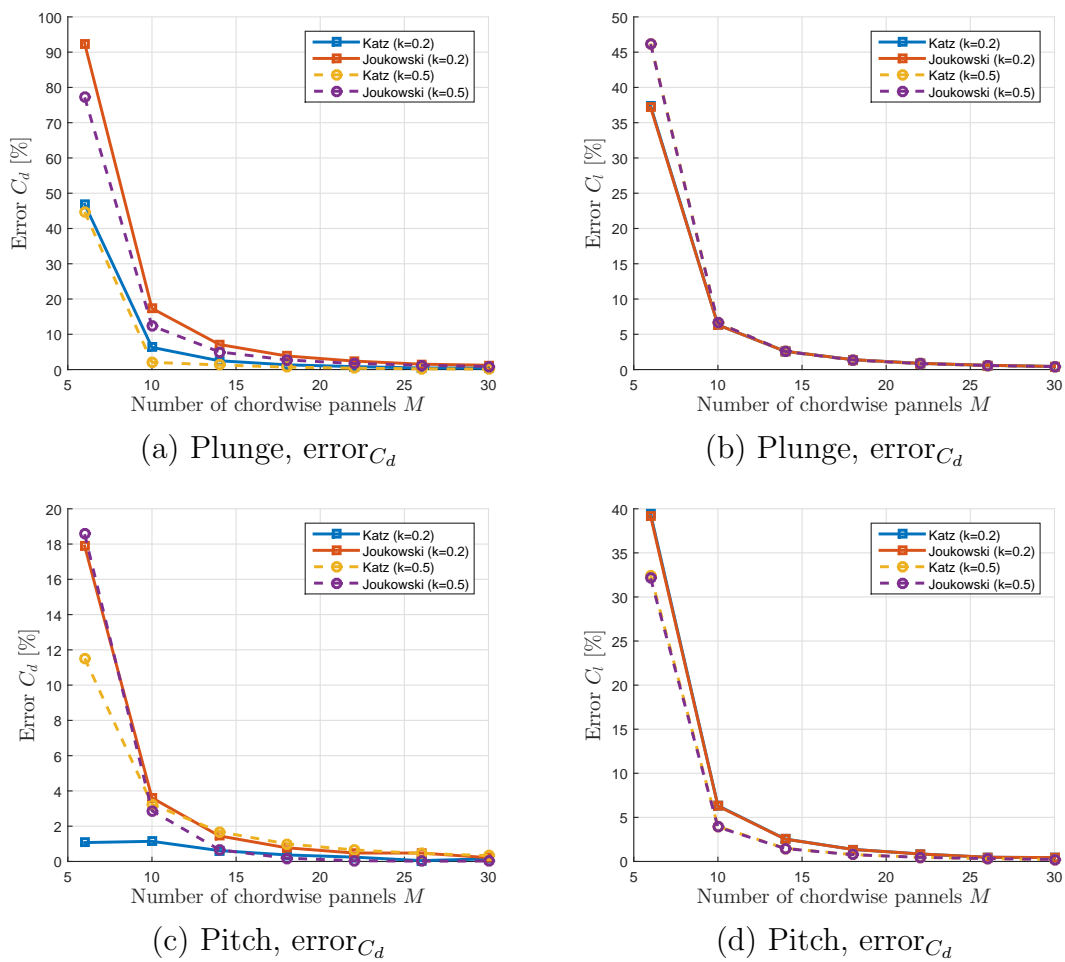
FIGURE 3.16: Convergence of drag and lift coefficients for of a NACA 2412 finite wing in plunge and in pitch – 3D.

The results are more or less similar than the ones obtained for the NACA 6409 finite wing.
First of all, the lift coefficient converges exactly at the same rate for both methods.

The convergence of the drag coefficient is a bit more complex. In plunge, Katz method shows a faster convergence than Joukowski for both reduced frequencies. As for the NACA 6409, the convergence rate is not impacted much by the modification of the reduced frequency.

In pitch, Katz methods converges almost immediately for the lower reduced frequency. But for $k = 0.5$, Joukowski's solution converges marginally faster than Katz's for $M \geq 10$.

Note that in steady case, the Katz solution was shown to converge faster than the one obtained with Joukowski (see Fig. 3.4).

3.6 Influence of wake parameters

3.6.1 Wake model

As explained before, two different wake models can be used : *free wake* or *flat wake*. Both models are investigated for a 3D NACA 2412 in pitching conditions.

The Fig. 3.17 represents the two wake shapes for a 3D NACA 2412 undergoing harmonic pitching motion. The amplitude of the pitch angle was set to $\overline{\alpha_p} = 8$ deg in order to show more easily the differences between the two wake models. Note that the colors only represent the vertical position of the wake.

As explained in Section 2.3, in a free wake model the wake simply moves with respect to the local flow velocity. This model shows really well the wake roll-up phenomenon and the real amplitude of the wake. The main drawback of this type of wake is that it is extremely time consuming (see Table.3.2). Note that the CPU time expressed in the table is the total time needed to compute the solution with both aerodynamic loads methods in parallel.

In the flat wake model, the wake is simply convected with the free stream and its shape does not vary with time.

	Flat wake CPU time [s]	Free wake CPU time [s]
Steady	226	898
Pitching	685	10541

TABLE 3.2: Computing time for free wake and flat wake models of a 3D NACA 2412 in steady and harmonic pitch. $M = 18$, $N = 24$.

The results for the lift and drag coefficients during the last period are compared for both wake models for an harmonic pitching in Fig. 3.18.

Note that the wake parameter impacts in the same way both aerodynamic loads computation schemes, because the computation of loads have nothing to do with wake propagation. Therefore the results presented for the Joukowski's solution in Fig. 3.18 are also applicable for the Katz method.
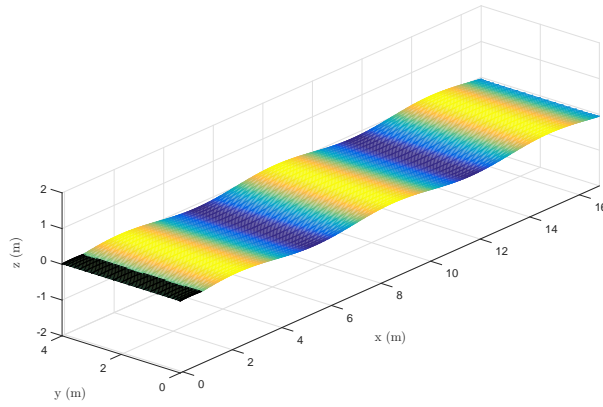
(a) Flat wake model
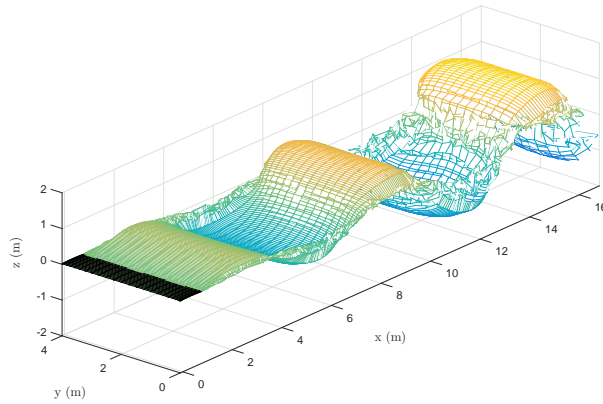
(b) Free wake model

FIGURE 3.17: Comparison of wake models for a NACA 2412 finite wing in pitch.

As expected, the wake model has very little to no influence at all on the coefficients. It is therefore logical to use only a flat wake model due to the lower computing time required to achieve the same result.

However the free wake model may become useful in case of wake interacting with each other, or to model the wake of a body,... but these phenomenon are not studied here and will not be considered for the flapping wings either.

3.6.2   Position of the first wake panel

As explained in Section 2.3, in theory, the trailing segment (= the first wake segment) should be placed in the interval covered by the trailing edge during the latest time step ($\mathbf{U}_\infty(t)\Delta t$) in order to account for the movement of the wing.

(a) Joukowski, C_d (b) Joukowski, C_l
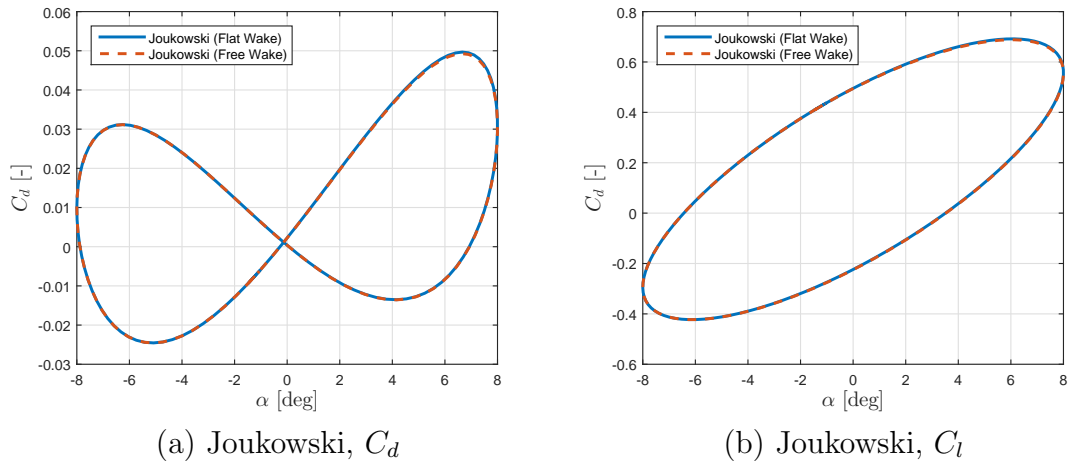
FIGURE 3.18: Comparison of drag and lift coefficient with two different wake
propagation models for a pitching 3D NACA 2412. $M = 18$, $N = 24$.

However, this would result in an underestimation of the induced velocities and
therefore an overprediction of the drag.

In practical, the first wake segment is commonly placed between $0.2 - 0.3\, \mathbf{U}_\infty(t)\Delta t$
in order to compensate this effect.

The Fig. 3.19 shows the aerodynamic coefficients in the case of a pitching
NACA 0012 airfoil (the same case that was extensively discussed in Section 3.4.1).
The results obtained for the drag are plotted for the different positions of the first
wake segments and they are compared with the results obtained using Garrick's
equations.

(a) Joukowski, C_d (b) Joukowski, C_l
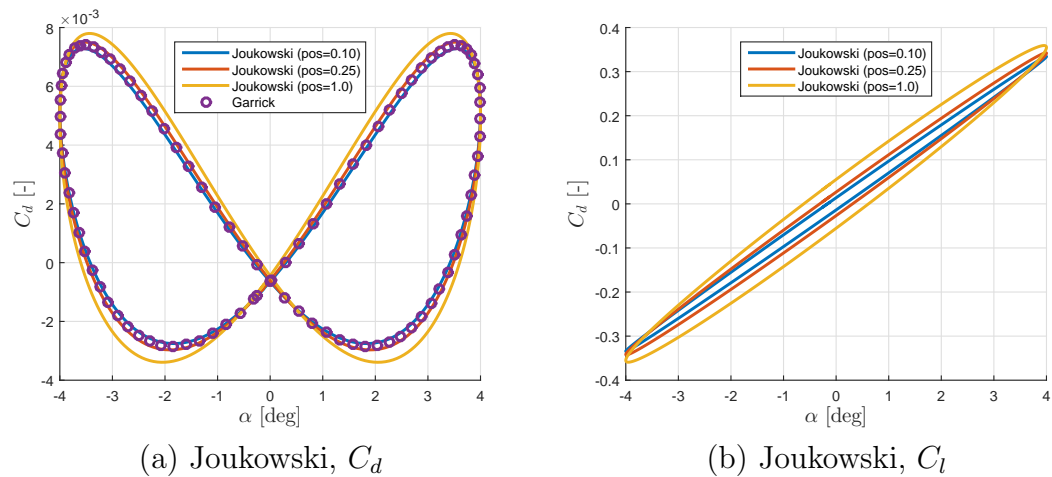
FIGURE 3.19: Comparison of drag and lift coefficient for different positions of
the first wake panel for a pitching 2D NACA 0012. $M = 18$, $N = 24$.

As expected, if the first wake panel is placed at $\mathbf{U}_\infty(t)\Delta t$ the solution given
by the UVLM diverges from the one found using Garrick's equations. The results

are much closer to Garrick's solution in the case of a first wake panel situated at $0.25\,\mathbf{U}_\infty(t)\Delta t$.

As for the wake model, this parameter impacts both Katz and Joukowski methods in the same way because the difference between these methods only occurs in the way aerodynamic forces are calculated and not in the way the flow properties are computed.

3.7   Summary

This chapter was focused on the reproduction and the extension of the study conducted by Simpson *et al.* [4].
The two different methods to compute the aerodynamic loads with the UVLM were discussed for three different conditions: steady, pure pitching and pure plunging. For each case, three different airfoils were studied in order to detect the influence of the camber on the results.

It was found that the results given by the two methods were extremely close to each other for the lift and drag coefficients. For harmonic pitching and plunging, it was also shown that the solution found for a NACA 0012 airfoil matches really well an analytical solution.
For all the movement studied, the chordwise convergence of the methods was analysed. This study showed that for finite wings the Joukowski method presents a better convergence than the Katz only for the NACA 0012. However, for cambered airfoils, the solution was found to converge marginally faster with the Katz method.

Finally, the impact of the wake parameters was studied. In this last section, it was proven that the free wake model did not change the results given by the vortex lattice simulation. However it increased dramatically the total computing time.
The position of the first wake panel was also analysed. A quick study showed that it was best to follow the directives given in Katz for the placement of the last bound vortex segment in order to have a relatively good solution.

Chapter 4

Flapping flight

This chapter will treat the problem of a flapping UAV studied experimentally by Abdul Razak in [2]. The methods developed previously for the aerodynamic loads will be applied to the wings used by Abdul Razak and the results will be compared with his wind tunnel experiments. For the cases that work the best with the UVLM a convergence study will be realised for the chordwise and spanwise paneling.

4.1   Configuration of the problem

4.1.1   Geometry

The UAV model studied here is based on the one used by Abdul Razak [2]. The design of the whole flapper is shown in Fig. 4.1.

Only the wings will be modeled in `Matlab` in order to apply the vortex lattice method. The body is not represented in the model, meaning that its wake will not be taken into account in the resolution. Note that both wings are separated from each other, therefore the vortex lattice solution developed for the previous chapter needs to be adapted to take into account multiple bodies, as explained in Chapter 2. This procedure will lead to a significant increase of computation time for the whole resolution (4 times larger for a two wings system than for a simple wing system).
The `Matlab` model of the surface and wake panels, vortex rings and collocation points for two NACA 6409 wings is shown in Fig. 4.2.
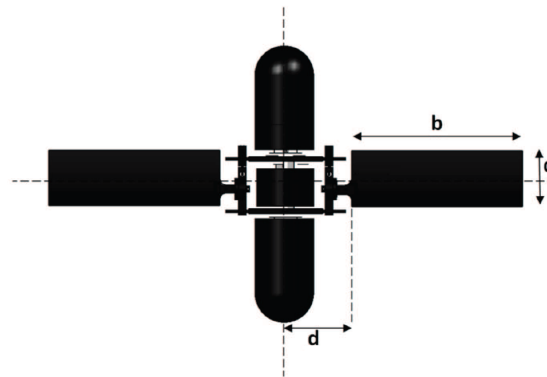
(a) Top view
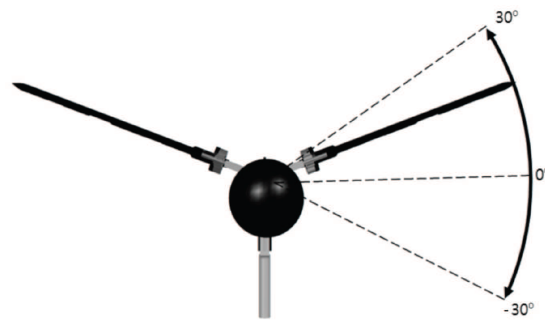
(b) Front view

FIGURE 4.1: Diagram of the flapping and pitching mechanical model, front and top view. Illustration from [2]
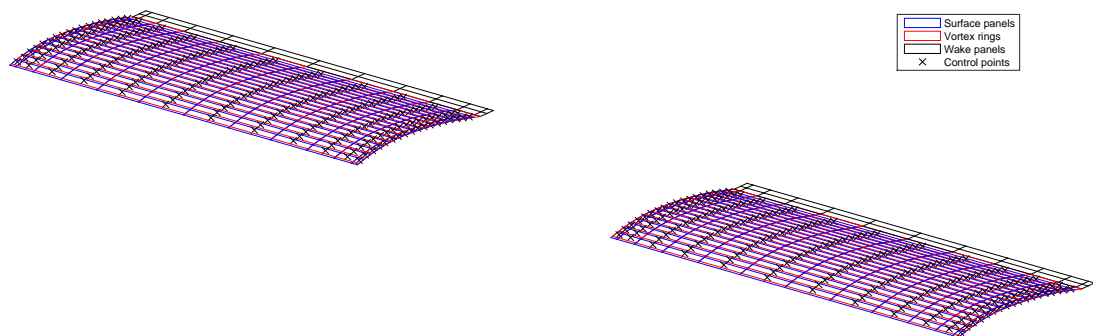
FIGURE 4.2: Surface and wake panels, vortex rings and collocation points. NACA 6409, $M = 18$, $N = 12$

4.1.2 Kinematics

The motion imposed to the wings can be divided in three different types:

- Pure flapping: the pitch angle is always zero, only the flap angle varies.
- Pitch lagging: both pitch and flap angles vary. The pitch angle lags the flap by 90 deg.
- Pitch leading: both pitch and flap angles vary. The pitch angle leads the flap by 90 deg.

These three cases are represented in Fig.4.3.
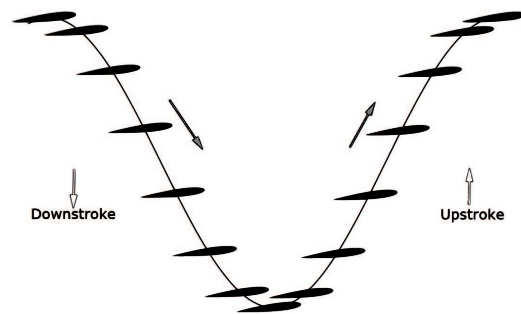
(a) Pure flapping
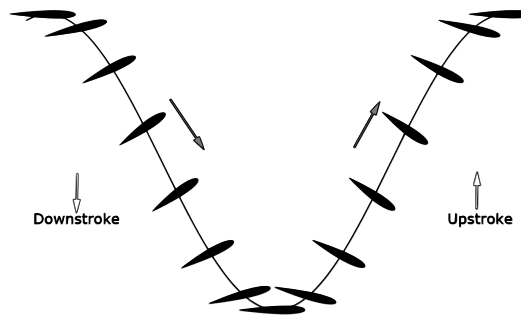
(b) Pitch lagging
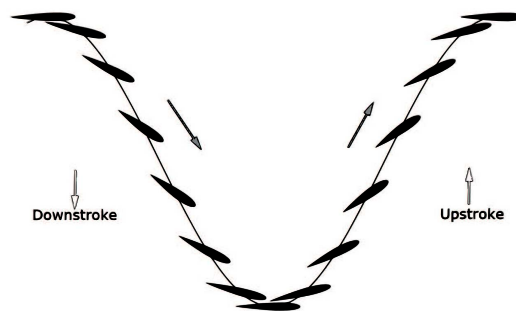
(c) Pitch leading

FIGURE 4.3: Visualisation of wing cross section undergoing pure flapping, pitch lagging and pitch leading motions. Illustration from [2].

The main difference between these three cases, is the behavior of the flow. In most of the pitch leading cases, the flow is expected to remain attached at all time, while it should detach periodically in many pure flapping cases and in all the pitch lagging cases. The constant detachment/reattachment of the flow in pure flapping and pitch lagging is known as dynamic stall. A summary of this phenomenon is given in [2], but as the UVLM does not work with these types of flow, it will not be discussed here.
Because the UVLM is only works with attached flows, it is expected to give better results for the pitch leading cases than for the other two.

For all the cases studied in this chapter, the vortex lattice simulations are conducted using the kinematics measured in wind tunnel (flap and pitch angles) as input. This is done in order to remain as close as possible to the experimental setup and to ensure the validity of the comparison with experimental measurements.

Effective angle of attack

The movement of the wing generates an effective angle of attack. In a combined flapping and pitching motion, this effective angle of attack α_{eff} comes from the translational velocity V_z perpendicular to the free stream velocity, and from the pitching motion of the wing. The effective angle of attack is given by

$$\alpha_{eff} = \alpha_p + \arctan \frac{-V_z}{U_\infty} \tag{4.1}$$

where V_z is counted positive when pointing up.
The effective angle of attack is a good way to tell if the flow is most likely to separate or not. For large values of α_{eff} (typically above 13-14 deg) the flow can detach, which would lead to the invalidity of the UVLM solutions.
The form of Eq. (4.1) suggests that during the downstroke ($V_z \leq 0$), the effective angle of attack will increase. Also, if the airspeed is increased, the second term of the equation would become smaller and therefore this would reduce the value of the effective angle of attack.
And obviously, the effective angle of attack is directly proportional to the pitching angle (α_p).

As the plunge velocity component (V_z) of the wing varies along the spanwise direction (because the flapping happens around wing root), the effective angle of attack is higher at wing tip and smaller at wing root. The vertical velocity V_z can be calculated from the value of the flap angle as

$$V_z = \dot{\gamma} r_s \tag{4.2}$$

where $\dot{\gamma}$ is the angular flapping speed (in radians) and r_s is the distance from one point of the wing to the flapping axis.
In order to have a flow attached (almost) everywhere on the wing, α_{eff} should be lower than a designated value, especially at wing tip.

In general, the bests results should be obtained with a small flapping frequency and a high airspeed, as these configurations ensure a smaller effective angle of attack and therefore, an attached flow everywhere.

4.2 Discretisation of the problem

4.2.1 Spatial discretisation

For this specific chapter, the same dimensions and discretisation are used for all the cases. The dimension of the wings match the ones used by Abdul Razak [2], in order to have a simulation as close as possible to the wind tunnel experiments. These data are summed in Table 4.1.

	Chord [m]	Span [m]	Distance to flapping axis [m]	M [-]	N [-]
NACA 0012	0.146	0.48	0.19	18	16
NACA 2412	0.146	0.48	0.19	18	16
NACA 6409	0.16	0.4	0.146	18	16

TABLE 4.1: Dimensions and discretisation of the wings used in flapping flight

Because there is two wings in the configuration studied here, the spanwise discretisation of each wing has been reduced (from $N = 24$ for the tests cases to $N = 16$ here) in order to keep relatively good computation times. A convergence study on both M and N will be conducted for some pitch leading cases.

The wings are meshed exactly as in the previous chapter (see Section 3.1). The chordwise dimension is the same for all panels, and the spanwise dimension is smaller for the panels at wing tip than for the ones at the center of the wing in order to detect more effectively the effects of the tip vortices on the drag (see Fig. 3.1 for a zoom on a portion of a wing).

4.2.2 Time discretisation

To ensure that wake panels have the same area that the trailing edge panels, the nondimensional time used so far is also employed here (see Eq. (3.1)). The drawback of this nondimensional time step is that the computation cost will increase a lot with the number of chordwise panels.

4.2.3 Wake modeling

As detailed in Section 3.6, the wake shape has a negligible influence on the results. Moreover, it is safe to assume that the wakes will not cross each other

because of the large distance (in comparison with their dimensions) separating the two wings, even for a free wake model. So their influence should be the same for both types of wake, like it was the case for a simple wing. In all the cases studied in this chapter, the flat wake approximation will be used.

The first wake panel position was also studied in the previous chapter. It was shown that the best results were obtained when the first wake panel was placed at $0.25\,\mathbf{U}_\infty(t)\Delta t$ aft of the wing's trailing edge. This position for the first wake segment will also be used for all the simulations in this chapter.

4.3   Remarks on experimental data

As said previously, all the experimental data come from [2]. Like for every experimental results, it is important to keep in mind that they are tainted with errors.

The first source of errors is the experimental setup itself (backlash in the mechanism, vibration of the mast carrying the model, imprecision in the motor, difficulty to set an exact value for the airspeed or flapping frequency,...). Moreover, the wings used in experiments are not perfect (the dimensions may have some small incertitude, the same goes for the camber) they also contain small defects on their surface,...

The second source of errors is the numerical treatment of the measured data. All tests required different measurements (for inertial and added mass effects) in order to determine the influence of the wings only (see Section 4.6 in [2]). These inertial and added mass effects were then subtracted from the total forces measured under flapping conditions. As the exact same flapping frequency is difficult to reproduce multiple times in the lab, the subtraction may lead from time to time to small errors that will appear as non physical peaks in the final filtered signal. Other parameters such as the cut-off frequency of the filter can lead to the apparition of oscillations in the final results.

However, in order to limit the impact of errors in the data presented, the experiments were conducted over a large number of periods and the results of all these periods were then averaged. In this thesis, all the experimental data are represented with their standard deviation in order to measure their reliability.

4.4   Pitch leading

This section will focus on the pitch leading kinematics. The only results available from [2] for this movement concern the NACA 6409 wings. The comparison of the coefficients given by the two vortex lattice methods over one period and the experimental data will only concern this airfoil. However, the convergence study will be also realised for the NACA 0012 and NACA 2412, in order to determine if the conclusions made for the simple cases in Chapter 3 are still valid for more complex kinematics. Note that the displacement measured for the 6409 wings will

be used as an input for the convergence studies of NACA 0012 and 2412, due to the absence of measurement with these airfoils.

As already explained, the results for this specific motion should be the most reliable ones because the flow is expected to remain attached everywhere for most of the time.

4.4.1 Kinematics analysis

An example of the kinematics for a NACA 6409 undergoing pitch leading is represented in Fig. 4.4 along with the effective angle of attack measured at mid span and at wing tip for two different airspeeds and flapping frequencies.

(a) $U_\infty = 6$ m/s , $f = 0.79$ Hz

(b) $U_\infty = 6$ m/s , $f = 1.23$ Hz

(c) $U_\infty = 9.4$ m/s , $f = 0.79$ Hz

(d) $U_\infty = 9.4$ m/s , $f = 1.23$ Hz
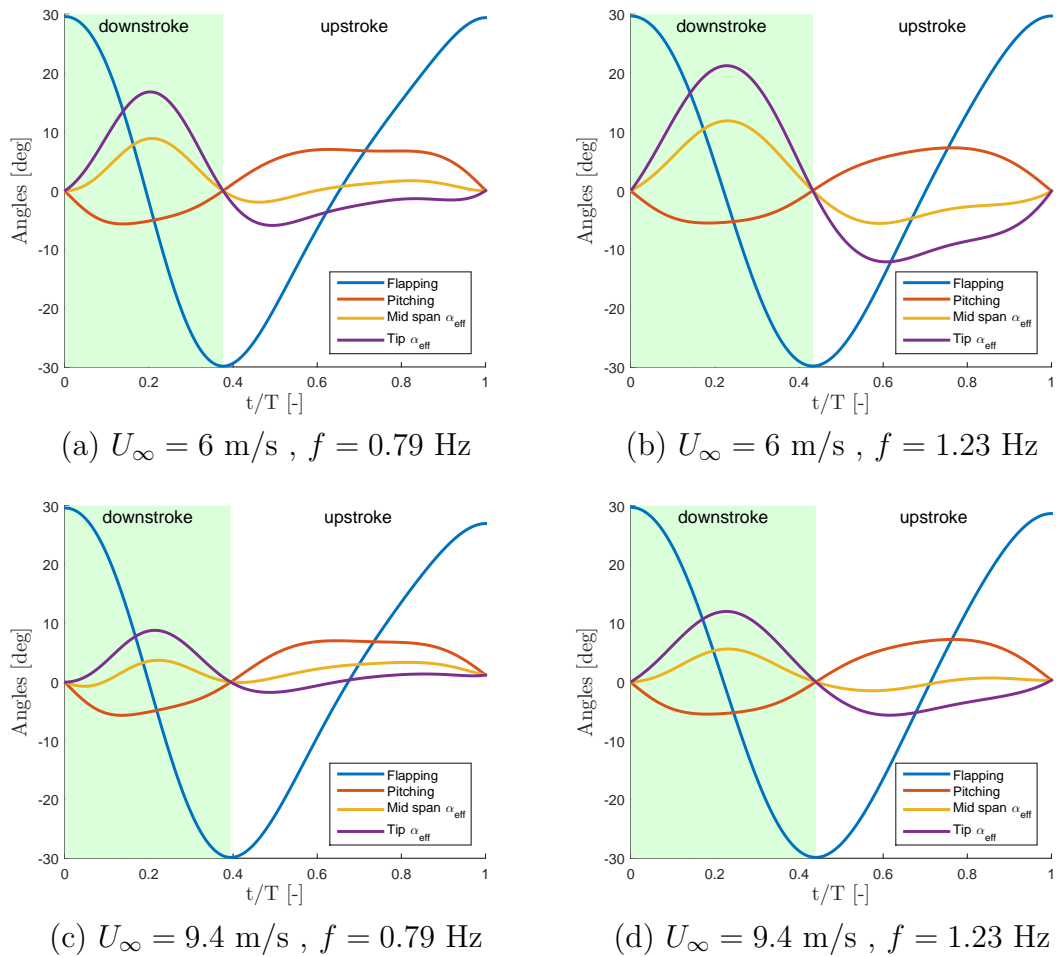
FIGURE 4.4: Wind tunnel data for flapping, pitching and effective angle of attack at mid span and wing tip in pitch leading.
NACA 6409, $\alpha_p \in [-6, 6]$ deg.

The movement starts with the wing at maximal flapping (γ) and at 0 pitching (α_p). During the first phase, the *downstroke*, the flapping angle is decreased progressively to its minimal value. In the same time, the pitching amplitude is also

decreased and reaches its minimal value at the middle of the downstroke (because the pitch angle leads the flap by 90 deg), then it start to increase again to reach 0 at the end of the downstroke, when the wing is at its lowest position. The second part of the motion consists of the *upstroke*: the exact opposite of the first phase. As seen on the figure, the downstroke phase is shorter than the upstroke. This is because the inertial forces during downstroke are higher due to gravitational acceleration and there is no counter weight or spring installed to balance the wing inertial forces [12].

During the downstroke, the effective angle of attack is positive and quite important, due to the increase of $-V_Z$ (especially at wing tip). As the wing is tilted forward during this part of the movement, the normal force is also tilted forward and thrust should be generated. During the upstroke, the wing is tilted backwards and should produce downforce. Depending on the value of the effective angle of attack, it may either produce thrust or drag. If α_{eff} is mainly positive across the span, thrust should still be generated, otherwise there should be drag.
Note that as the upstroke is longer than the downstroke, the vertical velocity is smaller and leads to a smaller effective angle of attack during the upstroke.

As explained previously, the effective angle of attack is higher at lower airspeed. The inspection of Fig. 4.4 suggests that the flow is probably separated near the wing tip for $U_\infty = 6$ m/s, when the wing is at mid downstroke. However, during the rest of the period, the effective angle of attack decreases to more reasonable values, and its legitimate to think that the flow reattaches.
For higher airspeeds, the effective angles of attack remain small enough to keep an attached flow during the whole period. Therefore, the results obtained with the UVLM for $U_\infty = 9.4$ m/s should be closer to the reality than the ones obtained for $U_\infty = 6$ m/s.
The impact of the flapping frequency can also be observed, as the effective angle of attack increases with the frequency.
In conclusion, the best results should be obtained for $U_\infty = 9.4$ m/s and $f = 0.79$ Hz, while the worst are expected for $U_\infty = 6$ m/s and $f = 1.23$ Hz.

4.4.2 Cambered airfoil: NACA 6409

Only this airfoil was tested by Abul Razak in wind tunnel for pitch leading. As this case should be the one presenting the best conditions for the analysis through the UVLM, the influence of all the flow parameters will be studied.

4.4.2.1 Influence of the airspeed

The first parameter studied is the airspeed. As explained previously, a higher airspeed should give better results as the flow is expected to be attached everywhere at all time. In order to analyse the airspeed's effect, the pitching amplitude and the flapping frequency were fixed respectively at $\alpha_p \in [-6, 6]$ deg and $f = 0.79$ Hz. This specific value for the flapping frequency was chosen in order to

keep α_{eff} as small as possible during the whole period. The angles corresponding to this case were shown in Fig. 4.4(a,c).

The Fig. 4.5 represents the influence of airspeed on the aerodynamic coefficients.

(a) C_d , $U_\infty = 6$ m/s

(b) C_l , $U_\infty = 6$ m/s

(c) C_d , $U_\infty = 9.4$ m/s

(d) C_l , $U_\infty = 9.4$ m/s
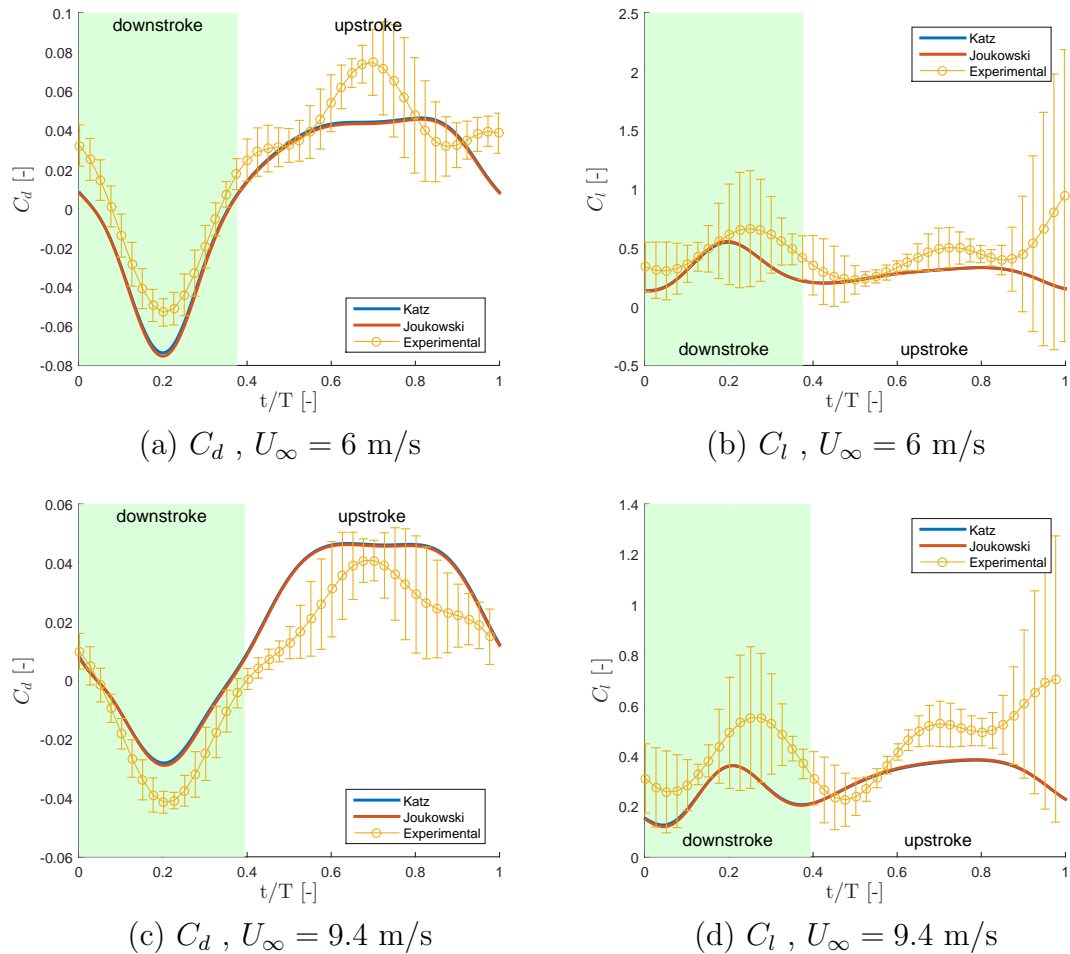
FIGURE 4.5: Influence of airspeed on the aerodynamic coefficients for a NACA 6409 in pitch leading, $f = 0.79$ Hz, $\alpha_p \in [-6, 6]$.

First of all, once again both Katz and Joukowski give almost exactly the same results for the drag and lift coefficients. The only small difference is that the Joukowski method seems to predict a little bit more leading-edge suction (and therefore more thrust) than Katz', especially for the highest values of α_{eff} measured. But this difference in perfectly negligible.

In general, the drag coefficient seems relatively well predicted by the UVLM. For the smaller airspeed, the drag is underpredicted with both Katz and Joukowski solutions, especially during the downstroke. This result is perfectly normal because some small separation is expected around wing tip during the downstroke ($\alpha_{eff,tip} \approx 17$ deg). As the UVLM can not represent detached flows, the drag created by the separation is not modeled and this leads to a smaller drag coefficient for the vortex lattice solutions. During the upstroke, the flow reattaches and

the UVLM is closer to the experimental data. There should be noted that the experimental data show a peak of drag at the middle of the upstroke that is not captured by the UVLM. This peak may be the result of mistakes in the treatment of raw data and may not be relevant. Still, the UVLM data are in general within the range of the standard deviation of the experimental measurements. So, for $U_\infty = 6$ m/s, the UVLM can be considered to capture well the behavior of the flow during the upstroke, but during the downstroke it underpredict a little bit the drag. However, because the separated area of the wing is relatively small, the underprediction error is limited.

In the case of $U_\infty = 9.4$ m/s, the drag seems to have more or less the same shape than the one measured in wind tunnel. However, the UVLM results are shifted up compared to the experimental ones, especially for the point at mid downstroke. This result is not due to an overprediction of drag with the UVLM, but rather to an underprediction of the leading-edge suction effect and therefore the thrust.

The lift coefficient for the lowest airspeed seems to be really well modeled. This result was not especially expected for the first peak because the flow should be separated around wing tip. Therefore the UVLM solution was expected to find a larger lift than the one measured during the downstroke. The upstroke part is well matched by the UVLM, with the exception of the very end of the period. However, the standard deviation of the measured lift indicates that the results obtained for the end of the period vary greatly. So, as the UVLM solutions are in the range of the standard deviation, they can be considered valid. Finally, the experimental data are shifted to the right compared to the UVLM solutions. This phenomenon is known as aerodynamic lag. This difference in lag between UVLM and experiments suggest that the UVLM tends predict a lower lag than in reality. For the highest airspeed the lift is also relatively well predicted, but not as well as for the lowest airspeed. This is surprising because it should be the best case for the UVLM. In fact, the UVLM tends to underpredict the lift of an attached flow. Because of the separation occurring with the lowest airspeed, the experimental lift is a little bit shifted downwards and therefore is closer to the solution brought by the UVLM. So in case of a small separation, the lift appears to be better modeled. Nonetheless, for $U_\infty = 9.4$ m/s, the UVLM is very close to the standard deviation around the measured lift, so it can be considered as a good model. It should also be noted that the the experimental results for the lift are in general less reliable than the ones for the drag. This is mainly due to the inertial forces that act in the same direction as the lift.

4.4.2.2 Influence of the flapping frequency

The flapping frequency is now studied. To analyse its effect, the pitching amplitude and the airespeed were fixed respectively at $\alpha_p \in [-6, 6]$ deg and $U_\infty = 9.4$ m/s. This specific value for the airspeed was chosen in order to keep α_{eff} as small as possible during the whole period. The angles corresponding to this case were shown in Fig. 4.4(c,d).

The Fig. 4.6 represents the influence of the flapping frequency on the aerodynamic coefficients.

(a) C_d , $f = 0.79$ Hz

(b) C_l , $f = 0.79$ Hz

(c) C_d , $f = 1.23$ Hz

(d) C_l , $f = 1.23$ Hz
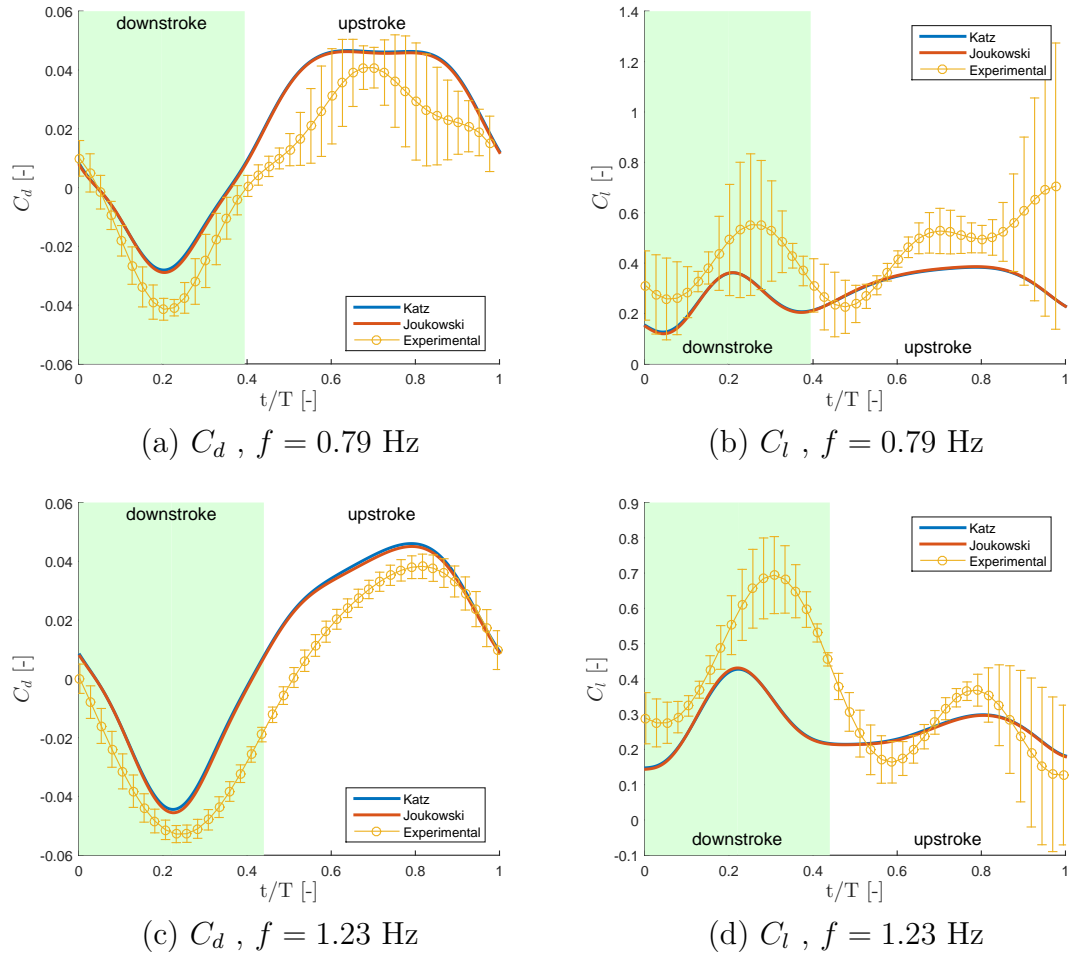
FIGURE 4.6: Influence of flapping frequency on the aerodynamic coefficients for a NACA 6409 in pitch leading, $U_\infty = 9.4$ m/s, $\alpha_p \in [-6, 6]$.

The graphs for the lowest frequency were already presented in the study of the airspeed's influence and will not be commented once again here.

The first interesting thing to notice is that for the higher frequency, the Joukowski method seems to predict a little bit more leading edge suction than Katz (even if the difference is still negligible). It seems that in general, Joukowski method predicts a larger thrust, especially for high values of effective angle of attack. Otherwise, both UVLM results for the lift and drag coefficient can be considered as equal.

As seen in Fig. 4.4(d), the value of α_{eff} is in general a little bit higher for the highest frequency than for the lowest, but α_{eff} remains small enough to consider the flow as attached everywhere.
Just like for the lowest frequency, the UVLM predicts a smaller thrust than the one measured in wind tunnel, which results in a drag coefficient always higher for

the UVLM than for the experiments. Nonetheless, the behavior of the drag is very well predicted for $f = 1.23$ Hz, even better than for the lowest frequency. This is probably not due to the vortex lattice method itself, but rather to errors in the experimental data for $f = 0.79$ Hz, as explained in the previous section (this can be observed by the larger values for the standard deviation for $f = 0.79$ Hz).

In the other hand, the lift is usually underpredicted with the UVLM, for both frequencies. The difference is really important for the two flapping frequencies and reaches even 35% for the peak during the downstroke. As explained previously for the airspeed, the aerodynamic lag is also smaller for the UVLM solutions than in reality. This large error for the lift coefficient probably comes from the experimental data because the most part of the inertial forces are acting in the same direction than the lift.

4.4.2.3 Influence of the pitching angle

The last parameter to study is the pitching angle. Two different cases are studied: $\alpha_p \in [-8, 4]$ deg and $\alpha_p \in [-4, 8]$ deg. The two cases are only analysed for $U_\infty = 9.4$ m/s as it will result most likely in flow attached everywhere. The measured angles are presented in Fig. 4.7.

The angles measured in all cases are similar. The important thing to notice is that the effective angle of attack is almost always smaller than 13-14 deg. This should ensure an attached flow in all cases.
As the smallest effective angles of attack are obtained with $f = 0.79$ Hz, this frequency was fixed for the study of the pitching amplitude impact. The results of this analysis are shown in Fig. 4.8.

Once again, the two UVLM solutions give the same results for the drag and lift coefficient, and the Joukowski method still predicts a little bit more thrust in general, but this can be neglected.

For both cases, the drag coefficient is really well predicted, especially during the downstroke. During the upstroke, the vortex lattice solutions show a large drag for a longer period of time, but in general there is no really big differences with the experimental measurements.
The fact that the drag amplitude is so well predicted for these cases is really interesting as it was not the case for the intermediate pitching angle $\alpha_p \in [-6, 6]$ (see Fig. 4.5(c)). It seems that some cases predict a better amplitude in general, but the other predict a better phase.

The lift is in general underpredicted during the downstroke, as it has always been the case so far. In general the aerodynamic lag is underpredicted as well for the lift coefficient.

(a) $\alpha_p \in [-8, 4]$ deg , $f = 0.79$ Hz

(b) $\alpha_p \in [-8, 4]$ deg , $f = 1.23$ Hz

(c) $\alpha_p \in [-4, 8]$ deg , $f = 0.79$ Hz

(d) $\alpha_p \in [-4, 8]$ deg , $f = 1.23$ Hz
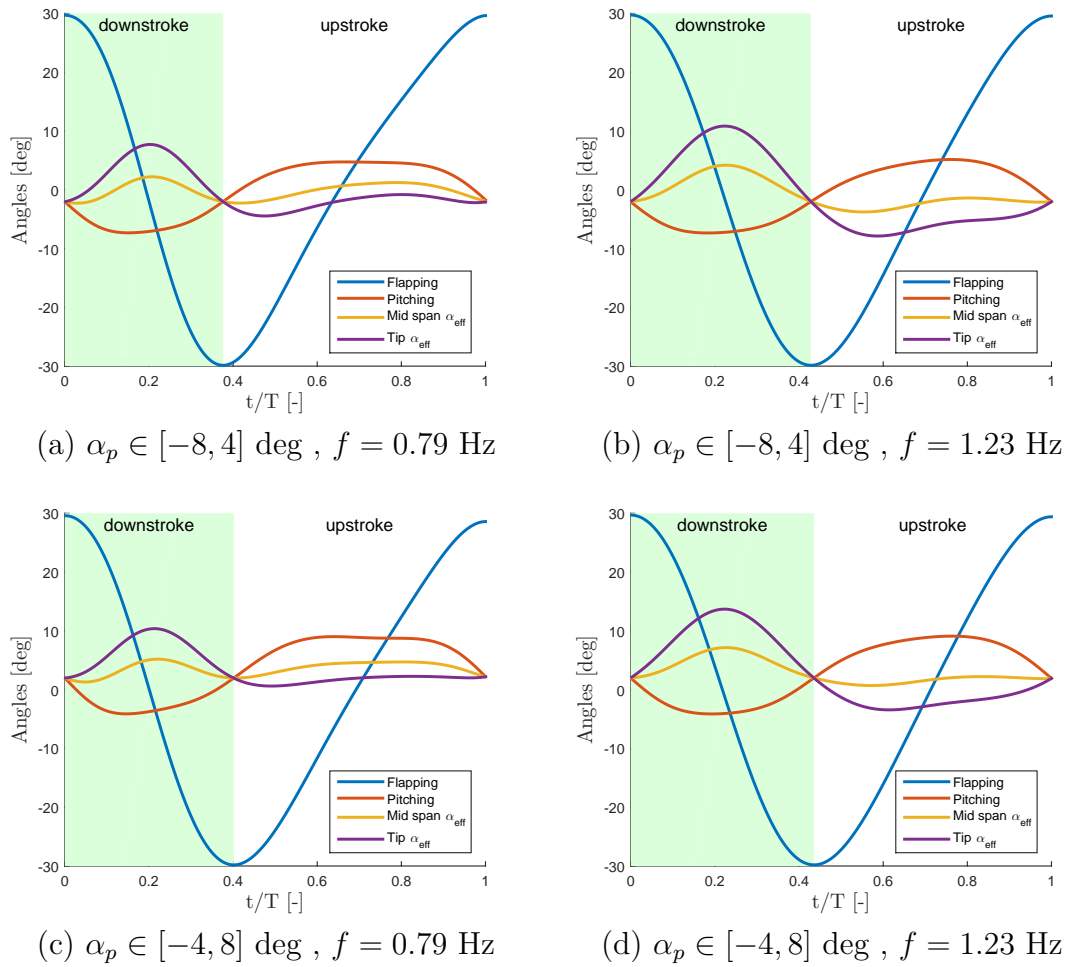
FIGURE 4.7: Wind tunnel data for flapping, pitching and effective angle of attack at mid span and wing tip in pitch leading. NACA 6409, $U_\infty = 9.4$ Hz.

(a) C_d , $\alpha_p \in [-8, 4]$ deg

(b) C_l , $\alpha_p \in [-8, 4]$ deg

(c) C_d , $\alpha_p \in [-4, 8]$ deg

(d) C_l , $\alpha_p \in [-4, 8]$ deg
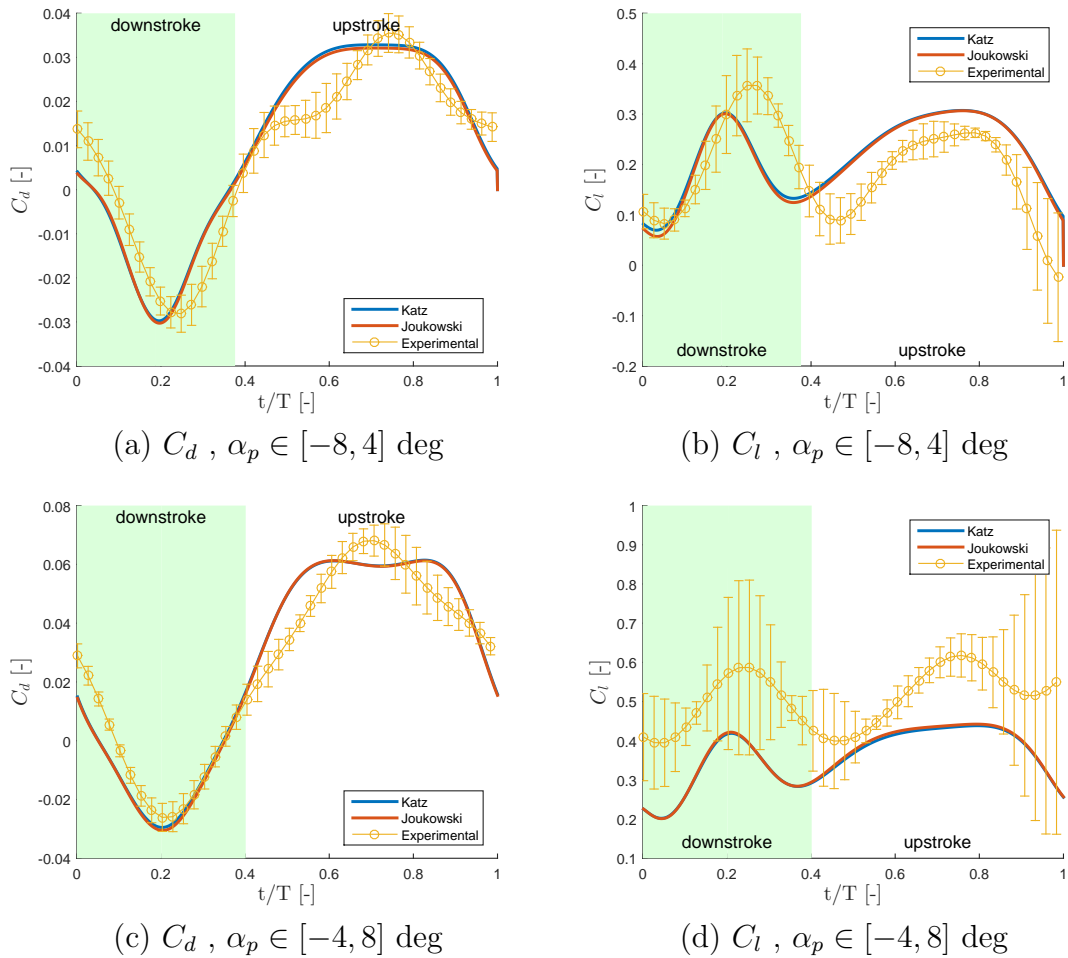
FIGURE 4.8: Influence of pitching angle on the aerodynamic coefficients for a NACA 6409 in pitch leading, $U_\infty = 9.4$ m/s, $f = 0.79$ Hz.

4.4.2.4 Chordwise convergence

The chordwise convergence is shown in Fig. 4.9 for both airspeeds and two flapping frequencies when the pitch angle varies from -6 to 6 deg. This study is conducted with a fixed number of spanwise panels on each wing $N = 16$.

(a) error_{C_d} , $U_\infty = 6$ m/s

(b) error_{C_l} , $U_\infty = 6$ m/s

(c) error_{C_d} , $U_\infty = 9.4$ m/s

(d) error_{C_l} , $U_\infty = 9.4$ m/s
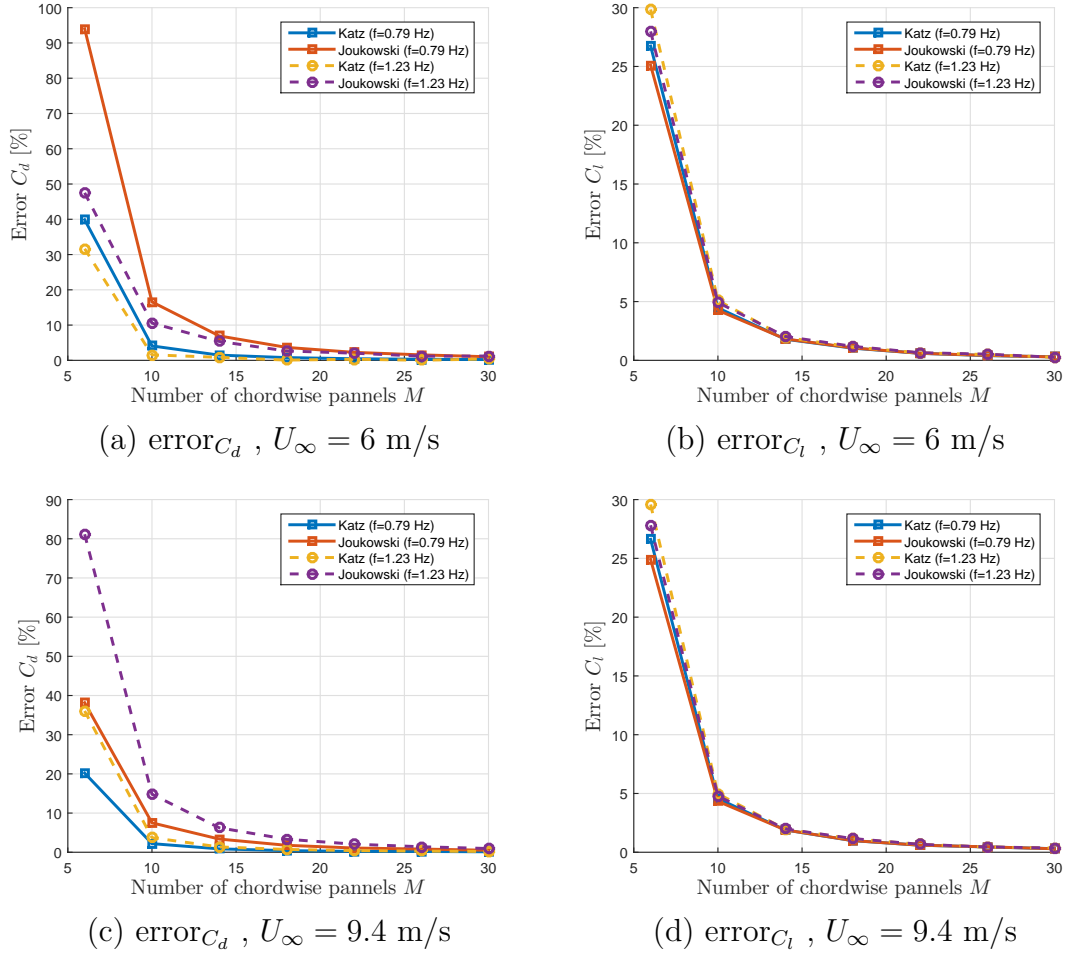
FIGURE 4.9: Chordwise convergence of drag and lift coefficients for different airspeed for NACA 6409 in pitch leading, $\alpha_p \in [-6, 6]$, $N = 16$.

As it has always been the case for the NACA 6409 airfoils, the Katz' method presents a better convergence in drag than Joukowski's. Note that, once again the difference is significant as Katz method could be considered converged for $M = 14$ while Joukowski have to wait until at least $M = 18$.

For the lift, both methods converge at the same rate independently of the flapping frequency. This was already the case for all the simulations with a NACA 6409 airfoil.

4.4.2.5 Spanwise convergence

The spanwise convergence is shown in Fig. 4.10 for both airspeeds and two flapping frequencies for the case of a pitch angle varying from -6 to 6 deg. This study is conducted with a fixed number of chordwise panels on each wing $M = 18$.

(a) error$_{C_d}$, $U_\infty = 6$ m/s

(b) error$_{C_l}$, $U_\infty = 6$ m/s

(c) error$_{C_d}$, $U_\infty = 9.4$ m/s

(d) error$_{C_l}$, $U_\infty = 9.4$ m/s
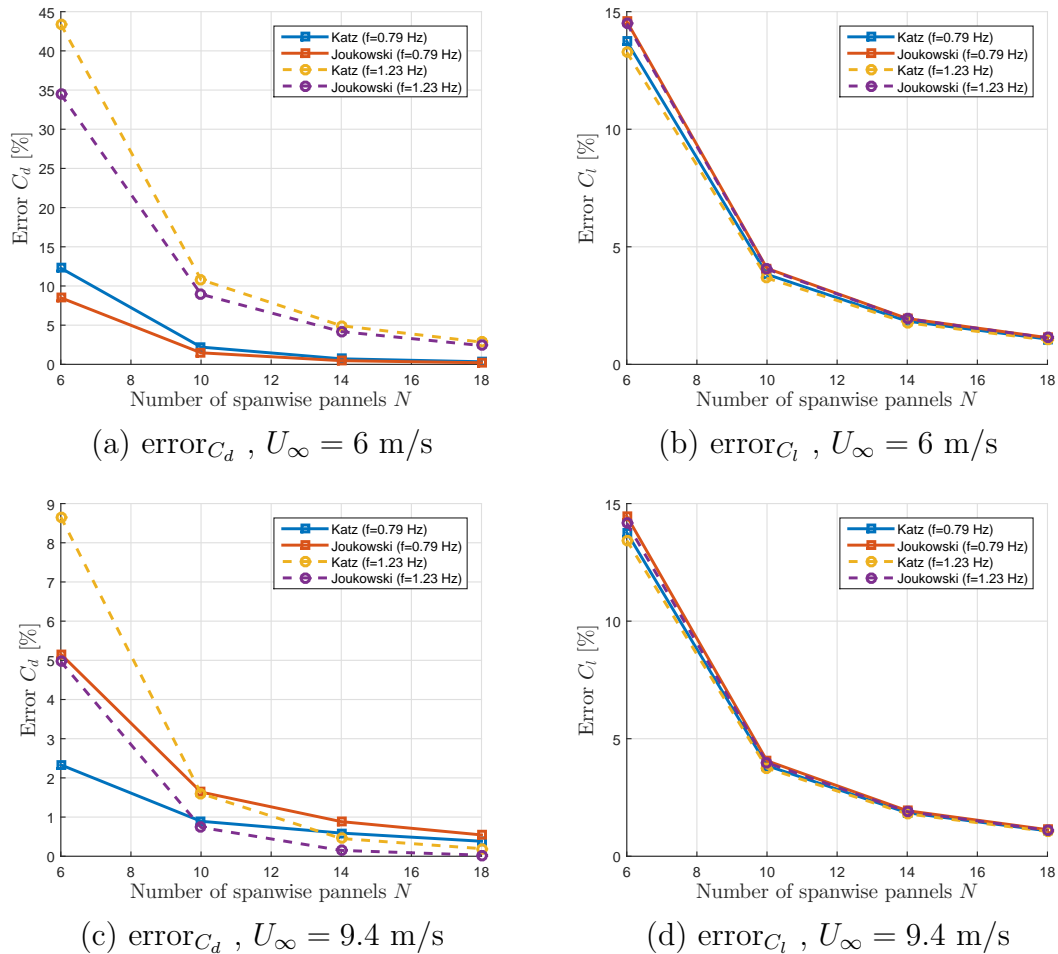
FIGURE 4.10: Spanwise convergence of drag and lift coefficients for different airspeed for NACA 6409 in pitch leading, $\alpha_p \in [-6, 6]$, $M = 18$.

Once again, the convergence of the lift is the same for both methods independently of the flapping frequency.

For the drag, the results are quite different from the chordwise convergence. Here, the Joukowski method presents a small advantage over the Katz for the two frequencies when $U_\infty = 6$ m/s. But with the increasing number of spanwise panels, both methods observe the same rate of convergence and they reach final convergence together.

The spanwise convergence is a little bit more complex for $U_\infty = 9.4$ m/s. In that case, the Katz method converges faster if $f = 0.79$ Hz, while Joukowski method

converges faster if $f = 1.23$ Hz. However, for the two frequencies both methods reach an error smaller than 2 % for the same discretisation. So they can be considered converged for the same paneling.

4.4.3 Symmetric airfoil: NACA 0012

As there was no available data for this airfoil, the kinematics used for the NACA 6409 were used as an input to compute the aerodynamic loads for a NACA 0012.

Chordwise convergence

The chordwise convergence for both airspeed and different frequencies for a NACA 0012 wing is presented in Fig. 4.11. Like for the NACA 6409, this study is conducted with a fixed number of spanwise panels on each wing $N = 16$.

(a) error_{C_d} , $U_\infty = 6$ m/s

(b) error_{C_l} , $U_\infty = 6$ m/s

(c) error_{C_d} , $U_\infty = 9.4$ m/s

(d) error_{C_l} , $U_\infty = 9.4$ m/s
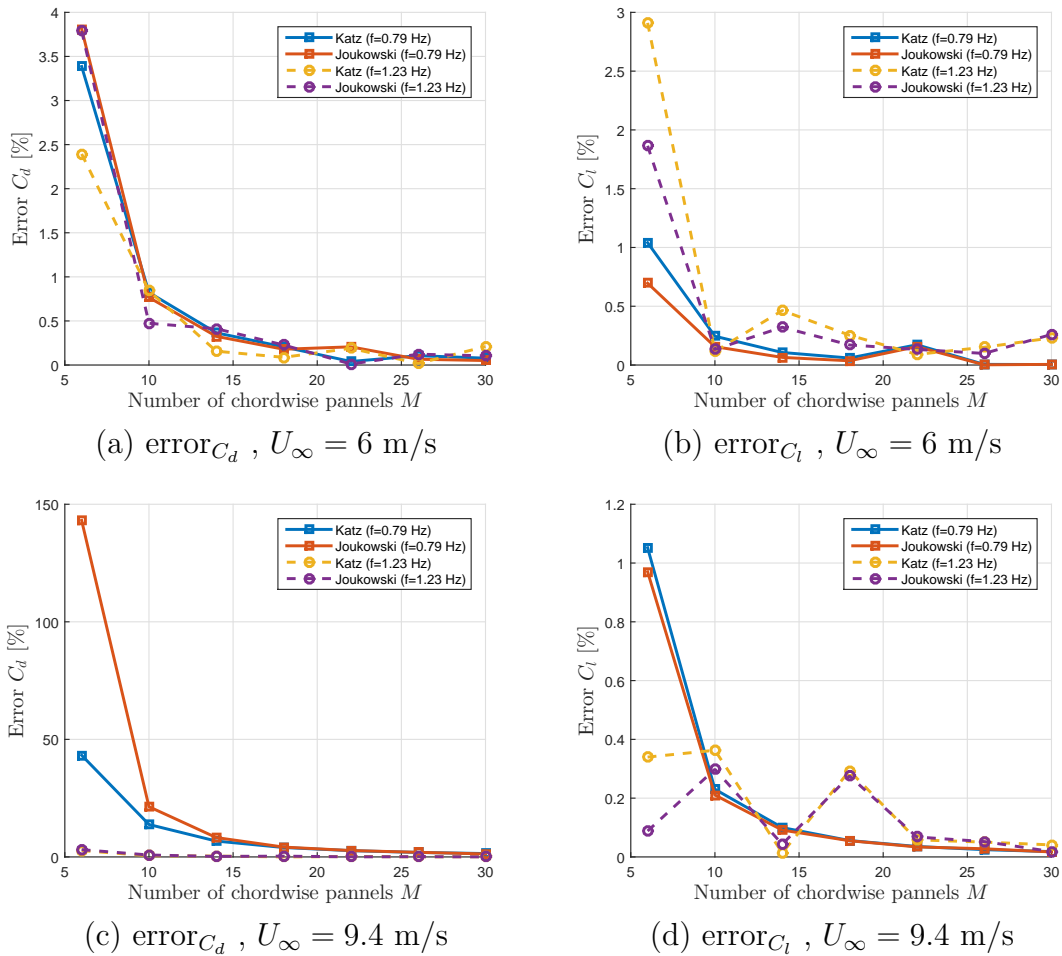
FIGURE 4.11: Chordwise convergence of drag and lift coefficients for different airspeed for NACA 0012 in pitch leading, $\alpha_p \in [-6, 6]$, $N = 16$.

The results for this airfoil are quite different than the ones obtained for the 6409 airfoil. With the exception of the drag for $U_\infty = 9.4$ m/s and $f = 0.79$ Hz, all the coefficients converge almost immediately (the error is smaller than 1% for the second discretisation tested). As the result is almost directly converged, it has no sense to tell that one method is faster than the other for these cases. Moreover, in general the convergence rate of both methods is almost the same.
For the specific case of $U_\infty = 9.4$ m/s and $f = 0.79$ Hz, the Katz method seems to have an advantage for the coarse paneling. However, the Katz' convergence rate is slower than Joukowski's and they finally end by converging together. So that they reach convergence at the same time.
In the end, for this airfoil, both method reach convergence at the same time.

Spanwise convergence

The spanwise convergence is represented in Fig. 4.12 for the same kinematics and chordwise paneling that were used for the NACA 6409.

(a) error$_{C_d}$, $U_\infty = 6$ m/s

(b) error$_{C_l}$, $U_\infty = 6$ m/s

(c) error$_{C_d}$, $U_\infty = 9.4$ m/s

(d) error$_{C_l}$, $U_\infty = 9.4$ m/s
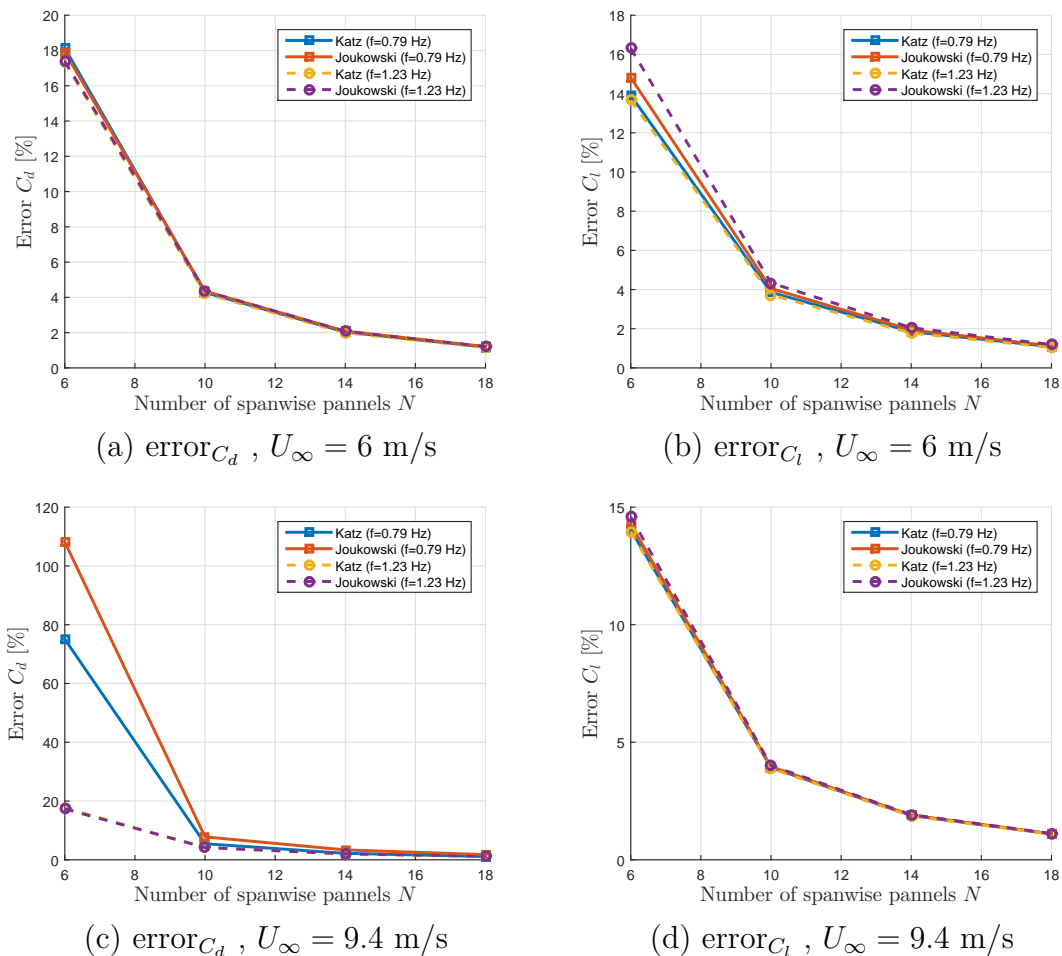
FIGURE 4.12: Spanwise convergence of drag and lift coefficients for different airspeed for NACA 0012 in pitch leading, $\alpha_p \in [-6, 6]$, $M = 18$.

Just like for the chordwise convergence, both method follow approximately the exact same convergence rate for the drag and the lift, once again with the exception of the case representing $U_\infty = 9.4$ m/s and $f = 0.79$ Hz. However, for that specific case they finally present the same error for the third discretisation tested.

4.4.4 Cambered airfoil: NACA 2412

Once again, the kinematics of the NACA 6409 were used as an input to deal with the absence of measurement with a 2412 airfoil.

Chordwise onvergence

The chordwise convergence is shown in Fig. 4.13 for both airspeeds and two flapping frequencies.

(a) error_{C_d} , $U_\infty = 6$ m/s

(b) error_{C_l} , $U_\infty = 6$ m/s

(c) error_{C_d} , $U_\infty = 9.4$ m/s

(d) error_{C_l} , $U_\infty = 9.4$ m/s
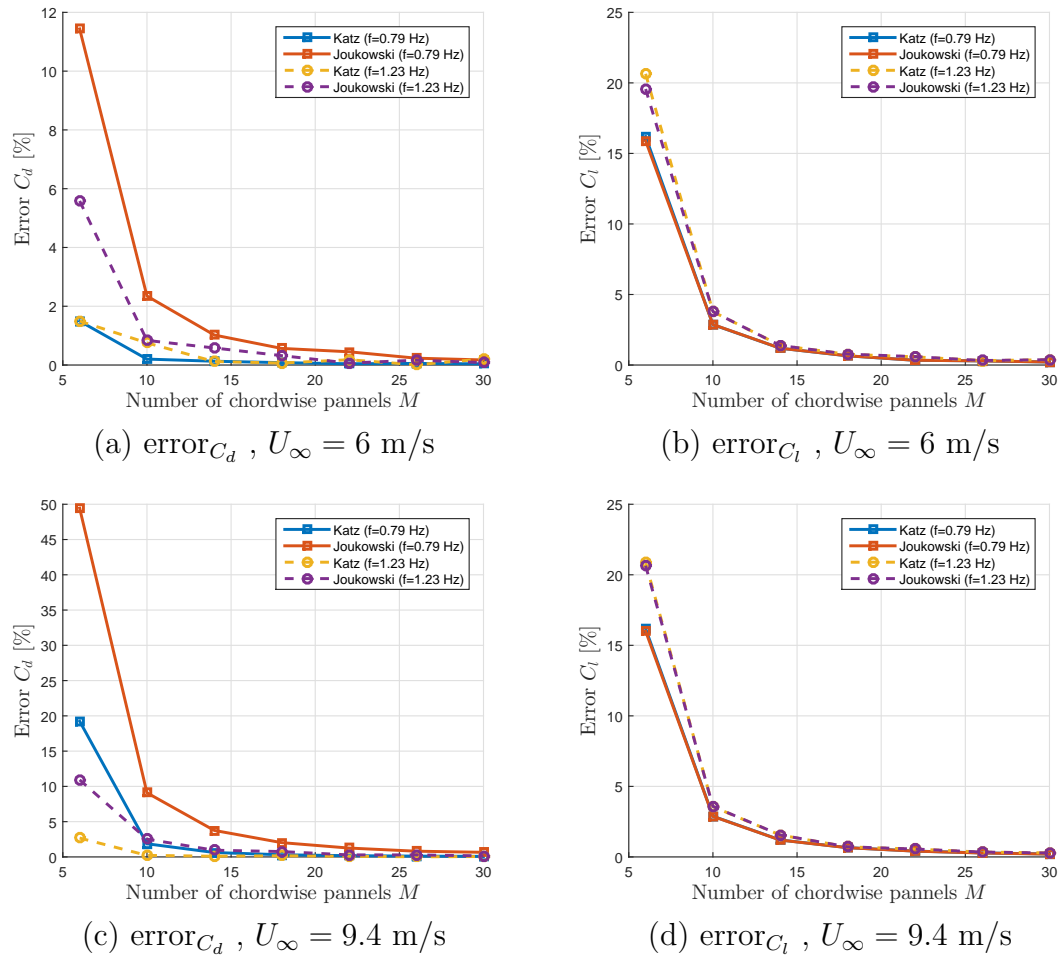
FIGURE 4.13: Chordwise convergence of drag and lift coefficients for different airspeed for NACA 2412 in pitch leading, $\alpha_p \in [-6, 6]$, $N = 16$.

It is obvious once again that the Katz method shows a better convergence than the Joukowski's for the drag coefficient. In general the solution given by Katz is converged around $M = 14$ while the one obtained with Joukowski requires at least $M = 18$.

The lift coefficient converges at the same rate for both methods, independently of the frequency, as usual.

Spanwise convergence

The spanwise convergence is represented in Fig. 4.14 for both airspeed and two flapping frequencies for the case of a pitch angle varying from -6 to 6 deg. Like for the 0012 airfoil, the spanwise convergence is the same for both methods.

(a) error$_{C_d}$, $U_\infty = 6$ m/s

(b) error$_{C_l}$, $U_\infty = 6$ m/s

(c) error$_{C_d}$, $U_\infty = 9.4$ m/s

(d) error$_{C_l}$, $U_\infty = 9.4$ m/s
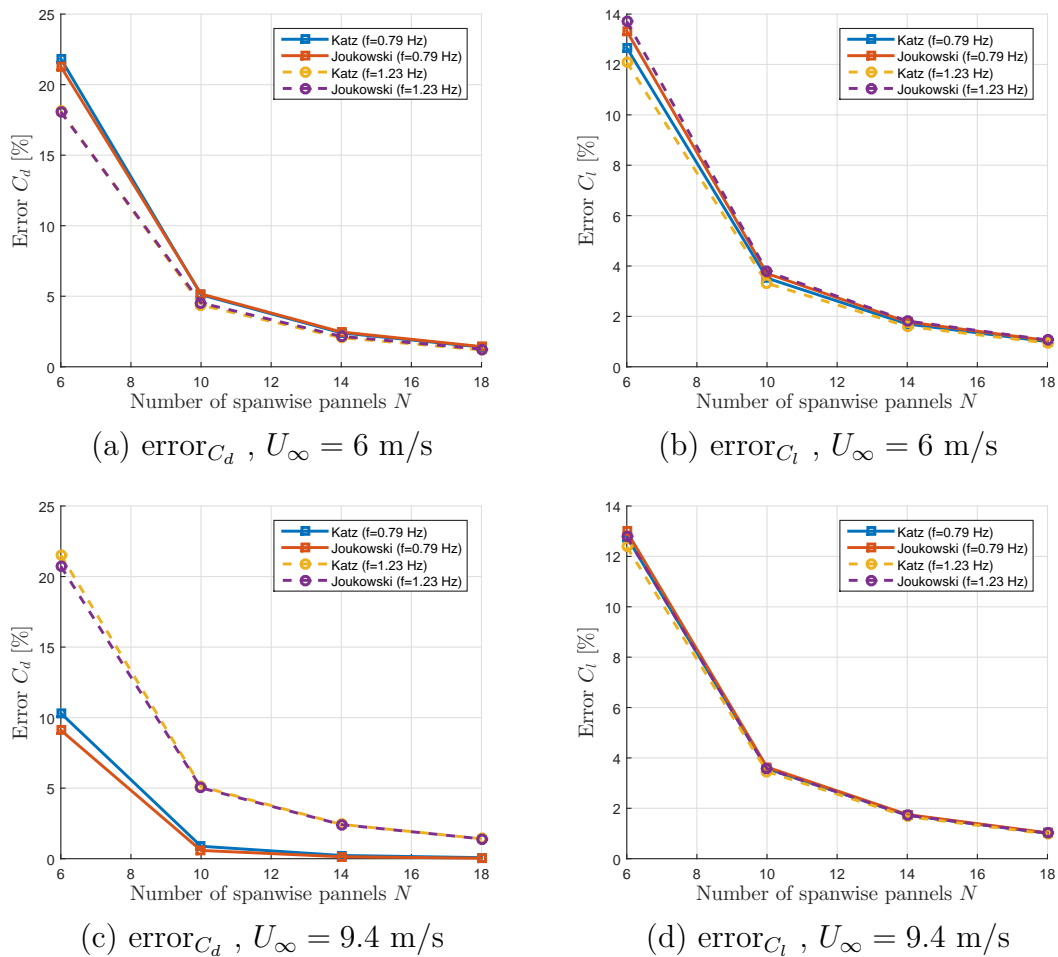
FIGURE 4.14: Spanwise convergence of drag and lift coefficients for different airspeed for NACA 2412 in pitch leading, $\alpha_p \in [-6, 6]$, $M = 18$.

In general, convergence is reached for $N = 16$.

4.5 Pure flapping

This case should experience some stall from time to time across the total period, therefore the vortex lattice method may not be applicable for all combinations of frequencies and airspeeds.

The study of this specific type of motion will be conducted with the NACA 0012 and NACA 2412 airfoils at an angle of attack $\alpha = 0$ deg.

4.5.1 Kinematics analysis

The Fig. 4.15 represents the evolution of the flapping, pitching and effective angles of attack for the NACA 2412 wings in pure flapping.

(a) $U_\infty = 6$ m/s , $f = 0.79$ Hz

(b) $U_\infty = 6$ m/s , $f = 1.23$ Hz

(c) $U_\infty = 9.4$ m/s , $f = 0.79$ Hz

(d) $U_\infty = 9.4$ m/s , $f = 1.23$ Hz
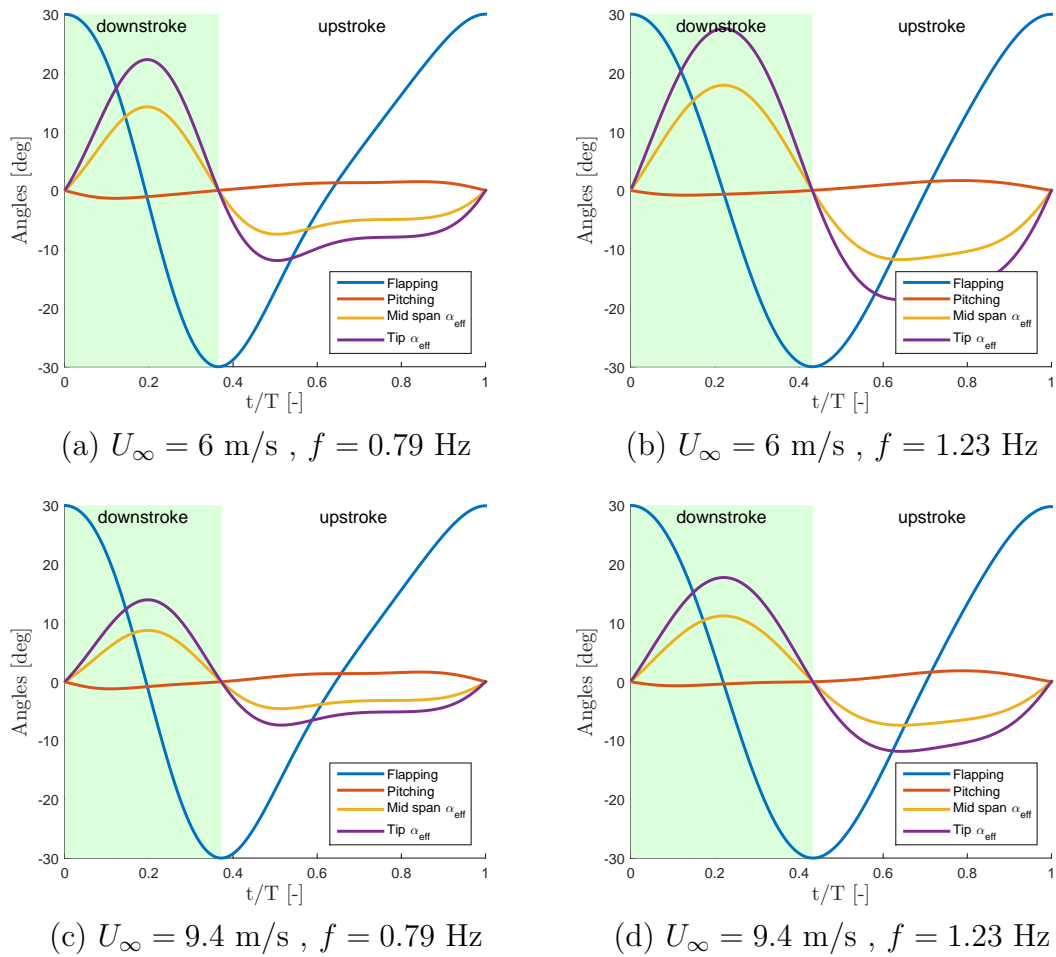
FIGURE 4.15: Wind tunnel data for flapping, pitching and effective angle of attack at mid span and wing tip in pure flapping. NACA 2412, $\alpha = 0$ deg.

All these values come from the experimental data. Even if the case is said to be "pure flapping", a small pitch angle is measured during the period, mainly

due to backlash in the mechanism. Just like for pitch leading, these flapping and pitching angles were used as an input for the vortex lattice resolution in order to make a valid comparison.

Note that the angles measured for the NACA 0012 have approximately the same values than the ones presented in Fig. 4.15 for the NACA 2412. So the comments based on the NACA 2412 remain valid for the other airfoil.

The first thing to notice with this type of flow is that the effective angle of attack take larger values than for pitch leading. At low airspeed ($U_\infty = 6$ m/s, Fig. 4.15(a,b)), α_{eff} is already above 13-14 deg at mid span and reaches values above 20 deg at wing tip. It is safe to assume that the flow will be separated on almost half of the wing as long as the effective angle of attack remains at such high values. Therefore the vortex lattice should not give a valid approximation of the solution.

For higher airspeed ($U_\infty = 9.4$ m/s, Fig. 4.15(c,d)), the effective angle of attack is in general a little bit lower. With the smaller flapping frequency, α_{eff} hardly exceed 12-13 deg, even at wing tip. In that case the flow can be considered as attached. For the higher frequency, the effective angle of attack reaches almost 20 deg at wing tip. The flow is expected to detach over at least a few centimeters before wing tip.

Except for the case presented in Fig. 4.15(b), the flow should remain attached during the upstroke, as the minimum effective angle of attack does not exceed -10 deg.

In conclusion, only the case presented in Fig. 4.15(c) should give good results with the UVLM due to the presence of an attached flow at all time.

4.5.2   Attached conditions

This section discusses the only case where the flow remains attached. The conditions allowing an attached flow are $U_\infty = 9.4$ m/s and a flapping frequency of $f = 0.79$ Hz. As there is no stall, the vortex lattice method should give reliable solutions in that specific case for both airfoils.

Results

The results obtained for the drag and the lift coefficient for the two airfoils tested are presented in Fig. 4.16.

At first let's consider the two vortex lattice solutions alone. For both airfoils the Joukowski method models a larger peak of thrust than Katz's, while the lift is the same during the whole period. The difference in drag between both methods shrinks when the effective angle of attack is decreased. This suggests that for higher angles of attack the Joukowski solution predicts a larger leading-edge suction (and therefore a larger thrust). As the thrust was underpredicted so far, it seems that for high angles of attack the Joukowski solution is the closest to
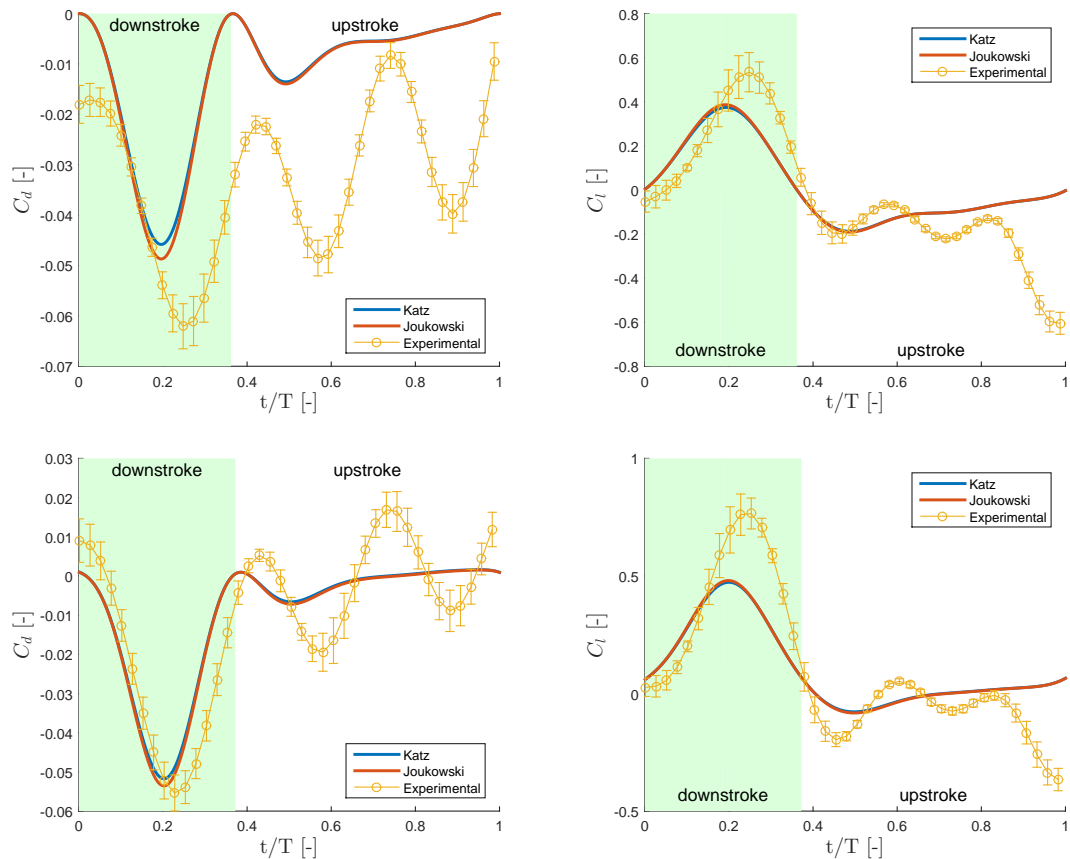
FIGURE 4.16: Drag and lift coefficient for NACA 0012 (top) and 2412 (bottom) airfoils. – Pure flapping (attached flow), $U_\infty = 9.4$ m/s , $f = 0.79$ Hz

the actual measurements. This result arises from the fact that Katz method relies on Bernoulli's equations and therefore on a small angle hypothesis, while the Joukowski method does not require any hypothesis on the angle of attack.

Note that, the peak of thrust corresponds to the highest effective angle of attack at wing tip. It was assumed for this analysis that the flow was totally attached for the values measured (13 deg at wing tip), but if there is a small separation around wing tip, the results of the UVLM may not be 100% reliable for this peak.

The evolution of the drag coefficient is now detailed. The first surprising result is that the measured data predicts some thrust at the beginning of the movement for the NACA 0012. In theory, this should not be possible as a symmetrical airfoil with 0 angle of attack should only produce an extremely small drag (due to viscosity of the flow, wing tip vortices and interference drag) but in no case at all it should produce thrust. This error may come from a bad filtering of the data or from errors in the measurement of static drag. However, if the experimental results are shifted up so that the first result matches 0, the thrust peak corresponds well with the UVLM solutions, with a small difference in aerodynamic lag. Therefore, one could say that for both airfoils, the drag coefficient is well predicted during the downstroke.

During the upstroke however the experimental results seem to oscillate. Once again, this behavior is not the expression of a physical phenomenon, but it could be caused by problems in the treatment of the measured data. As explained in Section 4.3, if there is a small difference in the frequencies used to measure the forces in wind-on conditions and to measure the forces coming from added mass and inertial effects, such peaks may appear after filtering. Anyways, the UVLM solutions seems to correspond to the mean of these oscillations (even for the NACA 0012 if the experimental results are shifted upwards as explained).

The results for the lift coefficient computed using both vortex lattice methods are in general more or less consistent with the ones obtained in wing tunnel. For both cases, the lag seems to be underevaluated with the UVLM as previously. For the downtroke the peak of lift is in general underestimated of about 25-30%. During the upstroke the lift is more or less well predicted with the exception of the very end of the period. For the lasts time steps the lift measured in wind tunnel seems to decrease of a significant amount. This result should not be possible as the graphs represent a whole period. In theory, the coefficients should end at the exact same value than they began, as it is the case for the UVLM results. Therefore this suggests that there is some small errors in the treatment of wind tunnel data.

In conclusion, the UVLM seems to predict quite well the results in that specific case, especially for the drag. Also, Joukowski method was found to model a little bit more precisely the leading-edge suction for large angles of attack. Finally, some additional study of the wing tunnel data may become useful in order to validate definitely these results.

4.5.3 Dynamic stall conditions

This section addresses the worst case possible, corresponding to the lowest airspeed ($U_\infty = 6$ m/s) with the highest flapping frequency ($f = 1.23$ Hz). In that case, the flow is expected to be separated during most of the downstroke over a large part of the wings but also during the upstroke for approximately half of the wing.
Of course the UVLM results are expected to be completely false in this case as the flow is detached over large portions of the wing and during a long time. However, the results found in this case may show if one method presents and higher offset than the other for stall conditions.

Results

The results obtained for the drag and the lift coefficient for the two airfoils tested are presented in Fig. 4.17.

As expected, the UVLM solutions do not match at all the experimental results, due to the separation of the flow.
Especially, both methods predict a large thrust during the downstroke while in fact the thrust is very small (because the drag increases during the separation).
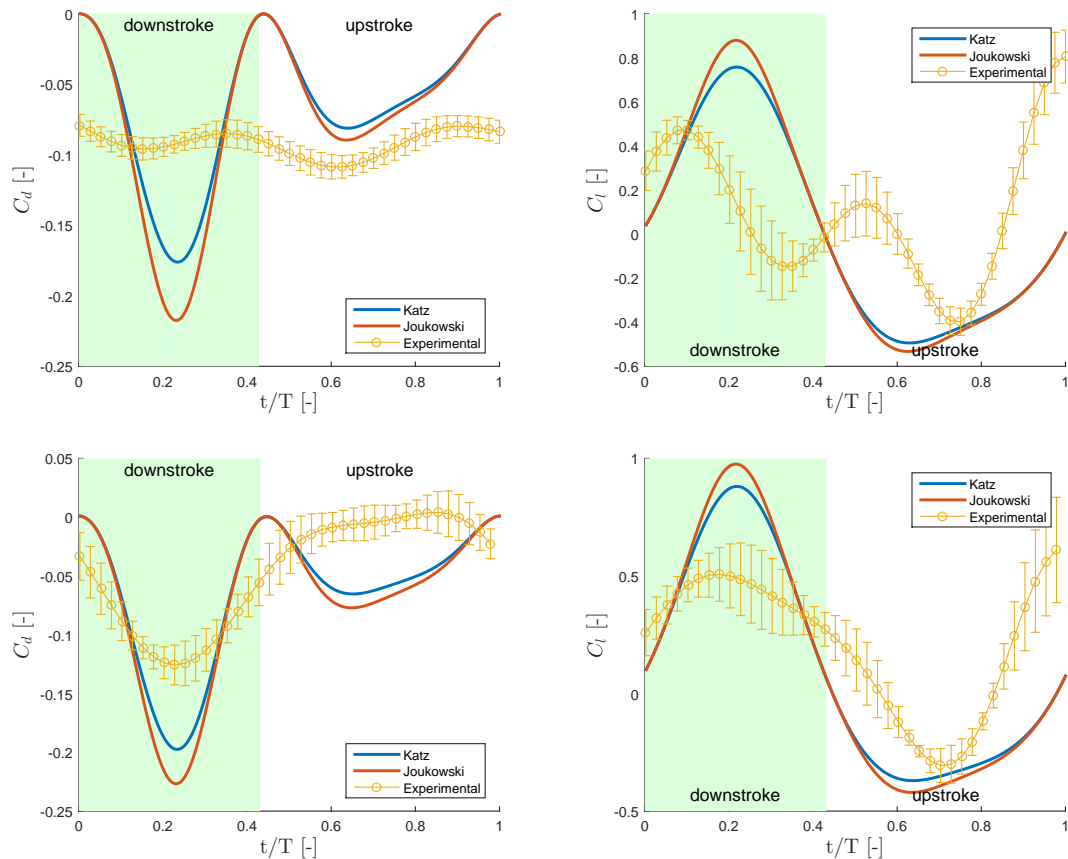
FIGURE 4.17: Drag and lift coefficient for NACA 0012 (top) and 2412 (bottom) airfoils. – Pure flapping (detached flow), $U_\infty = 6$ m/s , $f = 1.23$ Hz

In the same way, they both predict a higher lift during the downstroke while in reality the separation of the flow leads to loss of lift.

However, the interesting result is that, the Joukowski method models a larger leading-edge suction effect than Katz when the angle of attack is higher, as suggested from the study of attached flows.

In the case of an attached flow for high angle of attack (typically the one presented in the previous section), this becomes an advantage as the solution found with Joukowski is closer to the measured values. But as soon as the flow begins to separate, this becomes a disadvantage because the measured data will account for the increase of drag while the UVLM solutions will not. Therefore, the Joukowski solution will be ever further to reality than Katz.

In conclusion, the Joukowski method presents a real advantage in the modeling of the flow for high angles of attack. But in order to use this advantage, one should be certain that the flow is completely attached everywhere at anytime.

4.6 Pitch lagging

Just like for pure flapping, the wing is expected to experience separation during this type of motion; even more, the separated portion of the wings should be larger than for pure flapping.

Therefore, the vortex lattice method will probably not be able to model these flows.

4.6.1 Kinematics analysis

The Fig. 4.18 represents the evolution of the flapping, pitching and effective angles of attack for a NACA 2412 airfoil in pitch lagging with a pitch angle varying from -6 to 6 deg. All these values come from the experimental data.

(a) $U_\infty = 6$ m/s , $f = 0.79$ Hz

(b) $U_\infty = 6$ m/s , $f = 1.23$ Hz

(c) $U_\infty = 9.4$ m/s , $f = 0.79$ Hz

(d) $U_\infty = 9.4$ m/s , $f = 1.23$ Hz
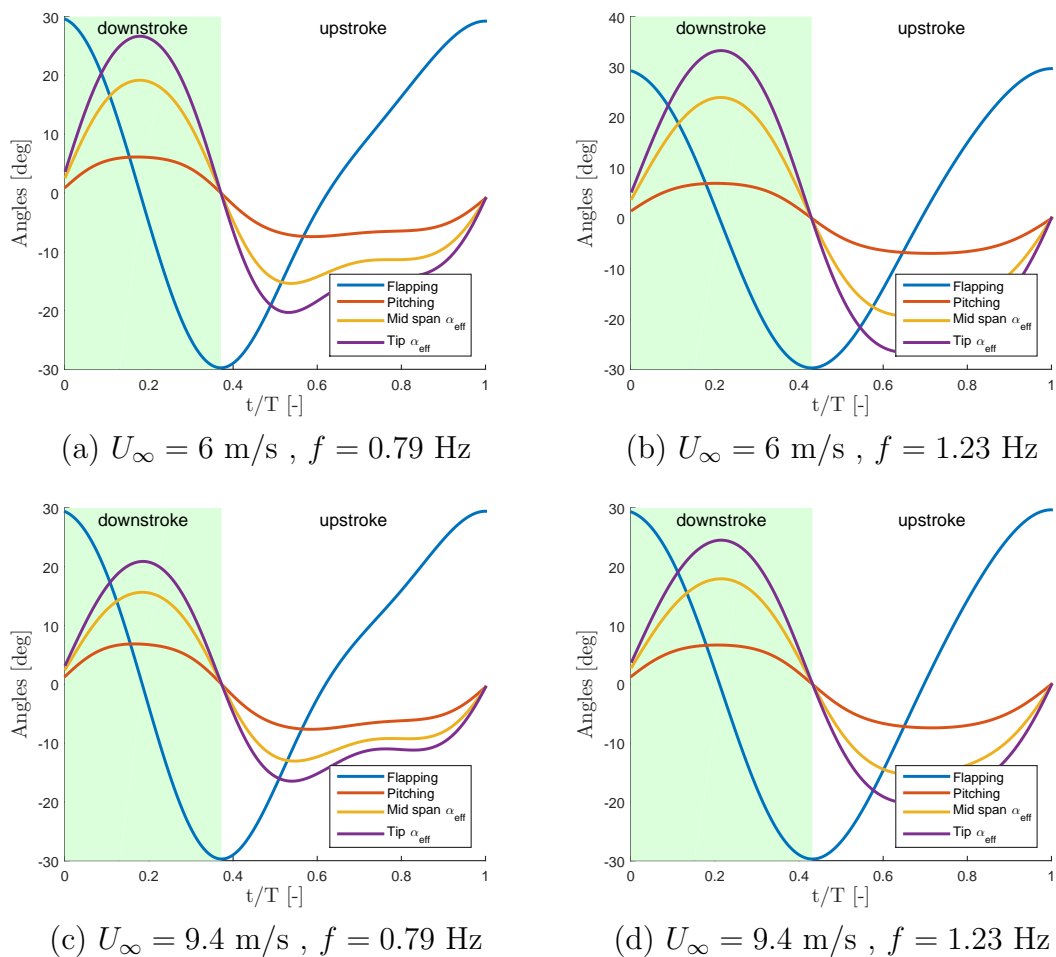
FIGURE 4.18: Wind tunnel data for flapping, pitching and effective angle of attack at mid span and wing tip in pitch lagging. NACA 2412, $\alpha_p \in [-6, 6]$ deg.

A quick inspection of the graphs reveals that α_{eff} is almost equal to 20 deg already at mid span in all the cases. Due to these excessive values for the effective

angle of attack, the flow will be separated over more than half of the wing. As the impact of separation on the UVLM solutions was treated previously for pure flapping, it will not be discussed once again for pitch lagging.

4.7 Summary

This chapter was focused on the analysis of flapping flight with the UVLM. Three different movements were studied: pitch leading, pure flapping and pitch lagging.

It was determined that the pitch leading should give the bests results with the UVLM as the flow is supposed to remain attached during the whole period. For this specific case, the problem of NACA 6409 wings was studied in detail. The different flow parameters were analysed in order to detect some big differences in the solution given by the two methods for the calculation of the aerodynamic loads with the UVLM. In pitch leading, the two methods were found to give similar results and to correspond quite well to the measurements done in wind tunnel.

For pure flapping and pitch lagging, the flow was presenting separation except for one specific case with a really high effective angle of attack. For this case, it was demonstrated that the Joukowski solution was closer to the reality than the Katz solution. In the case of highly separated flows, the UVLM was not applicable. However, a small comparison of the methods showed that the Joukowski was more wrong than the Katz solution as it modeled more leading edge-suction.

The convergence study was not very conclusive. In most of the cases, the Katz solution presented a slightly better convergence for the coarsest meshes, but both computation were found to reach convergence (typically an error smaller than 2%) for the same discretisation.

Chapter 5

Conclusion

5.1 Aerodynamic loads

The main purpose of this thesis was to compare and analyse two different methods used to calculate the aerodynamic forces with the unsteady vortex lattice method. The first method, called the Katz method was developed by Katz and Plotkin and relies mainly on the Bernoulli's equations in order to model the loads. The second method, called the Joukowski method, relies on the Joukowski's equations for the computation of forces.

The first part of this thesis consisted in the treatment of a single wing under simple kinematics (steady, harmonic plunging and harmonic pitching). This section showed that the two methods give similar results for all the kinematics studied. A convergence study was realised on the chordwise discretisation of the wings for the lift and drag coefficient. In almost all cases, the lift was converging at the exact same rate for both methods. This result was expected the lift is usually exactly the same for the two methods. The analysis of the drag proved that for a symmetric finite wing, the Joukowski method presents a better convergence than the Katz. For cambered airfoils, the solution was found to converge faster with the Katz method. However, in the vast majority of the cases studied, the two methods reached convergence (typically, an error smaller than 2%) for the same number of chordwise panels.
In conclusion, for these simple cases the two methods are equivalent. Nonetheless, the Katz method should be preferred, as it requires less computation time to achieve the solution.

The second part of this thesis addressed the problem of a flapping UAV. In that case, the model was adapted to account for the presence of a second wing. The problem of pitch leading was first studied, as this motion is known to present an attached flow during the entire period. The study of the pitch leading was conducted using only a NACA 6409 airfoil because the only available results concerned this airfoil. For these cases, the two methods gave also the same results for the drag and lift coefficients. In reality, the Joukowski method was predicting a little bit more leading-edge suction (and therefore thrust), but this difference was

negligible. In general, the two methods underpredicted the thrust for the attached flows. In the same way, the lift was also underpredicted. Otherwise, the general behavior of the drag and lift coefficient was really well modeled. The convergence study realised in pitch leading for three different airfoils showed that the Katz method tends to converge a little bit faster, especially for the coarsest discretisations. However, as for the simple cases, the two methods reached a converged state for approximately the same discretisation, which means that they can be considered as equivalent for this case too.

The study of pure flapping showed that only one case was expected to present an attached flow due to an effective angle of attack not too large. For this specific case, the difference between the Joukowski and the Katz methods was more evident. For high values of the effective angle of attack, the Joukowski method predicts a larger leading-edge suction than the Katz and therefore is closer to the experimental data. However, in the case of detached flows, the prediction of a higher thrust becomes a disadvantage. Indeed, in reality, the separation leads to a large increase of the drag coefficient. As the UVLM does not model the separation, this increase of drag is not captured. Therefore, the larger prediction of thrust leads to a much larger difference with the experimental results.

The pitch lagging was not discussed in details because it was shown to only present detached flows.

In the end, both method can be considered as equivalent for small angles of attack. However, as long as the flow remains attached everywhere, the Joukowski method should be preferred for modeling flow with high values of the effective angle of attack because it models a larger leading-edge suction.

As the two methods usually reach convergence for the same discretisation, the Katz solution should however be picked when it is possible as it requires less computing time.

5.2   Future works

Some improvement can be done on the codes in order to achieve a better result, especially in the flapping case.

5.2.1   Improvements of the UVLM

Katz and Plotkin suggest various improvement for the methods used to solve the potential flow theory (in [1], chapter 15). In particular, the model can be enhanced with the addition of the viscous effects in the equations. Moreover, some adaptations can be realised for wings at higher angle of attack, as it was the case during the downstroke for most of the movements studied here.

The thickness of the wings can also be modeled in the UVLM. With this, the leading-edge suction should be better predicted with the two aerodynamic loads computation methods. However, in reality the wings were really thin, so this effect should not be really important.

5.2.2 Improvements of the wake model

In the wind tunnel experiment, the body of the flapper shed a wake that interacted with the wake originating from the wings. Therefore, the body can be modeled with the UVLM without being taken into account for the computation of the forces. Then, the wake shed by the body could be computed and could interact with the wake shed by the wings. This would probably give even better results for a free wake model.

It was shown for simple cases that the position of the first wake panel could lead to big differences in the solutions given by the UVLM. This parameter should probably be the topic of a more complete study in order to determine the best value in order to be closer to the experimental data.

Bibliography

[1] J. Katz and A. Plotkin. *Low-Speed Aerodynamics*. Cambridge University Press, second edition, 2001.

[2] N. Abdul Razak. *Experimental Investigation of the Aerodynamics and Aeroelasticity of Flapping, Plunging and Pitching Wings*. PhD thesis, University of Liege, 2012.

[3] P. Chirarattananon and R. J. Wood. Identification of flight aerodynamics for flapping-wing microbots. In *2013 IEEE International Conference on Robotics and Automation (ICRA)*, Karlsruhe, Germany, May 2013 .

[4] R. Palaciois R.J.S. Simpson and J. Murua. Induced-drag calculations in the unsteady vortex lattice method. *AIAA Journal*, 51(7):1775–1779, July 2013.

[5] I.E. Garrick. Propulsion of a flapping and oscillating airfoil. Technical Report 567, NACA, 1937.

[6] T.E. Fritz and L. N. Long. Object-oriented unsteady vortex lattice method for flapping flight. *Journal of Aircaft*, 41(6):1275–1290, 2004.

[7] J. D. Anderson Jr. *Fundamentals of Aerodynamics*. Mc Graw Hill, fifth edition, 2010.

[8] R. Palacios J. Murua and J. M. R. Graham. Applications of the unsteady vortex-lattice method in aircraft aeroelasticity and flight dynamics. *Progress in Aerospace Sciences*, 55:46–72, August 2012.

[9] L. Chang-Sup. *Prediction of steady and unsteady performance of marine propellers with or without cavitation by numerical lifting-surface theory*. PhD thesis, Massachusetts Institute of Technology, May 1979.

[10] G. Dimitriadis P. Tickle J. R. Codd J. Gardiner, N. A. Razak and R.L. Nudds. Simulation of bird wing flapping using the unsteady vortex lattice method. In *IFASD*, 2013.

[11] U. Gulcat. Propulsive force of a flexible flapping thin airfoil. *Journal of Aircraft*, 2009.

[12] N. A. Razak and G. Dimitriadis. Wind tunnel experiments on a flapping drone. In *IFASD*, 2011.

Appendix A

Additional results for test cases

A.1 Pitching and plunging of airfoils
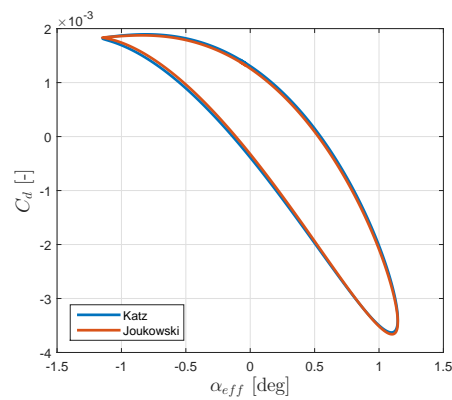
(a) C_d at $k = 0.2$
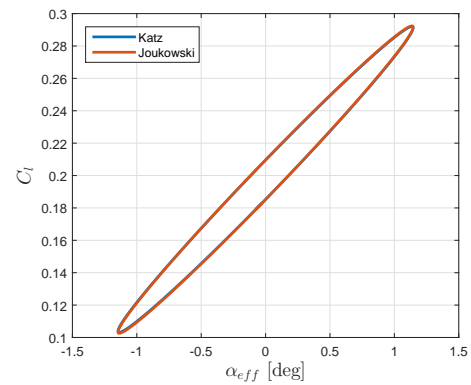
(b) C_l at $k = 0.2$
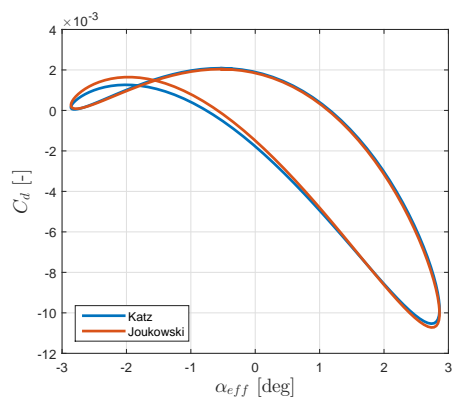
(c) C_d at $k = 0.5$
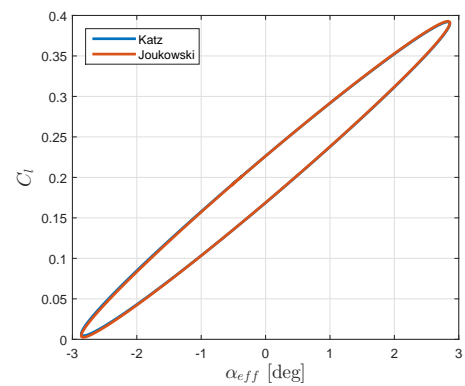
(d) C_l at $k = 0.5$

FIGURE A.1: Drag and lift coefficients for a NACA 2412 airfoil in plunge – 2D.

(a) C_d at $k = 0.2$

(b) C_l at $k = 0.2$

(c) C_d at $k = 0.5$

(d) C_l at $k = 0.5$
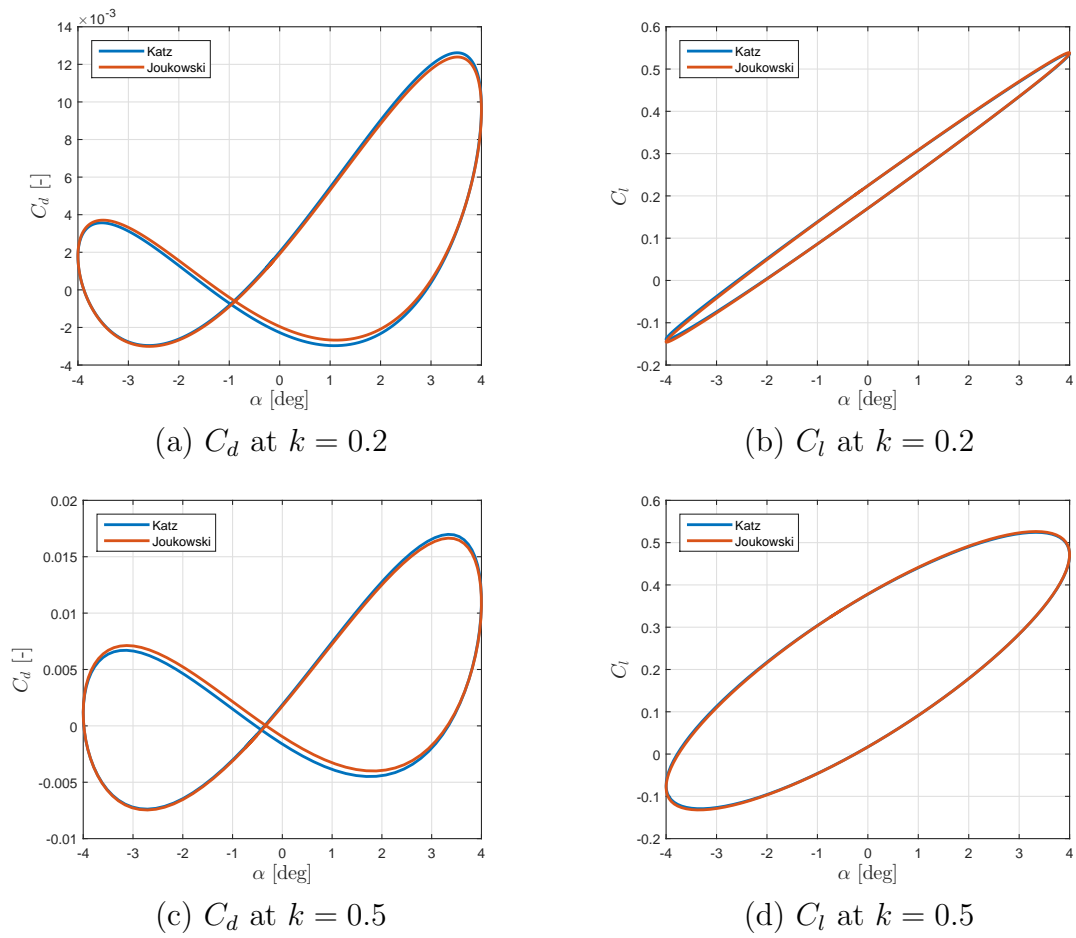
FIGURE A.2: Drag and lift coefficients for a NACA 2412 airfoil in plunge – 2D.